

Pontificia Universidad Católica del Perú

Escuela de Posgrado

Tesis

Robotic Manipulator inspired by Human Fingers based on
Tendon-Driven Soft Grasping

Tesis para obtener el grado académico de:
Magíster en Ingeniería Mecatrónica

Presentado por: Till Odenkirchen

Tutor Responsable (TU Ilmenau) : M. Sc. Jos´e Luis Z´arate Moya

Professor Responsable (TU Ilmenau) : Univ.-Prof. Dipl.-Ing. Dr. med (habil)Hartmut Witte

Professor Responsable (PUCP) : Prof. Dr-Ing. Dante Angel Elias Giordano

Junio - 2021

Aufgabenstellung für die Masterarbeit

von Herrn Till Odenkirchen

Thema: Robotic Manipulator Inspired by Human Fingers Based on Tendon-Driven Soft Grasping

The tendon-driven underactuated structures, widely used in robotic hands and grippers, have a close inspiration by human fingers. This device exhibits many types of grasping described by hand taxonomy, thanks to the biomimetic structure. Grippers use as a standard actuation method a set of rigid connections, joints, and springs, using external motors to give movement to the complete framework. A possible limitation of soft grippers is the miniaturization difficulty of the engine system, which may limit the use of technology in portable platforms. Another topic is the manufacture of skin, like that of human hands, to improve the friction of tendon-driven grippers with objects for better handling. The purpose of this work is to determine the best configuration in a robotic gripper based on parameters of size, weight, shape, and control to improve the gripping system, in particular, the manipulation of a fragile object.

Tasks:

- Characterization of force control in a gripper robotic system.
- Reduction of the influence of rigid manipulation by contact points sensors and mobility of the fingers.
- Testing and documentation of the methodology applied to this work.

Ausgabedatum: 03.11.2020

Verantwortlicher Hochschullehrer: Univ.-Prof. Dipl.-Ing. Dr. med. (habil.)
Hartmut Witte

Betreuer PUCP Lima: Prof. Dr.-Ing. Dante Elias

Betreuer an der TU Ilmenau: MSc. José Zárate

Ilmenau, 15.10.2020

Ort, Datum

Lima, 08.12.2020

Ort, Datum

Ilmenau, 16.10.2020

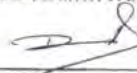
Ort, Datum

Ilmenau 16.10.2020

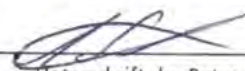
Ort, Datum



Unterschrift des verantwortlichen Hochschullehrers



Unterschrift des verantwortlichen Hochschullehrers



Unterschrift des Betreuers




Unterschrift des Studierenden

Statement of Authorship

I hereby declare that I am the sole author of this master thesis and that I have not used any sources other than those listed in the bibliography and identified as references.

Furthermore, I declare that I have not submitted this thesis at any other institution in order to obtain a degree.

Ilmenau, 07.05.2021
Place, Date


Till Odenkirchen

Kurzfassung

Die menschliche Hand ist in der Lage, verschiedene Greif- und Manipulationsaufgaben auszuführen und kann als einer der geschicktesten und vielseitigsten Effektoren angesehen werden.

In dieser Arbeit wurde ein Soft Robotic-Greifer entwickelt, der auf den Erkenntnissen aus der Literatur zur Taxonomie der menschlichen Greiffähigkeiten und den biomechanischen Synergien der menschlichen Hand basiert.

Im Bereich der Roboterhände sind sehnengetriebene, unteraktuierte Strukturen weit verbreitet. Inspiriert von der Anatomie der menschlichen Hand, bieten sie durch ihre Flexibilität passive Adaptivität und Robustheit.

Es wurde ein Sensorsystem implementiert, bestehend aus Force Sensing Resistors (FSRs), Biegungssensoren und einem Stromsensor, wodurch das System charakterisiert werden kann. Die Kraftsensoren wurden in die Fingerkuppen integriert. In Anlehnung an die menschliche Haut wurden Abgüsse aus Silikonkautschuk an den Fingerballen verwendet. Diese versprechen eine erhöhte Reibung und bessere Adaptivität zum gegriffenen Objekt.

Um den entwickelten Greifer zu evaluieren, wurden erste Tests durchgeführt. Zunächst wurde die Funktionalität der Sensoren, wie z.B. der als FSRs ausgewählten Kraftsensoren, getestet. Im weiteren Verlauf wurden die Greiffähigkeiten des Greifers durch Manipulation verschiedener Objekte getestet. Basierend auf den Erkenntnissen aus den praktischen Versuchen kann festgestellt werden, dass der entwickelte Greifer ein hohes Maß an Geschicklichkeit aufweist.

Auch die Adaptivität ist dank der verwendeten mechanischen Komponenten gewährleistet. Mittels der Sensorik ist es möglich, den Greifprozess zu kontrollieren. Die Ergebnisse zeigen aber auch, dass z. B. die interne Systemreibung die Verlustleistung des Systems stark beeinflusst.

Abstract

The human hand is able to perform various grasping and manipulation tasks, and can be seen as one of the most dexterous and versatile effectors known.

The prehensile capabilities of the hand have already been analyzed, categorized and summarized in a taxonomy in numerous studies.

In addition to the taxonomies, research on the biomechanical synergies of the human hand led to the following conceptions: The adduction/abduction movement is independent of the flexion/extension movement. Furthermore, the thumb is rather independent in its mobility from the other fingers, while those move synchronously within their corresponding joints. Lastly, the consideration of the synergies provides that the proximal and distal interphalangeal joints of a human finger are more intensely coordinated than those of the metacarpal joints.

In this work, a soft robotic gripper was developed based on the knowledge from the literature on the taxonomy of human gripping abilities and the biomechanical synergies of the human hand.

In the domain of robotic hands, tendon-driven underactuated structures are widely used. Inspired by the tensegrity structure of the human hand, they offer passive adaptivity and robustness through their flexibility.

A sensor system was implemented, consisting of FSRs, flex sensors and a current sensor, thus the system parameters can be characterized continuously. The force sensors were integrated into the fingertips. Molds of silicone rubber were used as finger pads to provide higher friction and better adaptivity to the grasped object on the contact areas of the finger, to mimic human skin.

Initial tests were carried out to evaluate the gripper. First, the functionality of the sensors, such as the force sensors selected as FSRs, was tested. In the further course, the gripping capabilities of the gripper were tested by manipulation of various different objects.

Based on the findings from the practical experiments, it may be stated that the gripper has a high degree of dexterity. Thanks to the mechanical components used, adaptivity is guaranteed as well. By means of the sensor system it is possible to control the gripping processes. However, the results also showed that, for example, the internal system friction dominates the system's power dissipation.

Acknowledgement

This thesis was written within the double degree program between the Pontificia Universidad Católica del Perú (PUCP) and the TU Ilmenau. The work was done at the Department of Biomechatronics at the Ilmenau University of Technology.

At this point I would like to thank all those who have always supported me in this work. Especially I would like to thank Mr. José Luis Zárate Moya (M. Sc.), who supervised my master thesis and always supported me as soon as I approached him with questions or discussion needs. He has always been extremely helpful at all times. Thank you very much!

I would also like to thank Prof. Dr.-Ing. Dante Elias, who supervised my thesis on the part of the PUCP. I would like to thank for the overwhelming hospitality I received during my time in Lima and for all the unforgettable experiences I had there. Thank you very much.

Besides Mr. Elias, I would also like to thank Dr.-Ing. Tom Ströhla, who was my contact person for the academic organization of the double degree program and Mrs. Corinna Wedekind, who made the scholarship possible.

I would also like to thank the entire Department of Biomechatronics under the leadership of Univ.-Prof. Dipl.-Ing. Dr. med (habil) Hartmut Witte for the smooth organization during these unusual times.

Last but not least, I would like to thank my family and friends, who also supported me during the preparation of my thesis.

Contents

List of Figures	I
List of Tables	III
Glossary	IV
List of Abbreviations	VI
Formula Directory	VII
List of Symbols	VIII
1 Introduction	1
2 Fundamentals and State of Art	2
2.1 Biomechanical Overview of the Human Hand	2
2.1.1 Functional Anatomy of the Human Hand	2
2.1.2 Biomechanics of the Human Digits	6
2.1.3 Prehensile Capabilities of the Human Hand	13
2.1.4 Synergies in Human Grasping	16
2.2 Soft Robotic Materials	17
2.3 Mechanical Fundamentals	17
2.3.1 Underactuation	18
2.3.2 Differential Mechanism	18
2.3.3 Contact Points	20
2.3.4 Compliant Mechanisms	21
2.4 Sensory Systems	22
2.4.1 Force-sensing Resistors	23
2.4.2 Flex Sensors	24
2.4.3 Current Sensors	26
2.5 Control Systems	28
2.6 State of the Art - Tendon-driven Soft Robotic Grippers	29
2.6.1 Actuation	34
3 Design of the Manipulator	35
3.1 Conceptual Design	36
3.1.1 Requirements for the Soft Robotic Gripper	36
3.1.2 Overall Function and Technical Principles	37
3.2 Mechanical Design	38
3.2.1 Design of the Finger	39
3.2.2 Design of the Compliant Joints	41
3.2.3 Design of the Tooth Gear Mechanism	42

3.3	Electrical Design	43
3.3.1	Selection: Position Sensors	44
3.3.2	Selection: Force Sensors	44
3.3.3	Election: Current Sensor	44
3.3.4	Calibration of the Sensors	45
3.3.5	Selection of the Actuator	48
3.3.6	Power Supply	48
3.4	Software Design	48
3.4.1	Calculations	48
3.4.2	Software Implementation	49
3.5	Fabrication	51
3.5.1	3D-Printing	52
3.5.2	Silicon Molds	53
4	Practical Experiments	54
4.1	Test Measurements with the Implemented Sensors	54
4.1.1	Test Measurements with the FSR	54
4.1.2	Test Measurements with the Flex Sensor	55
4.1.3	Test Measurements with the Current Sensor	56
4.2	Test of the Grasping Capabilities	58
4.3	Test of the Sensors during Grasping	59
5	Evaluation of the Soft Robotic Gripper	61
5.1	Evaluation of the Sensor Functionality	61
5.2	Evaluation of the Grasping Capabilities	61
6	Discussion	64
6.1	Design strengths and weaknesses	64
7	Conclusion and Outlook	65
	Bibliography	v
A	Appendix	XIII
A.1	Complementary Sections	XIII
A.1.1	Calibration of the Flex Sensor	XIII
A.1.2	Calibration of the Force Sensor	XIV
A.2	Complementary Figures	XV
A.3	Complementary Tables	XVIII
A.3.1	List of Requirements	XVIII
A.3.2	Solution Concepts	XXIV
A.3.3	Evaluation Matrices	XXV
A.4	Technical Drawings	XXVI

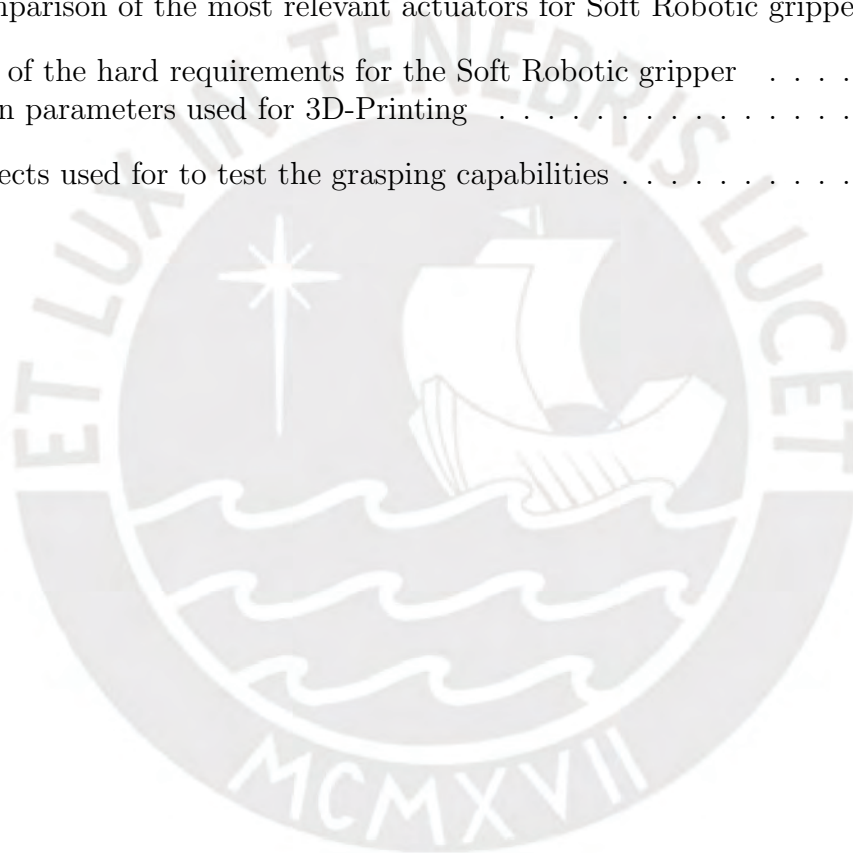
List of Figures

2.1	Kinematic skeleton of the human hand	3
2.2	Comparison of the extensor and flexor tendons of the human left hand	4
2.3	Lateral, schematic illustration of the human hand, containing local coordinate systems and marker locations used for the anthropometry	5
2.4	Motion range of the finger joints	6
2.5	Flexion of the human finger	7
2.6	Conceptual illustration of an underactuated finger	8
2.7	Conceptual tendon-driven finger with n phalanges	12
2.8	Abducted and adducted position of the thumb	13
2.9	Comparison of the opposition types of the human grasping and the respective integration of two Virtual Fingers	14
2.10	Results of the grasp span analysis, representing a smaller subset of grasp types, that can be used to grasp most objects	15
2.11	Tridigital prehension with 2 virtual fingers	15
2.12	Two-level hierarchy of prehensile control, including the concept of VF	16
2.13	Transmission mechanism with two outputs in an underactuated system	18
2.14	Commonly used differential mechanisms in robotic grasping	19
2.15	Seesaw mechanism	20
2.16	Schematic illustration of the difference between distributed and concentrated compliance	21
2.17	Possible geometries of flexure hinges to realize one, respectively two DOFs . .	22
2.18	Basic construction of a FSR	23
2.19	Basic Circuits for conversion of data with variable resistors	24
2.20	Schematic drawing of an optical flex sensor	25
2.21	Schematic drawing of a capacitive bend-angle sensor	25
2.22	Schematic drawing of a conductive ink based flex sensor	26
2.23	Schematic illustration of the Hall-effect	27
2.24	Fuzzy control scheme to control a robotic hand with FSRs	28
2.25	Examples for Soft Robotic grippers	29
2.26	Biomimetic hand by Xu et al.	30
2.27	Grasping demonstration of the “Synergy-based Three-Fingered Hand”, integrated into the GRASP Taxonomy	31
2.28	Comparison of medium-complexity Robotic Grippers from the Yale Open-Hand Project	32
3.1	Graphical illustration of the design methodology according to the VDI 2206 and VDI 2221	35
3.2	Basic System Structure	37
3.3	Technical principle of a finger with 3 phalanges and compliant joints	38
3.4	CAD-Model of the assembled Soft Robotic Gripper	39
3.5	Design of the fingertip	40
3.6	Tendon routing of the Soft Robotic fingers	41

3.7	Hinge design in detasFLEX	42
3.8	Manually lockable gear mechanism to change between different grasp modes	43
3.9	Range of motion of the gear mechanism to realize adduction/abduction. The adduction/abduction movement is between 0° and 90°	43
3.10	Exemplary illustration of the wiring of a FSR with the corresponding reference resistor	45
3.11	Schematic drawing of the elected Flex Sensor	45
3.12	Linear current sensor from Microbot with an Allegro [®] Hall-effect based IC	46
3.13	Calibration of the flex sensor with a RC-circuit	46
3.14	Technical principle for the referencing process	47
3.15	Characteristic curve of the Interlink FSR [®] 400	47
3.16	Class diagram of the Soft Robotic Gripper software	50
3.17	Soft Robotic Gripper Tool: A GUI to control the developed gripper	50
3.18	Flow chart of the data acquisition	51
3.19	Fabrication of the Soft Robotic Gripper with a 3D-Printer	52
3.20	Cleaning the silicone rubbers after curing	53
4.1	Example for the test measurements: FSR of the right finger	55
4.2	Example for the test measurements: Flex sensors during a Medium Wrap	56
4.3	Power Sphere grip to determine the functionality of the current sensor	57
4.4	Curve of the current of the servo motor when trying to grab an orange	57
4.5	Soft Robotic Gripper performing various grasps	59
4.6	Sequences of a Medium Wrap during the manipulation of a plastic cup	59
4.7	Curve of the Force of the FSR of the left finger while trying to grab a shot glass with a Medium Wrap	60
5.1	Prehensile capabilities of the Soft Robotic gripper	62
5.2	Roll-back Phenomenon during the grasp of a banana	63
A.1	Referencing of the flex sensor with an angle disc	XIII
A.2	Calibration of the flex sensors with a multimeter	XIV
A.3	Setup of the calibration by means of a beam with a flat contact surface for optimum loading of the active zone of the FSR	XIV
A.4	Dorsal view of the calibration setup	XV
A.5	Schematic drawing of the collateral ligaments and volar plate at the MCP joint	XVI
A.6	Classification of gripping technologies in relation to different object geometries	XVI
A.7	Taxonomy realized by the anthropomorphic hand by Xu et al.	XVII

List of Tables

2.1	Segment length coefficients of the 3 phalanges of the most important digits	5
2.2	Motion ranges of the human interphalangeal joints of the index finger	6
2.3	Static friction coefficients for some common materials	20
2.4	Examples for the different categories of grasping technologies	29
2.5	Comparison of the Model M ² , Model T42 and Model O	32
2.6	Comparison of State of the Art tendon-driven, robotic Grippers	33
2.7	Comparison of the most relevant actuators for Soft Robotic grippers	34
3.1	List of the hard requirements for the Soft Robotic gripper	36
3.2	Main parameters used for 3D-Printing	52
4.1	Objects used for to test the grasping capabilities	58



Glossary

Definitions

Afferent Information sent to the brain from e.g. muscle

Efferent Information sent from the brain to e.g. muscle

Anatomical Terms

Body Parts

Pollex Thumb

Carpus Wrist

Metacarpus Wrist

Digit Finger

Anatomical Directions

Anterior In front of, front

Axial Around a central axis

Bilateral Involving both sides of the body

Caudal Toward the back, toward the tail

Contralateral On opposite sides of the body

Distal Away from, farther from the origin

Dorsal Near the upper surface, toward the back

Inferior Below, under

Intermediate Between two structures

Ipsilateral On the same side of the body

Lateral Toward the side, away from the mid-line

Medial Toward the mid-line, middle, away from the side

Parietal	Relating to a body cavity wall
Posterior	After, behind, following, toward the rear
Proximal	Near, closer to the origin
Rostral	Toward the front
Superior	Above, over
Unilateral	Involving one side of the body
Ventral	Toward the bottom, toward the belly
Visceral	Relating to organs within body cavities

Anatomical Movements

Abduction	Moving the fingers away from the middle finger
Adduction	Moving the fingers toward the middle finger
Circumduction	Circular movement as a combination of different individual movements (e.g. adduction, abduction, flexion and extension)
Extension	Moving the base of the finger away from the palm
Flexion	Moving the base of the finger towards the palm

Presented Grasp Types

Precision Grasps		Power Grasps	
InfP	Inferior Pincer	AT	Adducted Thumb
L	Lateral	ET	Extension Type
PP	Palmar Pinch	FH	Fixed Hook
PE	Parallel Extension	LD	Large Diameter
PreD	Precision Disk	LT	Light Tool
PreS	Precision Sphere	MW	Medium Wrap
P2F	Prismatic 2 Finger	PowD	Power Disk
TIP	Tip Pinch	PowS	Power Sphere
TP	Tripod	SD	Small Diameter

List of Abbreviations

AC	Alternating current
ADC	Analog-digital converter
AHAP	Anthropomorphic Hand Assessment Protocol
AMR	Anisotropic Magnetoresistance
CMC	Carpometacarpal
DC	Direct current
DIP	Distal interphalangeal
DOF	Degree of freedom
EDC	Extensor digitorum communis
ER	Electro-rheological
FDM	Fused deposition modeling
FDP	Flexor digitorum profundus
FDS	Flexor digitorum sublimis
FEA	Fluidic elastomer actuator
FSR	Force sensing resistor
GAS	Grasping Ability Score
GUI	Graphical user interface
IC	Integrated circuit
IDE	Integrated development environment
iHY	iRobot-Harvard-Yale
LMPA	Low melting point alloy
MCP	Metacarpophalangeal
MR	Magneto-rheological
MRI	Magnetic Resonance Imaging
PC	Principle components
PCA	Principle components analysis
PIP	Proximal interphalangeal
SMA	Shape memory alloy
TPU	Thermoplastic polyurethane
VF	Virtual finger

Formular Directory

Notations

$\mathbf{a}, \mathbf{b}, \dots$	Vector
A_x, b_x, \dots	scalar in x-direction
$\mathbf{A}, \mathbf{B}, \dots$	Matrix
\circ	Reciprocal product of screws in the plane

Constants

g	$9.806\,65 \frac{\text{m}}{\text{s}^2}$	Standard acceleration due to gravity
e	$1.602 \times 10^{-19} \text{ A s}$	Elementary electric charge
ρ_{H_2O}	$997.532 \frac{\text{kg}}{\text{m}^3}$	Density of water at 296 K

List of Symbols

Symbol	Description	Unit
B_j	Segment length coefficient, $j \in \{1, 2, 3, 4\}$	
HL	Hand length	[mm]
$SL_{j,f}$	Segment length, $f \in \{I, II, III, IV, V\}$	[mm]
C	Capacitance	[F]
q	Electrical charge carrier	[C]
U_H	Hall voltage	[V]
I	Electrical current	[A]
l	Length	[mm]
F_L	Lorentz force	[N]
R_M	Measuring resistance	[Ω]
B	Magnetic flux	[T]
I_M	Motor current	[A]
R_{flex}	Electrical resistance of the flex sensor	[Ω]
R_{FSR}	FSR resistance	[Ω]
d	Thickness	[mm]
V_{cc}	Alimentation voltage	[V]
V_{out}	Output voltage	[V]
b	Width	[mm]

1 Introduction

Even though there is a long and successful history of robot development for industrial environments, there are still few applications of robots interacting with people. One of the causes is the perception problem, which complicates the use a lot, meaning the permanent use of sensors to understand the ambient. Additionally, common grippers are still not close to the broad capabilities of the best known effector, the human hand [Mas18]. Common manipulation robots usually use the following procedure. Initially, the contact points between the gripper and the object are determined. Accordingly, a collision-free trajectory is planned afterwards. Crucial for this procedure is that only the determined contact points are allowed to interact with the desired object. Once the gripper is in the position to lift the object, it grasps blindly and only successfully if the calculated trajectory is correct and the pre-grasp location is good enough to grab the object. To overcome the necessity of this high precision, the use of soft, underactuated structures has been initiated, leading to higher adaptivity. The fabrication of those has been favored by the continuing progress in technology of 3D-printing, which even makes soft materials like thermoplastic polyurethane (TPU) printable. Thus, the possibility of rapid prototyping for soft robots was induced.

Motivation and Objectives

Since the first experimental setups with tendon-driven grippers in the late 1970s [Shi+18; Tow00] there has been an enormous increase in knowledge about the design and versatility of grippers. These grippers, inspired by human fingers, show an underactuated behaviour due to their morphology (see 2.3.1). In order to be able to exert an appropriate force on an object, it is essential to implement an exteroceptive sensor system. As the main objective is to develop a 3-finger robotic manipulator with a design inspired by the human finger, there is also a need to integrate a system for proprioception for a precise control. Based on the human finger (see 2.1), this work also aims to reduce the effect of rigid manipulation, which includes modifying the contact points with the object to be gripped similar to human skin. The entire development process follows the guidelines of the VDI 2206.

2 Fundamentals and State of Art

The following part of this work is intended to illustrate the fundamentals, which are required to develop a suitable configuration of a tendon-driven Soft Robotic gripper with human inspired fingers. In the development of human-inspired robotic grippers mainly exist two approaches for the design: a purely theoretical, mathematical investigation on grasping and manipulation or more focussed on functional prototypes in a rather intuitive way [BG06]. This part of the work aims to give an insight on both sides, to combine the knowledge. First, the anatomical background is given, demonstrating the human hand's morphology (Sec. 2.1.1) and its biomechanics (Sec. 2.1.2), as well as a brief summary of the human prehensile capabilities (Sec. 2.1.3) and synergies in human grasping (Sec. 2.1.4). Second, to lead to the development of force control, the sensory possibilities and their functionality will be discussed (Sec. 2.4). Finally, the issue of the mathematical fundamentals for the description of the finger's mechanics shall be broached (Sec. 2.1.2).

2.1 Biomechanical Overview of the Human Hand

This section first describes the anatomy of the human hand (Sec. 2.1.1). Followed by an overview on the commonly used grasps for the manipulation of fragile objects (Sec. 2.1.3), it leads to a more detailed biomechanical analysis of the human fingers used for those grasps (Sec. 2.1.2).

2.1.1 Functional Anatomy of the Human Hand

The human hand is able to perform various grasping and manipulation tasks, making it the most “dexterous and versatile effector known (e.g. opposable thumb, palm mobility etc.)” [LAK13, p. 2046]. The main use of this effector is prehension, referring to a static hand posture, in which an object is held safely, irrespective of the hand orientation [Fei+16]. Additionally, there is the possibility of in-hand motion, which will not be looked further into here. The enormous level of dexterity requires a certain complex framework made of bones and tendons. This chapter yields to give an insight of the morphology and topography of the human hand with focus on the fingers, especially on the functional characteristics (i.e. kinematics).

In addition to its prehensile capabilities, the human hand is also a very accurate and sensitive sensory receptor [Kap74, p. 164]. The human hand is divided into three parts: wrist

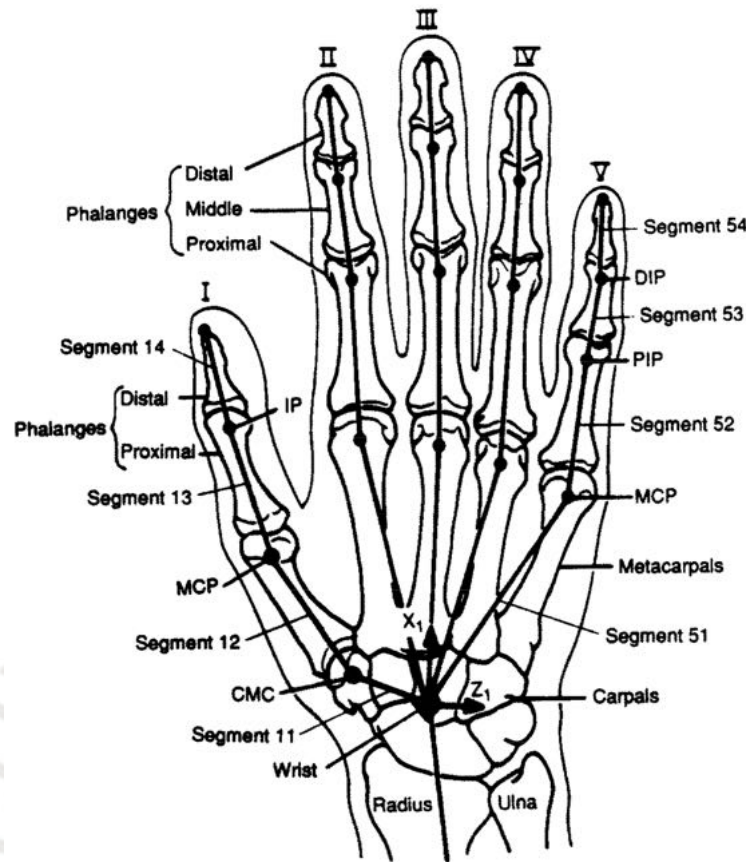


Figure 2.1: Kinematic skeleton of the human hand, adapted from [BA92, p. 152]

I Thumb III Middle finger V Little finger
II Index finger IV Ring finger

(*carpus*), *metacarpus* and fingers (*digiti*) and is usually formed by 27 bones. Each finger consists of three phalanges: *phalanx proximalis*, *mediae*, *distalis*, except the thumb (*pollex*), which persists in two phalanges [Aum+17] (see Fig. 2.1). Depending on the position, the synovial joints between the phalanges are named distal interphalangeal (DIP), proximal interphalangeal (PIP), metacarpophalangeal (MCP) and carpometacarpal (CMC) joint. While the DIP and PIP joint only have one degree of freedom (DOF), the MCP has one extra DOF, forming a so-called saddle joint [XT16, p. 3487]. In total, the hands framework has 15 joints (not considering the carpal and metacarpal joints), which results in more than 20 DOF [Fei+16]. Generally speaking, the thumb, index and middle finger are the most important fingers in common grips [Fei+09; Fei+16; Cut89].

The joint, respectively the finger motion, is limited by the length of the ligaments (see A.5 as an example for the MCP joint). When the finger is in a flexed position, the ligaments are tensed. Once the finger is extended, the ligaments become less stressed, which, in case of the MCP, permits e.g. the index finger to be moved laterally [XT16; Kap74].

As seen in Fig. 2.2, there are two types of tendons connecting the bones and muscles: the extensor (Fig. 2.2a) and flexor tendons (Fig. 2.2b). While the first mentioned are in charge

of straightening the finger, the others induce a force to bend the particular finger, operated by the muscles in the forearm, the so-called extrinsic muscles. Besides those, the so-called intrinsic muscles exist, which are a small group of muscles providing passive reflex-mediated stiffness to the fingers [XT16]. The tendons are guided by the *synovial sheaths* (see Fig. 2.5c), which allow the tendons to move with reduced friction [Kap74, p. 190]. Those sheaths are made of a fibrous tissue wrapped around each tendon (see. Fig. ??). Akin to the flexor tendons, the extensor tendons (see Fig. 2.2a) are also pulled by extrinsic muscles and guided by fibro-osseous tunnels [Kap74, p. 196].

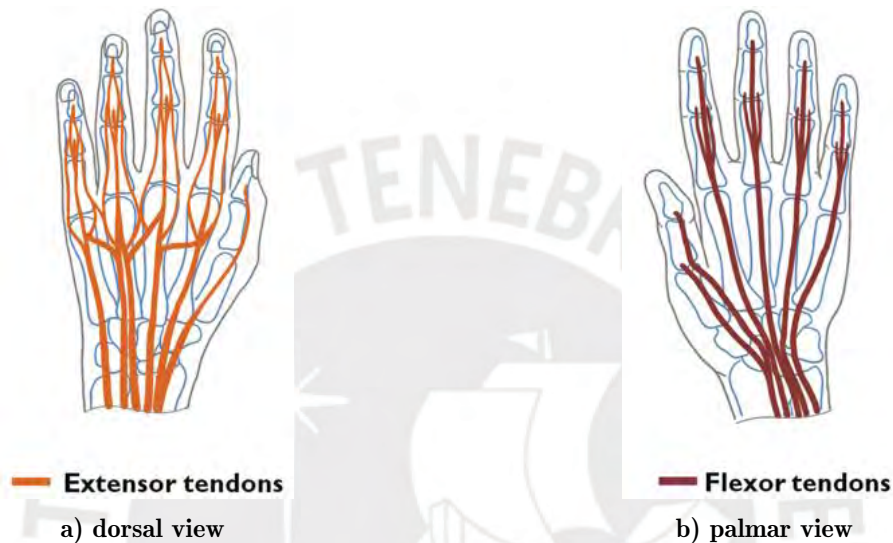


Figure 2.2: Comparison of the flexor and extensor tendons of the left human hand, modified from [XT16, p. 3489]

In addition to the knowledge on the tensegrity structure of the human hand, it is necessary to know about the metric data on the human hand and then take a look on the kinematics afterwards (see Sec. 2.1.2).

Buchholz et al. did an anthropometric analysis of the human hand [BAG92] to collect statistically-based parameters to describe the hand's kinematics (see Fig. 2.3), needed for the kinematic model in their subsequent publication [BA92]. The authors define the thumb as digit I, the index finger as digit II and so on (see Fig. 2.1).

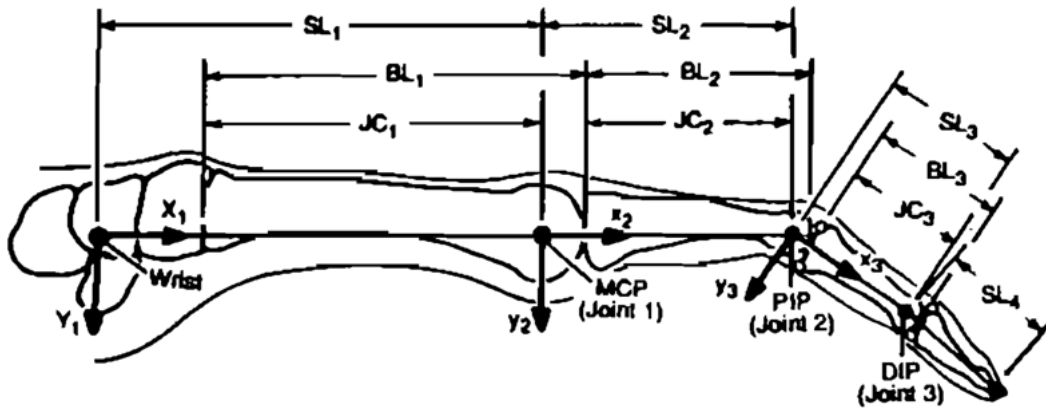


Figure 2.3: Lateral, schematic illustration of the human hand, containing local coordinate systems and marker locations used for the anthropometry [BAG92, p. 265]

Their study of two female and four male hands yielded to the following coefficient B_j ($j \in \{1, 2, 3, 4\}$) to calculate the segment length $SL_{j,f}$ ($f \in \{I, II, III, IV, V\}$) in relation to hand length HL (see Tab. 2.1). The segment length is defined by the distance between two centers of rotation (joints), for example the MCP and PIP joint (see Fig. 2.3).

Since it has already been established that the thumb, index finger and middle finger are the most important digits, only the associated coefficients are listed here for the sake of simplicity.

Table 2.1: Segment length coefficients B_j of the 3 phalanges (2 in case of the thumb) of the 3 most important digits, based on the survey of two female and four male hands [BAG92]

Segment j	Digit		
	I (thumb)	II (index)	III (middle)
2	-	0.245	0.266
3	0.196	0.143	0.17
4	0.158	0.097	0.108

With the help of these coefficients it is possible to estimate the respective segment length for each finger within a certain range of deviation, only by the knowledge of the hand's length HL .

$$SL_{j,f} = B_j \cdot HL \quad (2.1)$$

In the process of the thesis, these findings will be used to determine the design of the robotic fingers (see Sec. 3.2.1).

Once the most relevant grasps are pointed out in the following section, the concrete mechanism behind the human finger and the mechanical model shall be pointed out (see Sec. 2.1.2).

2.1.2 Biomechanics of the Human Digits

As mentioned in Sec. 2.1.1, the human finger consist in three phalanges, except in case of the thumb. Connected by the tendons, they are driven by the extrinsic muscles, which are located in the forearm. This actuation offers a corresponding motion range of each joint of the hand which is illustrated in the following figure (see Fig. 2.4). The PIP and DIP joint are hinge joints (1 DOF), while MCP joints are morphologically spherical joints, but the third DOF is limited by ligaments (see Fig. A.5).

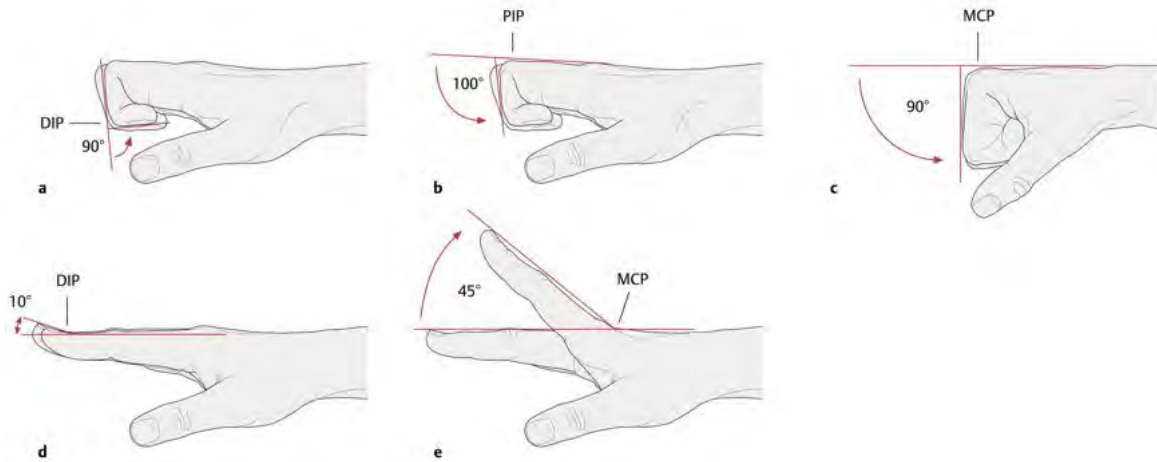


Figure 2.4: Motion range of the finger joints [SSS14, p. 297]

- a) Flexion of the DIP joint
- b) Flexion of the PIP joint
- c) Flexion of the MCP joint
- d) Extension of the DIP joint
- e) Extension of the MCP joint

The ranges of motion in Figure 2.4 taken from literature [Aum+17; SSS14] are mostly consistent with scientific studies. For example, Ingram used the CyberGlove (Virtual Technologies, Palo Alto, CA, USA) to record the movements of the right hand. This study showed that, the MCP joint reaches up to $103^\circ \pm 16^\circ$. Additionally, they provided the range for abduction of the index finger as $35^\circ \pm 5^\circ$. Due to Ingram et al.'s practical approach, the motion ranges of their study will be used in this work.

Table 2.2: Motion ranges of the human interphalangeal joints of the index finger

Joint	Flexion [°]	Extension [°]	Range [°]	Source
MCP	78	25 (passive 90)	103	[Ing+08], passivity [Kap74]
PIP	84	-1	85	[Ing+08]
DIP	59	23 (30 passive)	82	[Ing+08], passivity [Kap74]

Angles measured starting from the calibration as pressing the hand down against a flat surface with four fingers parallel and the thumb aligned against the side of the palm.

As seen in Figure 2.5a, the flexor digitorum sublimis (FDS) mainly flexes the PIP joint and the flexor digitorum profundus (FDP) (see Fig. 2.5b) primarily flexes the DIP joint, but also

affects the PIP, as there does not exist a particular antagonist [Kap74]. Together with the extensor digitorum communis (EDC), the flexor forms a postural synergy (see Sec. 2.1.4) [Kap74].

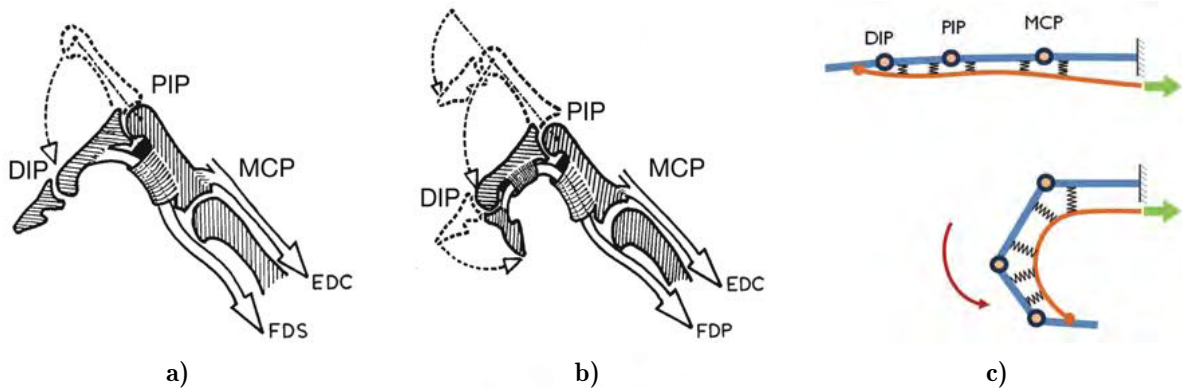


Figure 2.5: Flexion of the human finger

- a) Flexion of the PIP joint with the FDS
- b) Flexion of the DIP joint with the FDP, both modified from [Kap74, p. 195]
- c) Schematic illustration of tendon sheaths during flexion and its mechanical analogy of the tendon sheath as springs in the lateral view [XT16, p. 3489]

As demonstrated in Fig. 2.5c, the sheaths of the human hand can be modeled as a series of elastic pulleys. It can be observed that in the case of flexion, the moment arms are lengthened by the tendon sheaths, and thus major gripping forces can be obtained.

Mathematical Model of the Human Finger

In the analysis of the kinematics of the hand, a mathematical approximation by assuming that the joints are ideal and connected by simple line segments [BA92] is usually used. Hence, it is possible to model the system as a rigid-body model. Each interphalangeal joint forms a hinge joint, only being able to perform flexion and extension. Thus, they have one DOF. Birglen et al. [BLG08]'s model is also such a rigid-body model. Their framework was developed to provide a framework the gap between the otherwise rather intuitive development methods or the purely mathematical methods. For enveloping grasps, like the Medium Wrap (see 2.1.3), the framework aims to analyze contact forces of robotic fingers, which offers the possibility to compare the theoretical and the actual build model. However, due to simplicity only the general static model will be described.

A major advantage of analytical approaches is that they significantly reduce the number of iterations in the production of intuitively designed systems [Hus+17].

In the following, the mathematical model will be explained.

As seen in Figure 2.6, the system is driven by the input torque T_a . Using the method of virtual power, one obtains the following equation

$$t^T \omega_a = \sum_{i=1}^n \xi_i \circ \zeta_i, \quad (2.2)$$

including the input torque vector \mathbf{t} , the joint velocity vector ω_a , the twist of the i^{th} contact point ξ_i and the corresponding wrench ζ_i . The operator \circ combines the sum of twists with the according wrenches as the reciprocal product of screws in the plane for example.

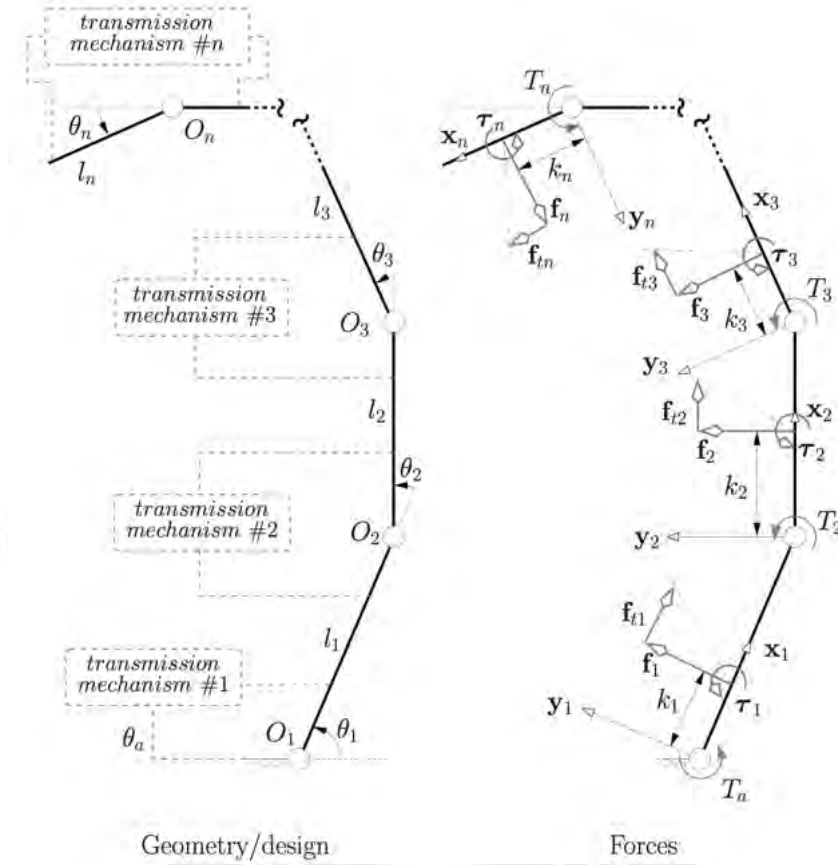


Figure 2.6: Conceptual illustration of an underactuated finger [BLG08]

Each joint of the conceptual model is characterized by a local coordinate system. For the consideration of the finger we use the local coordinate system of the MCP joint x_1, y_1 , the PIP joint x_2, y_2 and the DIP joint x_3, y_3 . However, the model is also valid for n links with the according coordinate system x_n, y_n . The model is limited by the assumption that each phalanx i only has one contact point with the grasped object. In case of the human fingers the number of joints is $n = 3$.

If now the spring stiffnesses K_i are included, the torque vector \mathbf{t} can be expressed as follows.

$$\mathbf{t} = \begin{bmatrix} T_a \\ T_2 = -K_2\Delta\theta_2 \\ T_3 = -K_3\Delta\theta_3 \\ \dots \\ T_n = -K_n\Delta\theta_n \end{bmatrix}, \quad \omega_a = \begin{bmatrix} \dot{\theta}_a \\ \dot{\theta}_2 \\ \dot{\theta}_3 \\ \dots \\ \dot{\theta}_n \end{bmatrix}, \quad (2.3)$$

where T_i is the torque at the i^{th} joint, K_i is the stiffness of the i^{th} spring, $\Delta\theta_i$ is the rotation of the i^{th} joint relative to the entire configuration. The angular velocity ω_i is split into its x and y components v_i^x and v_i^y of the i^{th} phalanx. For the i^{th} phalanx, the tangential forces f_{ti} , f_i and τ_i are notated as seen in Equation 2.4.

$$\xi_i = \begin{bmatrix} \omega_i \\ v_i^x \\ v_i^y \end{bmatrix}, \quad \zeta_i = \begin{bmatrix} f_{ti} \\ f_i \\ \tau_i \end{bmatrix}. \quad (2.4)$$

The twist of the i^{th} contact point ξ_i can be specified as

$$\xi_i = \sum_{k=1}^i \dot{\theta}_k \xi_i^{O_k}. \quad (2.5)$$

$\xi_i^{O_k}$ is the joint twist of the point O_k in relation to C_i , the contact point. The last mentioned can be expressed as

$$\xi_i^{O_k} = \begin{bmatrix} 1 \\ \mathbf{E} \mathbf{r}_{ki} \end{bmatrix} \quad (2.6)$$

because the joints between the phalanges are considered to be of revolute type. The vector r_{ki} is the connection from O_k to the contact point C_i of the i^{th} phalanx. \mathbf{E} represents the matrix of the planar cross product.

$$\mathbf{E} = \begin{bmatrix} 0 & -1 \\ 1 & 0 \end{bmatrix} \quad (2.7)$$

If friction is considered, the edge of the friction cone of the i^{th} phalanx is defined by $f_{ti} = \pm \mu_{i-static} f_i$. $\mu_{i-static}$ is the static coefficient of friction at the i^{th} contact point. Generally $\mathbf{f}_t = \boldsymbol{\mu} \mathbf{f}$ is valid, where

$$\mathbf{f} = \begin{bmatrix} f_1 \\ f_2 \\ \dots \\ f_n \end{bmatrix}, \quad \mathbf{f}_t = \begin{bmatrix} f_{t1} \\ f_{t2} \\ \dots \\ f_{tn} \end{bmatrix} \quad (2.8)$$

and

$$\boldsymbol{\mu} = \begin{bmatrix} \mu_1 & 0 & \dots & 0 \\ 0 & \mu_2 & \dots & 0 \\ \dots & \dots & \dots & \dots \\ 0 & 0 & \dots & \mu_n \end{bmatrix}. \quad (2.9)$$

It is to say, that $\mu_i \neq \mu_{i-static}$ always applies. The relation between \mathbf{f}_t and \mathbf{f} is made by the matrix $\boldsymbol{\mu}$, but both maintain unknown. Analogously, $\boldsymbol{\tau} = \boldsymbol{\eta}\mathbf{f}$ can be written, where

$$\boldsymbol{\tau} = \begin{bmatrix} \tau_1 \\ \tau_2 \\ \dots \\ \tau_n \end{bmatrix} \quad (2.10)$$

and

$$\boldsymbol{\eta} = \begin{bmatrix} \eta_1 & 0 & \dots & 0 \\ 0 & \eta_2 & \dots & 0 \\ \dots & \dots & \dots & \dots \\ 0 & 0 & \dots & \eta_n \end{bmatrix} \quad (2.11)$$

Hence, it is possible to note the wrench ζ_i as

$$\zeta_i = f_i \mathbf{x}_i^* + f_i \mathbf{y}_i^* + \tau_i \mathbf{z}_i^* = f_i (\mathbf{y}_i^* \mu_i \mathbf{x}_i^* + \eta_i \mathbf{z}_i^*) \quad (2.12)$$

where the unit wrench to a pure force along \mathbf{y}_i is $\mathbf{y}_i^* = [\mathbf{y}_i^T \ 0]^T$. Analogously applies $\mathbf{x}_i^* = [\mathbf{x}_i^T \ 0]^T$ and $\mathbf{z}_i^* = [0 \ 0 \ 1]^T$. These approaches lead to

$$\xi_i \circ \zeta_i = \sum_{k=1}^i \dot{\theta}_k \zeta_i^{O_k} \circ f_i (\mathbf{y}_i^* \mu_i \mathbf{x}_i^* + \eta_i \mathbf{z}_i^*) \quad (2.13)$$

$$\xi_i \circ \zeta_i = f_i \left(\sum_{k=1}^i \dot{\theta}_k \mathbf{r}_{ki}^T \mathbf{x}_i - \mu_i \sum_{k=1}^i \dot{\theta}_k \mathbf{r}_{ki} \mathbf{y}_i + \eta_i \sum_{k=1}^i \dot{\theta}_k \right). \quad (2.14)$$

This can be summed up to

$$\mathbf{t}^T \boldsymbol{\omega}_a = \mathbf{f}^T (\mathbf{J} \dot{\boldsymbol{\theta}}) = \mathbf{f}^T (\mathbf{J} \mathbf{T} \boldsymbol{\omega}_a) \quad (2.15)$$

with

$$\mathbf{J} = \mathbf{J}_1 - \boldsymbol{\mu} \mathbf{J}_2 + \boldsymbol{\eta} \mathbf{J}_3 \quad (2.16)$$

The only dependencies of the matrix \mathbf{J} consist in the location of the contact point on the phalanges, the relative orientation of the phalanges and the friction coefficients, whereas \mathbf{T} depends on the transmission mechanism, driving the phalanges. Via the matrix \mathbf{T} the vector $\boldsymbol{\omega}_a$ is made dependent on the time derivatives of the phalanx joint coordinates. Thus one

receives

$$\dot{\boldsymbol{\theta}} = \mathbf{T}\boldsymbol{\omega}_a \quad (2.17)$$

Through the previous Equations ??, the matrices \mathbf{J}_1 , \mathbf{J}_2 and \mathbf{J}_3 can be characterized.

$$\mathbf{J}_1 = \begin{bmatrix} k & 0 & 0 & \dots & 0 \\ \mathbf{r}_{12}^T \mathbf{x}_2 & k_2 & 0 & \dots & 0 \\ \dots & \dots & \dots & \dots & \dots \\ \mathbf{r}_{1n}^T \mathbf{x}_n & \mathbf{r}_{2n}^T \mathbf{x}_n & \mathbf{r}_{3n}^T \mathbf{x}_n & \dots & k_n \end{bmatrix} \quad (2.18)$$

where $\mathbf{r}_{ii}^T \mathbf{x}_i = k_i$ is the distance between the i^{th} joint and the i^{th} contact point. Analogously follows

$$\mathbf{J}_2 = \begin{bmatrix} 0 & 0 & 0 & \dots & 0 \\ \mathbf{r}_{12}^T \mathbf{y}_2 & 0 & \dots & 0 \\ \dots & \dots & \dots & \dots & \dots \\ \mathbf{r}_{1n}^T \mathbf{y}_n & \mathbf{r}_{2n}^T \mathbf{y}_n & \mathbf{r}_{3n}^T \mathbf{y}_n & \dots & 0 \end{bmatrix} \quad (2.19)$$

and

$$\mathbf{J}_3 = \begin{bmatrix} 1 & 0 & 0 & \dots & 0 \\ 1 & 1 & 0 & \dots & 0 \\ \dots & \dots & \dots & \dots & \dots \\ 1 & 1 & 1 & \dots & 1 \end{bmatrix}. \quad (2.20)$$

Finally one obtains

$$\mathbf{J}^T = \begin{bmatrix} k_1 + \eta_1 & \mathbf{r}_{12}^T (\mathbf{x}_2 - \mu_2 \mathbf{y}_2) + \eta_2 & \dots & \dots & \mathbf{r}_{1n}^T (\mathbf{x}_n - \mu_n \mathbf{y}_n) + \eta_n \\ 0 & k_2 + \eta_2 & \dots & \dots & \mathbf{r}_{2n}^T (\mathbf{x}_n - \mu_n \mathbf{y}_n) + \eta_n \\ \cdot & 0 & \dots & \dots & \mathbf{r}_{3n}^T (\mathbf{x}_n - \mu_n \mathbf{y}_n) + \eta_n \\ \dots & \dots & \dots & \dots & \dots \\ 0 & 0 & \dots & 0 & k_n + \eta_n \end{bmatrix}. \quad (2.21)$$

Empirically, it is noticeable that the η_i are often very small, so that they will be neglected from here on. In addition, the coefficient of friction μ_1 does not exist, since this phalanx due to its kinematic constraints cannot slide.

To proceed the framework on has either to determine the matrix \mathbf{T} or this typical matrix of underactuation.

$$\begin{bmatrix} \dot{\theta}_1 \\ \dot{\theta}_2 \\ \dot{\theta}_3 \\ \dots \\ \dot{\theta}_n \end{bmatrix} = \begin{bmatrix} X_1 & X_2 & X_3 & \dots & X_n \\ 0 & 1 & 0 & \dots & 0 \\ 0 & 0 & 1 & \dots & 0 \\ \dots & \dots & \dots & \dots & \dots \\ 0 & 0 & 0 & \dots & 1 \end{bmatrix} \begin{bmatrix} \dot{\theta}_{a1} \\ \dot{\theta}_2 \\ \dot{\theta}_3 \\ \dots \\ \dot{\theta}_n \end{bmatrix} \quad (2.22)$$

With the method of superposition, one receives the generally valid equation

$$\dot{\theta}_{a_{i-1}} = \dot{\theta}_{i-1} x_i \dot{\theta}_{a_i} \quad (2.23)$$

where x_i is the transmission ratio of the i^{th} stage. This equation determines the output velocity of the current stage from the input velocity of the next stage (see Fig. 2.6).

For example, in case of a tendon-driven system, where the transmission ratio is known, the parameters are

$$x_1 = 1 \quad \text{and} \quad x_i = \frac{r_{2i}}{r_{2i-1}}, i > 1. \quad (2.24)$$

Due to the knowledge of the transmission ratio x_i the first line of the matrix \mathbf{T} (X_i (Eq. 2.22) can be stated

$$\begin{cases} X_1 = 1 \\ X_j = -\prod_{i=1}^j, \quad j = 2, \dots, n \end{cases}$$

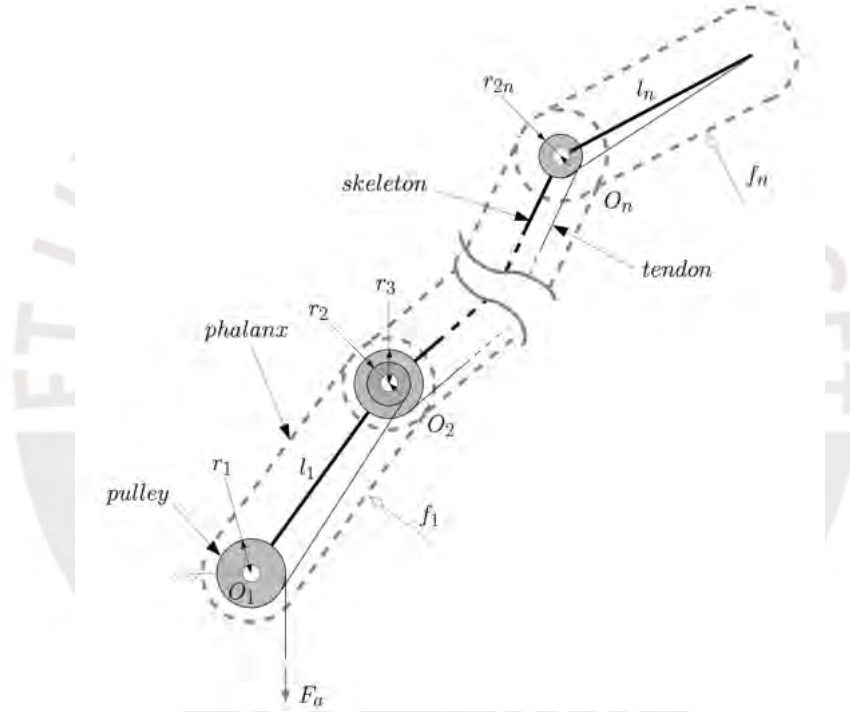


Figure 2.7: Conceptual tendon-driven finger with n phalanges [BLG08]
input force F_a ; pulley radii $r_1, r_2, r_3, \dots, r_{2n}$
, segment length l_1, \dots, l_n

Based on this, one obtains

$$\mathbf{T}^T = \begin{bmatrix} 1 & \mathbf{0}_{n-1}^T \\ -\frac{r_2}{r_1} & \\ -\frac{r_2 r_4}{r_1 r_3} & \\ \dots & \mathbf{1}_{n-1} \\ -\prod_{i=1}^n \frac{r_{2i}}{r_{2i-1}} & \end{bmatrix} \quad (2.25)$$

where r_{2i-1} is the pulley located at the base and r_{2i} is the pulley located at the end of the i^{th} phalanx.

2.1.3 Prehensile Capabilities of the Human Hand

To elect an adequate objective for the realized grasp, it is necessary to study the human grasp types. This part of the work aims to ease the selection of an appropriate type of grasp to be set as goal for the developed gripper according to the requirement to manipulate fragile objects. Furthermore, it is necessary to investigate typical dimensions in human grasps to further specify the design of the gripper.

The human GRASP taxonomy, developed by Feix et al., provides a large, yet compact review of current taxonomies of human prehension [Fei+09]. It differs the grasp types by the three categories *Power*, *Intermediate* and *Precision Grasp*, subclassifying each category by the position of the thumb as *abducted* or *adducted* (see Fig. 2.8). The study includes the taxonomies of Cutkosky [Cut89], and Kapandji [Kap74] and places them into a new taxonomy called the GRASP taxonomy. Due to their meticulous procedure, which sums up around 30 grasp types, their terminology shall be used in this work.

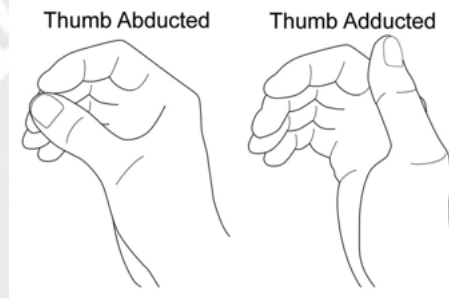


Figure 2.8: Abducted and adducted position of the thumb [Fei+16, p. 69]

The majority of grasps is characterized by an opposed, abducted position of the thumb in relation to the four other digits. Factually, this makes the thumb the most relevant digit of the human hand [FBD14, p. 74]. Feix et al. demonstrated that the thumb is used in 32, the index finger in 33 and the middle finger in 28 types of the grasps, occurring in their GRASP taxonomy.

Depending on the number of involved real fingers, the functional units of those form a so-called *virtual finger (VF)* during manipulation, a concept which has been introduced by Arbib et al. [AIL85] in 1985. This functional unit is determined by the direction of the applied force (see Fig. 2.9) [Ibe87, p. 1154]. For example, the so-called *Palmar Pinch* (Fig. 2.9a), the *Medium Wrap* (Fig. 2.9b) and the *Lateral* (Fig. 2.9c) consist in two VF. In the context of robotic manipulation this units can be controlled individually.

Referring to the main objective, the manipulation of fragile objects, the review of the GRASP taxonomy of human grasps by Feix et al. leads to the *Precision Grasps* [Fei+16]. This class of grasps is also characterized by a mostly abducted thumb (see Fig. 2.8) and uses at least two VF (see GRASP Taxonomy [Fei+16]). Another characteristic for most of the *Precision*

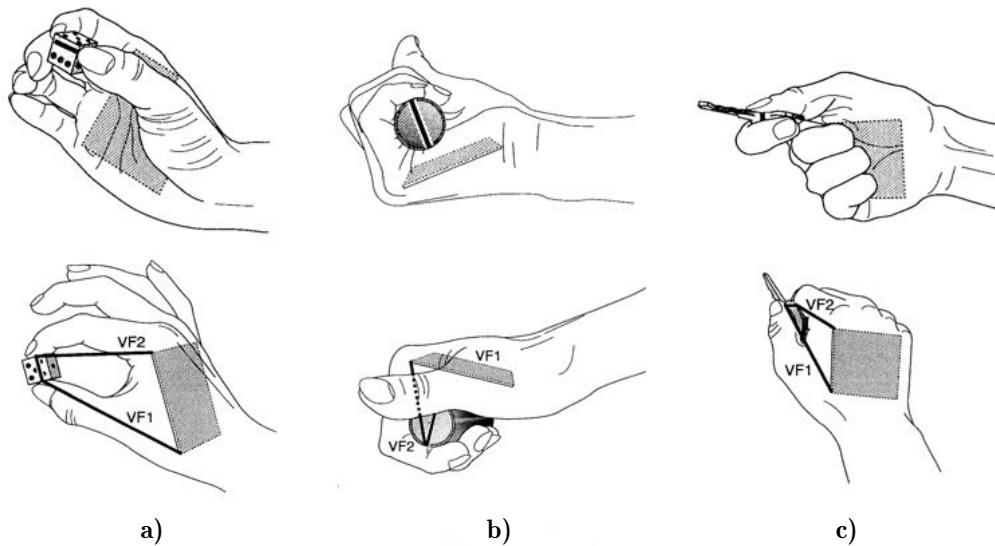


Figure 2.9: Comparison of the opposition types of the human grasping and the respective integration of two Virtual Finger, modified from [MI94, p. 32]

- a) Pad opposition, parallel to the palm, *Palmar Pinch*
- b) Palm opposition, perpendicular to the palm, *Medium Wrap*
- c) Side opposition, transverse to the palm, *Lateral*

Grasps is the *Pad Opposition* (see Fig. 2.9a). The pad opposition “occurs between hand surfaces along a direction generally parallel to the palm” [MI94, p. 31]. The opposition type is another criteria for the taxonomy of grasps, as there are also *Palm* (see Fig. 2.9b) and *Side Opposition* (see Fig. 2.9c), which are not looked into further, due to the focus on *Precision Grasps*.

An earlier study by Feix et al. yielded the perception, that statistically, the *Medium Wrap* (Fig. 2.9b) is the most commonly used grasp type, followed by the *Lateral* (Fig. 2.9c) and the *Thumb-2 Finger Grasp* (Fig. 2.11) (hereafter called *Prismatic 2 Finger* [Fei+16]) (see Fig. 2.10). It should be mentioned that the study is limited to the analysis of grasps by two housekeepers and machinists, who executed almost 10 000 grasp instances.

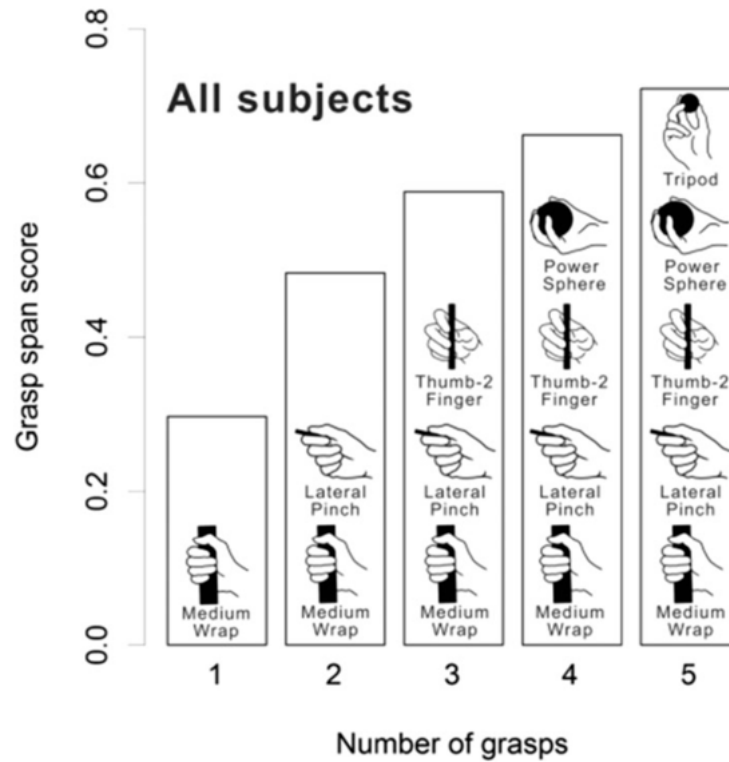


Figure 2.10: Results of the grasp span analysis, representing a smaller subset of grasp types, that can be used to grasp most objects [FBD14, p. 320]

According to the study by Feix et al., the *Prismatic 2 Finger Grasp* is one of the most important grasps for the manipulation of small, lightweight objects. Besides the geometrical advantages of a median grasp size of 1 cm, this grip fits well to the goal of lifting at least 20 g (see Sec. A.3.1) as a subordinated objective of this work [FBD14]. In addition to this, Kapandji stated that *tridigital grips* are the most popular grips. They use the thumb, index and middle finger [Kap74, p. 258]. Figure 2.11 demonstrates such a grasp, known as the *Tripod Grip*. Even though there are three real fingers involved in the *Tripod Grip*, the results by Baud-Bovy et al. suggest that this case can be seen as a two VF grip [BBS01, p. 615].



Figure 2.11: Tridigital prehension with 2 VF, modified from [Kap74, p. 259]

These perceptions regarding the use of certain types of grasps for the manipulation of small and fragile objects show that the *Prismatic 2 Finger Grasp* and the *Tripod Grip* are the best grasps to meet these requirements. This is further supported by the study of Townsend, who identified that a typical robotic gripper uses less than five fingers with three phalanges per finger [Tow00]. Hence, this work's approach is to develop a gripper with three fingers with three phalanges each. Although the use of two fingers, respectively two VF would be

enough, the third finger permits more possibilities in grasping.

Due to simplicity, only the mechanics of the index finger will be described in the following part.

2.1.4 Synergies in Human Grasping

The term “postural synergy” comes from neuroscience and signifies a high level mechanism that governs the manner in which the hand is shaped to grasp objects. Which in this case means that the brain does not command the hand joint per joint, but through few input variables, for example the synergies that generate coordinated movements of the fingers. The exceptional grasping capabilities of the hand are achieved partially through these same synergies. Santello et al. suggested that few postural synergies explain most of the variance in hand grasping configurations by accomplishing a principle components analysis (PCA). In the context of technical realization, synergies offer possibilities to overcome the complexity of the human hand without having to accept big limitations in dexterity [SFS98; Che+20]. Indeed, the PCA revealed that more than 80% of the hand posture information can be described with two scalar values [BA07] (see Fig. 2.12). Mathematically, the synergies suggest that a joint configuration vector q can be described by fewer elements, gathered in the synergy vector $\sigma \in \mathbb{R}^s$, as $q = q(\sigma)$ [Gab+11]. However, the results by Santello et al. and subsequent studies were discussed because they might have been a mere byproduct of anatomical factors. A transcranial magnetic stimulation revealed the same synergies occur in the neuronal domain [GC06], which strengthened the theory of functional synergies in human grasping.

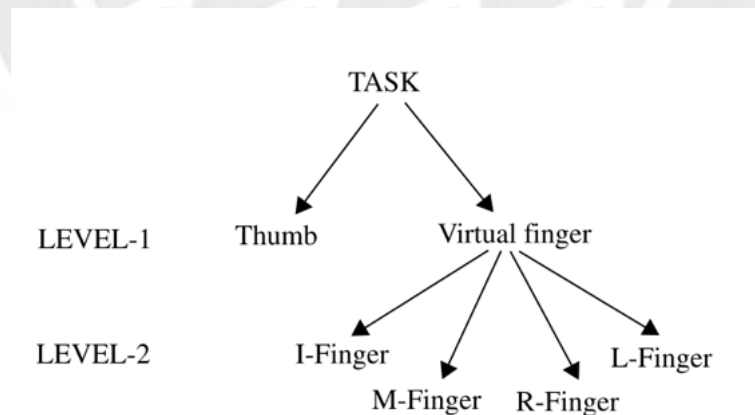


Figure 2.12: Two-level hierarchy of prehensile control, including the concept of VF [Lat08, p. 208]

Due to an analysis of the force direction of each individual finger in comparison to the direction of the total force showing minor deviation, Latash suggests that multi-finger synergies stabilize the direction of force produced by the VF [Lat08]. Further studies [Ing+08] expanding to a non-laboratory environment and using advanced measurement parameters have shown the following: The thumb is the most independent digit and the index finger is

the most independent finger of the human hand, even while the other corresponding fingers move synchronously. The study demonstrated that the first principle components (PC) reflect the actuation of the extension and flexion of the DIP, PIP and MCP joints of the four fingers. In addition, it was observed that PIP and DIP joints are more finely articulated than the MCP joint. At last, the adduction-abduction movement is independent from the flexion-extension movement. Those three perceptions form the most important biomechanical characteristics for this work. As consequence, there is a need for three transmission modules [Che+20].

In conclusion with the previous findings, namely that the *Tripod Grip* and the *Prismatic 2 Finger* are most significant for the manipulation of small, fragile objects, it can thus be concluded that for these grasps that have 2 VF two actuators are sufficient.

2.2 Soft Robotic Materials

In order to achieve efficient grasping, it is necessary to maintain the relation between the applied force and the reaction (e.g. when lifting an object against gravity without supporting it against gravity from below). Hence, the friction at the contact points and the form closure are really important. Generally speaking there are three main issues in multifingered robotic grasping: impact forces can vary if the fingers are not driven equally, rigid fingers are not able to grasp objects with uneven surfaces properly and rigid systems suffer more from usage because of the not existing attenuation [SG96]. To overcome those problems the use of soft finger pads made of silicon or resin casting of flexible urethanes has been introduced [Zis+14; MOD13]. Other studies use flexible joints of polyurethane to enhance the adaptability of the fingers. These flexible joints also have the advantage of withstanding many repeated movements and impacts. Furthermore, they also dampen vibrations [Hus+17].

2.3 Mechanical Fundamentals

This part of the work is intended to give an overview of the mechanical fundamentals on which the work is based.

At first the theory of underactuation will be described (Sec. 2.3.1), followed by a brief summary of commonly used differential mechanisms in robotic grippers (2.3.2). After that, the basics of contact point mechanics (Sec. 2.3.3) are explained. The last part is focussed on the fundamentals of compliant mechanisms (Sec. 2.3.4).

2.3.1 Underactuation

Due to the complex morphology of the human hand, a lot of robotic grippers have been designed with less fingers and even less motors, which results in coupling various DOFs to one actuator [Mas18]. Such a mechanical system can be seen as underactuated once the number of degrees of freedom is higher than the number of actuators [Shi+18, p. 1]. The adaptivity of grasps benefits highly from underactuation because the fingers of the grippers adapt to the shape of the object they grip. This also simplifies the control of the gripper. Mathematically, the following equation by Grübler determines the DOF [Vol78, p. 41]:

$$F = b(n - 1) - \sum_{i=1}^g (b - f) \quad (2.26)$$

In the plane view of a finger the following equation applies.

$$F = 3(n - 1) - 2g_1 - g_2 \quad (2.27)$$

Where n is the number of gear links, g_1 is the number of joints with one DOF and g_2 is the number of joints with two DOFs.

2.3.2 Differential Mechanism

The concept of underactuation, i.e. a system with fewer actuators than the degree of freedom, requires a uniform force distribution. The reason for this is the intrinsic adaptivity of sub-actuation. This manifests itself in the fact that fingers that are not yet blocked continue to move when others are already blocked. Thus, irregularly shaped objects can be grasped [BG06]. Differential mechanisms are used to achieve such an even distribution of forces on the fingers. In general, the objective of the analysis of the mechanism is to derive a function

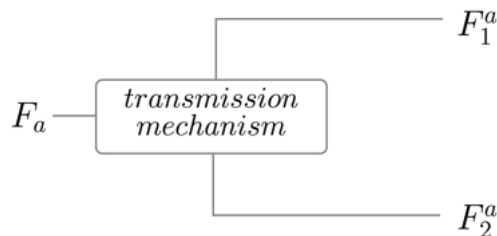


Figure 2.13: Transmission mechanism with two outputs in an underactuated system [BLG08, p. 141]. Input force F_a , two output forces respectively F_1^a and F_2^a .

of the input forces in relation to the actuation forces to the output. This function is

$$\mathbf{F} = \mathbf{T}^f \mathbf{t}^\circ \quad (2.28)$$

with

$$\mathbf{F} = \begin{bmatrix} F_1^a \\ F_2^a \end{bmatrix} \quad \mathbf{t}^\diamond = \begin{bmatrix} F_1^a \\ F_2^a \end{bmatrix}. \quad (2.29)$$

A differential mechanism is a “mechanism for which the degree of freedom is two and which may accept two inputs to produce one output or, may resolve a single input into two outputs” [Boe+91]. In the context of grasping the most commonly used differential mechanisms are the following three types: pulley differentials, linkage seesaw differentials (also known as whiffle-/whiffletree mechanisms) and gear differentials.

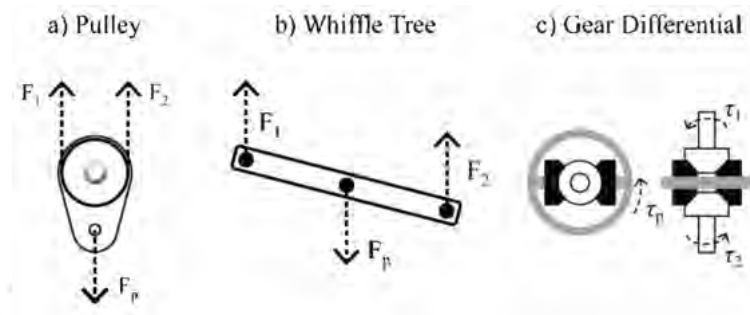


Figure 2.14: Commonly used differential mechanisms in robotic grasping [MOD13]
 a) pulley differential, b) linkage seesaw differential, c) gear differential

Due to the easier assembly and integration only the seesaw mechanism will be looked into further.

Based on a structure as shown in Figure 2.15, the transmission matrix can be written as

$$\mathbf{T}^f = \frac{1}{c} \begin{bmatrix} b_2 & \sin \alpha_2 \\ b_1 & -\sin \alpha_1 \end{bmatrix} \quad (2.30)$$

where c is the sum of the corresponding distances from the axis of the prismatic joint to A_1 and A_2 , i.e.,

$$c = b_1 \sin \alpha_2 + b_2 \sin \alpha_1 \quad (2.31)$$

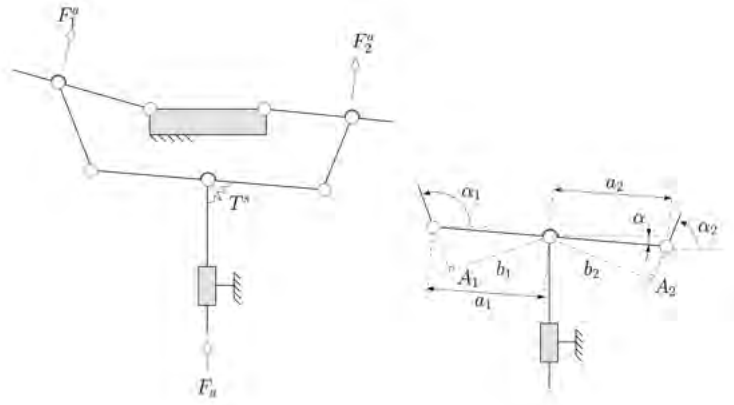


Figure 2.15: Seesaw mechanism

Floating pulley transmission for equalizing the force transmission [MOD13].

2.3.3 Contact Points

Following the definition of Murray et al., “a contact is described by a mapping between forces exerted by a finger at a point on the object and the resultant wrenches in some object reference frame” [MLS94, p. 256]. They suggested the use of a *soft-finger model* to obtain a more realistic contact model.

The *soft-finger model* not only allows forces, but also torques about the surface’s normal. Those torques are limited to achieve more simplicity in the model.

Contacts can be modeled as a force applied at a point on the object together with a moment along the normal of the contact surface. According to this model, four parameters are needed to describe each contact.

Table 2.3: Static friction coefficients for some common materials [HLB16]

Material 1	Material 2	Conditions	μ
Nylon	Nylon	Dry	0.2
Nylon	Steel	Dry	0.4
Polyethylene	Polyethylene	Dry	0.2
Polyethylene	Steel	Dry	0.2

Requirements on material

- attenuation of impact forces
- conformability
- strain dissipation

2.3.4 Compliant Mechanisms

The sector of human-mimetic robotics is advancing more and more and outperforms traditional robots by the use of biological mimicry of the human hand for example. Compliant mechanisms help to mimic, for example, the ligaments of the fingers.

Compliant mechanisms are characterized by their ability to deform under external loading due to intrinsic compliance, distributed or concentrated. A distributed compliance is present as soon as the length of the compliant area is ten times smaller than the length of the body or the system ($L/l \geq 10^1$), otherwise it is called a concentrated compliance ($L/l < 10^1$) [Zen14]. Figure 2.16 visualizes the difference between the two types. If there is compliance

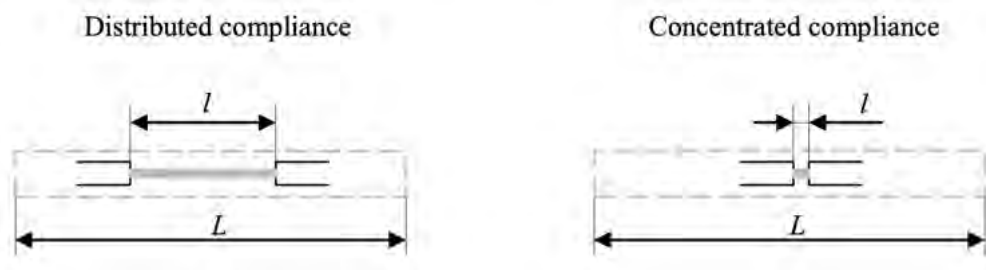


Figure 2.16: Schematic illustration of the difference between distributed and concentrated compliance [ZL19, p. 4]

in a system, it can be divided into the following categories: variable compliance, which is further divided into reversible and irreversible compliance, and constant compliance. Usually, technical rigid-body and compliant systems are equipped with constant compliance [Zen14]. Depending on whether a compliant mechanism moves as a function of a rigid body joint and a compliant joint or only a compliant joint, it is called a partially or fully compliant mechanism. This categories can be extended with the former definition of thy type of compliance. As an example, the human finger (see Sec. 2.1) can be described as a fully compliant mechanism with concentrated compliance. The synovial joints of the DIP and PIP joint have one DOF each, while the MCP joint has two DOFs. In the context of compliant mechanism, their mechanical behavior can be emulated by notch flexure hinges with only rotational movements (see Fig. 2.17).

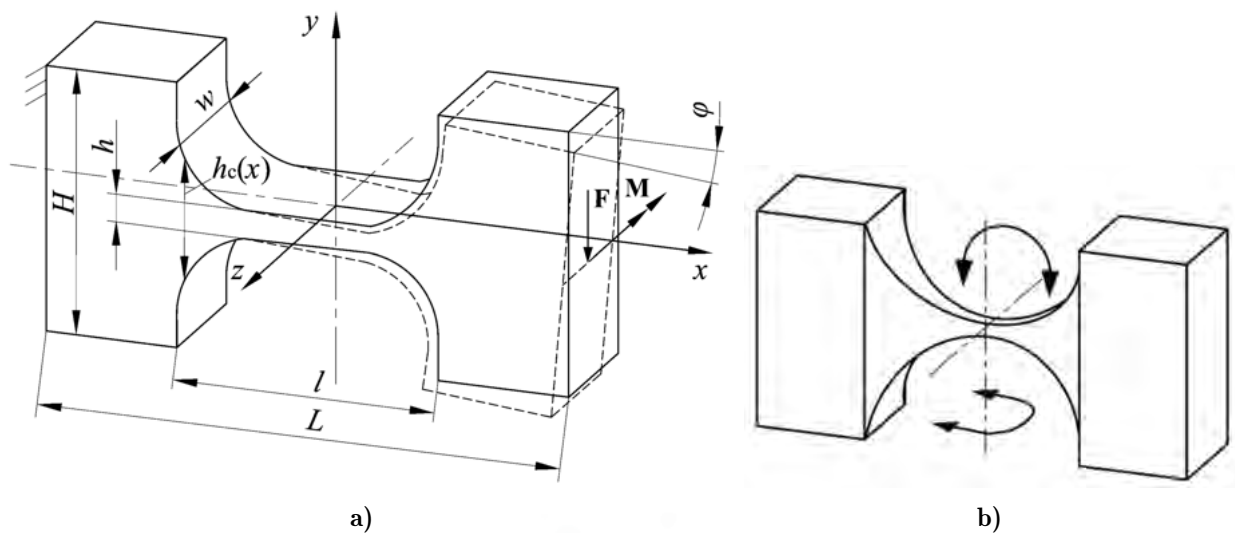


Figure 2.17: Possible geometries of flexure hinges to realize one DOF, respectively two DOFs [ZL19]

- a) Flexure hinge with 1 DOF with its geometric parameters, deflected by φ by a load F, M
 b) Flexure hinge with 2 DOFs

As seen in Figure 2.17a, the properties of the notch flexure hinges are defined by the following two groups:

- the basic hinge/link dimensions l, L, h, H, w, W ,
- the hinge contour height function $h_c(x)$ (Eq. 2.32).

Given by the chosen notch geometry, the most important characteristics of the hinge contour height function $h_c(x)$ are its symmetry and that minimum of h_c is at the mid-point and that the hinge cross-section is rectangular [ZL19].

$$h_c(x) = h + \frac{H-h}{\left(\frac{l}{2}\right)^n} |x|^n, n \in \mathbb{R}, 1.1. \leq n \leq 50 \quad (2.32)$$

Based on these notch flexure hinges, the *rigid-body replacement* approach will be exerted later (Sec. 3.2.2). This approach consists in four basic steps:

- synthesis of a suitable rigid-body mechanism;
- replacement of the hinges and basic design of the compliant mechanism
- goal-oriented, specific geometric design of the flexure hinges and
- verification of results and proof of requirements.

2.4 Sensory Systems

In the following section, various sensors which can be used in position control and for determination of the applied force to achieve force control in the developed gripper will be

discussed. To this, there will be a brief overview on flex/bend sensors (Sec. 2.4.2), force sensing resistors (FSRs) (Sec. 2.4.1) and current sensors (Sec. 2.4.3).

2.4.1 Force-sensing Resistors

FSRs [YP97] are thermally stable devices, which change their electrical resistance according to an applied force or pressure. The most basic configuration consists of two membranes separated by a spacer, which builds an air gap (see Fig. 2.18). The upper membrane is coated with carbon-based ink. When the sensor is now pressed, the conductive ink completes a

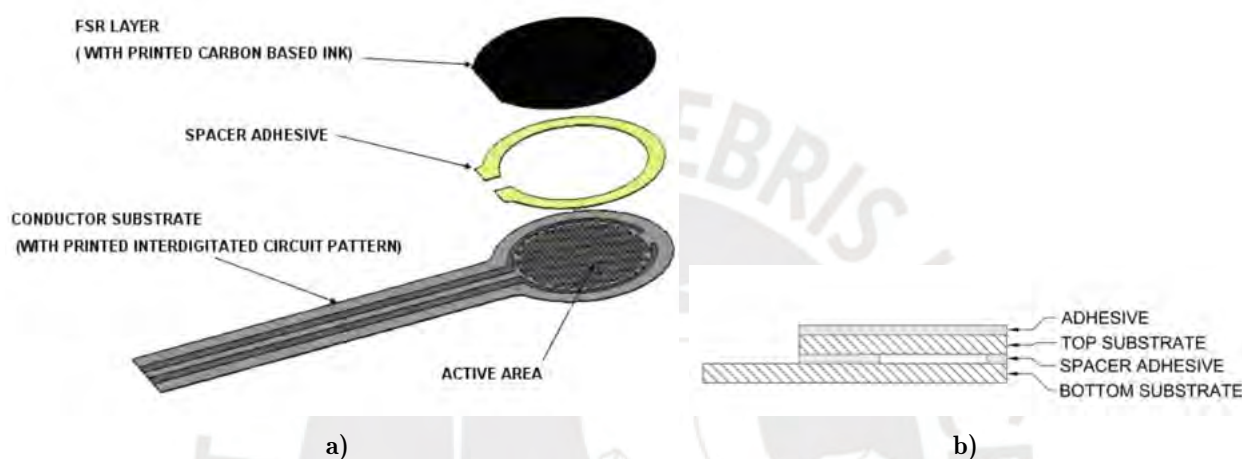


Figure 2.18: Basic construction of a FSR, from [Int16]

- a) Composition of conductive ink layer, spacer and conductor substrate with active area
- b) Layer stack-up

specific circuit with the lower membrane. This lower membrane has two sets of interdigitated fingers that are electrically distinct, respectively insulated from each other. Depending on the amount of pressure, the number of shorted traces varies, thus the electrical resistance of the sensor changes as well.

$$V_{out} = \frac{R_M V_{cc}}{R_M + R_{FSR}} \quad (2.33)$$

A voltage divider (see Fig 2.19a) can be used to relate the applied force to the output voltage V_{out} . This circuit consists of the measuring resistance R_M and the resistance of the FSR R_{FSR} (see Eq. 2.33). Another option to convert the read value is using a circuit, made of a resistor and a capacitor, called RC-circuit (see 2.19b). This principle uses the basic electronic property of resistors and capacitors where the time t_{RC} for charging is measured.

At the beginning, the capacitor is empty, but when a voltage is applied, the capacitor C is charged as a function of the ohmic resistor R . If the capacitor was uncharged at time $t = 0$,

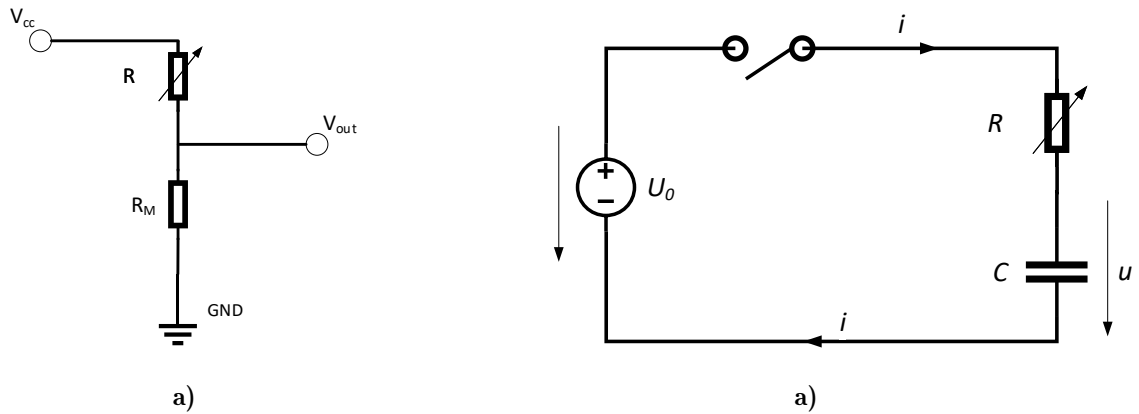


Figure 2.19: Basic Circuits for conversion of data with variable resistors

- a) Voltage Divider with supply voltage V_{cc} , variable resistance R , reference resistor R_M and output voltage V_{out}
 b) RC-circuit with voltage source U_0 , current i , variable resistance R , capacitance C and output voltage u

then $u(0) = 0$ is valid for the capacitance model and the relation can be expressed as the following equation (Eq. 2.34) for small time periods [MR17].

$$u(t) \approx \frac{U_0}{RC}t \quad (2.34)$$

Where the time constant is $RC =: \tau$.

However there are more complex ways to convert the analog value, such as an operational amplifier circuit or a Wheatstone bridge [BLG08].

This sensor offers a good shock resistance, small size, light weight and is economic, yet the accuracy suffers [Int16]. Apart from force-sensing resistors, there are also force-sensing capacitors, however they are not looked into further due to simplicity.

2.4.2 Flex Sensors

Flex or bend sensors are used in a wide range of applications. The best publicly known is probably the “Power Glove” from Mattel (El Segundo, CA, USA) for the Nintendo Entertainment System (Nintendo Co. Ltd., Kyoto, Japan). Besides from this commercial product, the flex sensors are also commonly used in the development of goniometric gloves for the analysis of the hand’s kinematics (e.g. Sigma Glove (Sheffield University)).

The measuring principle of flex sensors initially was based on optical flex sensors [Zim82], which were later joined by capacitive flex sensors [NR97] and sensors with conductive ink [Lan96]. While the sensor is stuck to a surface or within a mechanism, the amount of deflection or bending is detected.

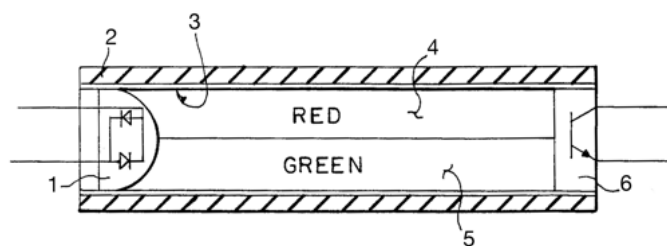


Figure 2.20: Schematic drawing of an optical flex sensor, adapted from [Zim82]
 1 Light source; 2 flexible tube; 3 reflective interior wall;
 4, 5 two different color areas; 6 photosensitive detector

Optical flex sensors [Zim82] are made of a flexible tube with a reflective inner wall. The measurement of deflection is achieved by detecting the direct transmitted and reflected light rays (4, 5) with a photosensitive detector (6) opposed to the light source (1) at the other end of the tube. The photosensitive detector changes its electrical resistance according to the light intensity.

Capacitive flex sensors [NR97] consist of two conductive layers with a comb-patterned structure (1, 2) fixed to an insulating base layer (3, 4) separated by dielectric material. The base layer usually is made of plastic because it is economic, flexible and easy to fabric. All layers are bonded together. The capacitive flex sensor is able to detect deflection in both

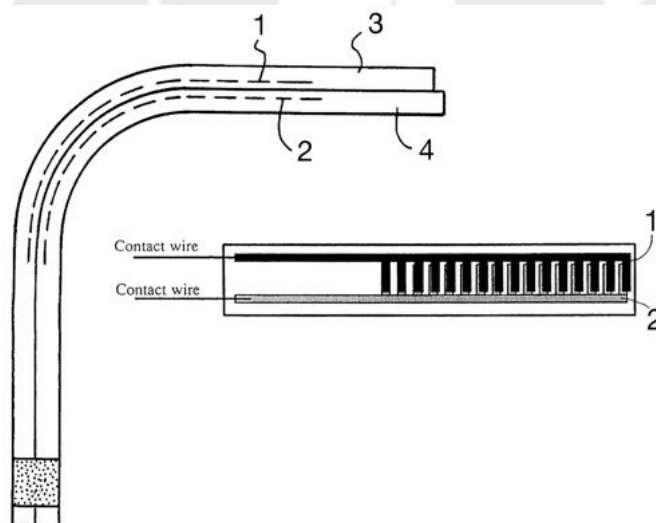


Figure 2.21: Schematic drawing of a capacitive bend-angle sensor, adapted from [NR97]
 1, 2 Conductive electrodes; 3, 4 insulating base layer

directions [NR97]. The measuring principle persists of the change of capacitance between the two conductive layers, which differs when the sensor experiences flexion/extension. To determine the bending, the capacitive sensor is operated with an oscillator whose frequency is proportional to the characteristic capacitance C of the sensor. The output signal can be converted into an analog or digital signal by the use of a frequency-to-voltage converter.

Conductive ink based sensors [Lan96] are formed by a phenolic resin substrate (2) with conductive ink (3), which has segmented conductors (1) mounted on top (see Fig. 2.22a).

The sensor works as a flexible potentiometer, given that the conductive ink changes its electrical resistance when it is bended. This change in resistance is due to cracks in the graphene of the ink. The segmented conductors are used to control the conductivity of the sensor element by varying their size.

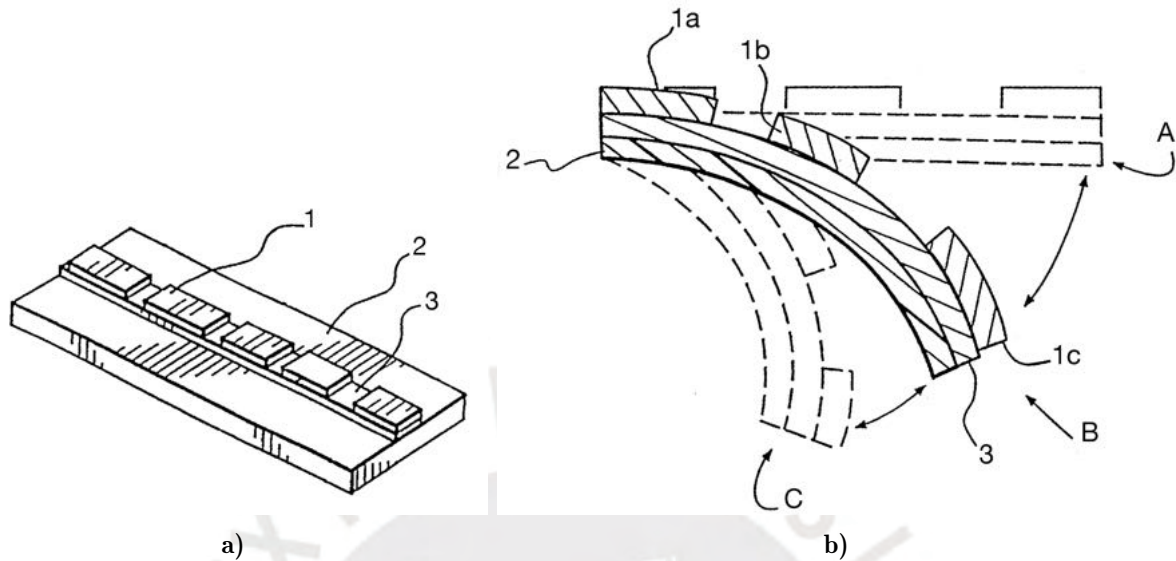


Figure 2.22: Schematic drawing of a conductive ink based flex sensor, adapted from [Lan96]
1a,b,c Segmented conductor; **2** phenolic resin substrate; **3** deposited conductive ink; **A** non-deflected configuration; **B** bent configuration; **C** further bent configuration

Due to the changing electrical resistance, the conductive ink based flex sensors can be simplified as a potentiometer depending on the deflection of the sensor. For a simple force-to-voltage conversion, a voltage divider (Fig. 2.19a) can be attached to the circuit. The following equation (Eq. 2.35) describes the output voltage V_{out} , where R_M is the measuring resistance, which is chosen to configure the force sensitivity range. V_{cc} is the alimentation voltage and R_{flex} is the resistance of the entire flex sensor.

$$V_{out} = \frac{R_M V_{cc}}{R_M + R_{flex}} \quad (2.35)$$

Another way to convert the analog value of flex sensors is a RC-circuit (see 2.4.1).

In conclusion, flex sensors offer good repeatability with adequate accuracy [SN17]. In addition, the sensors are cost-effective and easy to implement.

2.4.3 Current Sensors

To track the power consumption of electric devices, especially motors, current sensors form an economic and simple solution. Due to the use of only low-voltage components, only according measuring principles are discussed. Direct current (DC) can be sensed via shunt resistors, copper trace, Hall Effect, Fluxgate, AMR Effect, Core-less open-loop or Fiber-Optic current

sensors [Zie+09]. In comparison with the other sensors, the Hall effect sensors provide a sensing solution with “low losses, galvanic isolation, high bandwidth and good accuracy” [Zie+09]. Due to the simple integration and the good availability by numerous products for the Arduino/Microcontroller sector, only the Hall-effect Sensor will be described further. Among all magnetic field sensors, the Hall-effect sensors are one of the most commonly used.

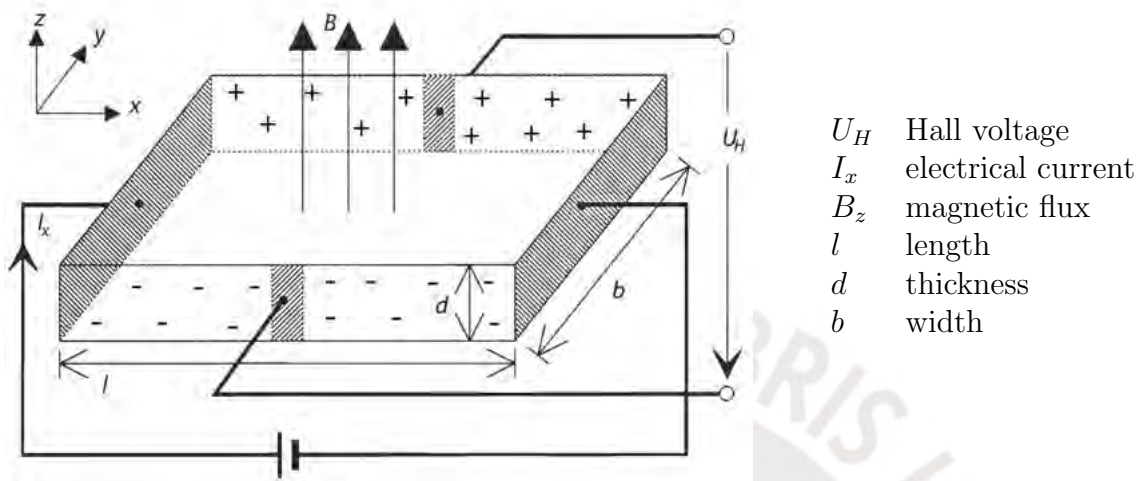


Figure 2.23: Schematic illustration of the Hall-effect, modified from [Pau+14]

The measurement principle is based on the Hall effect, which describes that the Hall voltage U_H occurs when a current I_x flows through a rod-shaped probe of conductive material with the dimensions l , d and b . This effect belongs to the galvanomagnetic effects which occur when a magnetic field has a component perpendicular to the current direction (see Fig. 2.23) [Her18]. Due to the Lorentz law and the corresponding Lorentz force F_L (Eq. 2.36) each current carrier experiences a force by the magnetic field B_z , which can be expressed as the following equation.

$$F_L = -qv_x B_z \vec{e}_y \quad (2.36)$$

(q : electrical charge carrier; v_x : velocity of the charge carrier)

The Lorentz force shifts the charge carriers in the y -direction. As figure 2.23 shows, in this case there is an electron surplus ($-$ charges) at the front of the probe and an electron deficiency ($+$ charges) at the back (see Fig. 2.23). The corresponding magnitude of potential difference is called Hall voltage U_H . Equation 2.37 describes the proportional relationship of the Hall voltage U_H to the magnetic field B_z .

$$U_H = \frac{I_x B_z}{nqd} \quad (2.37)$$

Due to the advances in integrated circuit (IC), it is possible to implement sensors with this measuring principle in a economic and highly-integrated way.

2.5 Control Systems

Controllers automatically influence the physical variables in a technical system. Through the controller disturbances are mostly compensated, thus the system is kept at a defined point. In case of the use of FSRs Birglen et al. [BLG08] suggest the use of Fuzzy Control like seen in Figure 2.24. However, it is to mention that their approach to prevent slippage be the use

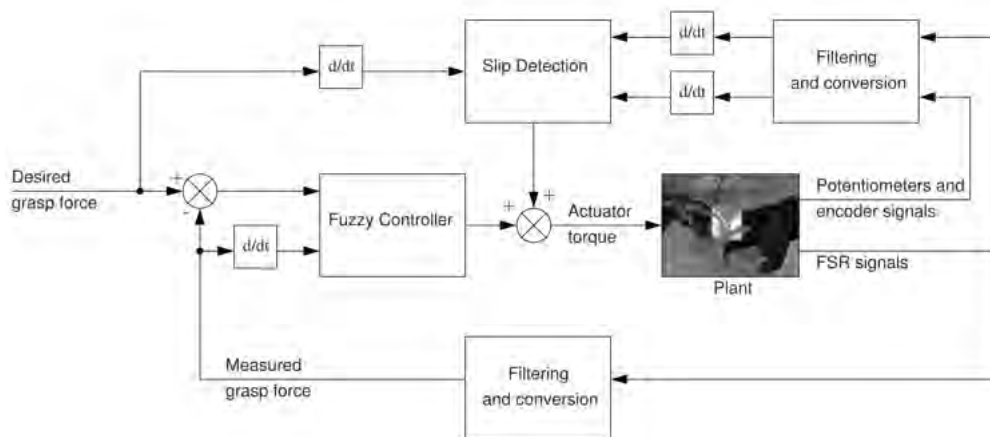


Figure 2.24: Fuzzy control scheme to control a robotic hand with FSRs [BLG08]

of fuzzy control was too slow.

2.6 State of the Art - Tendon-driven Soft Robotic Grippers

The following chapter is intended to inform about the current state of the art in research and development of tendon-driven Soft Robotic grippers. To give a more comprehensive overview, the commonly used actuation principles apart from tendon-based designs are presented, followed by a more detailed view on the state of the art tendon-driven, anthropomorphic grippers.

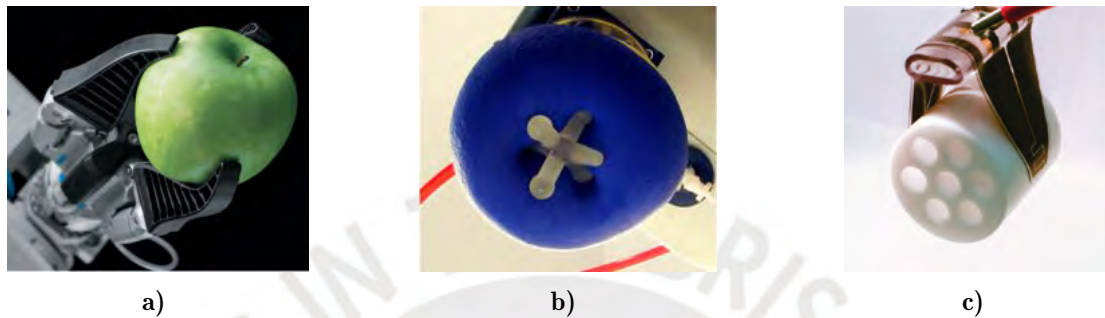


Figure 2.25: Examples for Soft Robotic grippers

- a) *Actuation:* Fin Ray[®] Gripper [Fes13]
- b) *Controlled Stiffness:* Jamming-based gripper picking up an object [Bro+]
- c) *Controlled Adhesion:* Electro-adhesion based Gripper [Shi+16]

The grasping technologies in the field of Soft Robotics are widely distributed. In general, they can be divided into the three main categories of *Actuation*, *Controlled Stiffness* and *Controlled Adhesion*. Table 2.4 provides references to scientific work on the respective categories.

Table 2.4: Examples for the different categories of grasping technologies, adapted from [Shi+18]

Category	Technology	Examples
Actuation	Passive structure with external motors (Fig. 2.25a)	[Fes13; MD17; XDM11; KLV19]
	Fluidic elastomer actuator (FEA)	[DB14; Taw+19]
	Shape memory alloy (SMA)	[Wan+17]
Controlled Stiffness	Granular jamming (Fig. 2.25b)	[Bro+]
	Low melting point alloy (LMPA)	[Nak+02]
	Electro-rheological (ER) and magneto-rheological (MR) fluids	[Pet+10]
Controlled Adhesion	Electro-adhesion (Fig. 2.25c)	[Shi+16]
	Geckoadhesion	[Men+12]

The considered classification of gripping technologies can be further divided in terms of suitability for specific object geometries (see Fig. A.6). The analysis of this classification shows that gripping by *Actuation* and *Controlled Stiffness* is best suited for convex object geometries, while *Controlled Adhesions* performs better with deformable objects. For non-convex geometries, *Controlled Stiffness* has small advantages to *Actuation* [Shi+18].

Due to the fact that the focus of this work is in the area of tendon-operated grippers, which belong to the *Actuation* category, only associated ones will be considered in more detail in the following.

Remarkable tendon-driven, human-inspired gripper have been invested intensively over the last years. Their advantage is the ability to mimic the human hand with the help of stiff and elastic parts. Their anthropomorphic design, a so-called tensegrity structure is commonly used together with tendon-driven grippers. As described before, the human hand offers a technically unprecedented dexterity (see Sec. 2.1). Xu et al. developed such an anthropomorphic gripper [XT16]. The complexity of their design even enables to cover various grasps of the aforementioned taxonomy (see Sec. 2.1.3). It should be said that they compared the realized grasps with the ones in Cutkosky’s taxonomy [Cut89], revised and newly integrated in the taxonomy used in this work by Feix et al. [Fei+16]. Hence, in terms of the GRASP Taxonomy, the robotic hand is able to perform the following *Precision Grasps*, relevant for this work. For circular objects there are the Precision Disk (PreD), Precision Sphere (PreS), Tripod (TP) grasps, while the hand can realize the Prismatic 2 Finger (P2F), Tip Pinch (TIP) and Palmar Pinch (PP) grasps for prismatic objects (see Fig. A.7).



Figure 2.26: Biomimetic hand by Xu et al. Anthropomorphic design, driven by 10 servo motors [XT16]

Their biomimetic hand consists of five digits that are driven by a total of ten servo motors. This complex construction results in a total weight of 942 g. The most remarkable feature of the gripper is its high level of anthropomorphism. Based on laser/MRI scans, they 3D-printed the bones and completed the structure by adding laser-cut extensor hoods with intrinsic muscles, tendon sheaths, tendons and ligaments. To actuate their hand, they use three actuators for the thumb, two servos for the flexion and extension of the ring and little finger and finally, two motors each for the index and middle finger to realize flexion and extension.

Another example for a tendon-driven robotic hand is presented by Chen et al. [Che+20]. They introduced the “Synergy-Inspired Three-Fingered Hand”, which intends to overcome the complexity of human grasping by the use of hand synergies (see Sec. 2.1.4) in form of a compliant and underactuated mechanism. Their design implements three fingers, each driven by one servo motor. The speciality of this design consists in the use of a differential mechanism enabling adduction/abduction of the three finger. Their preliminary results show that the grasping ability of their hand is in no way inferior to anthropomorphic grippers they mentioned in their paper ([BA07; Xu+14; Xio+16; CXY15]). According to the execution of the Anthropomorphic Hand Assessment Protocol (AHAP) [LH+19], their hand provides enough functionality to show human-like grasping ability. The AHAP quantifies the grasping ability and anthropomorphism of artificial hands and helps to evaluate different designs (see Sec. 5.2).



Figure 2.27: Grasping demonstration of the “Synergy-based Three-Fingered Hand” by Chen et al., integrated into the GRASP Taxonomy [Fei+16], modified from [Che+20] Precision Sphere (PreS); Tripod (TP); Lateral (L); Parallel Extension (PE); Fixed Hook (FH); Palmar Pinch (PP); Medium Wrap (MW); Large Diameter (LD). Two non-grasping postures: IP (index pointing/pressing); P (platform)

In the context of the grasp taxonomy by Feix et al., this robotic hand is able to perform at least eight grasp types: Precision Sphere, Tripod, Lateral, Parallel Extension, Fixed Hook, Palmar Pinch, Medium Wrap and Large Diameter.

While the “Synergy-based Three-Fingered Hand” is already less anthropomorphic than the first mentioned “Biomimetic Robotic Hand”, the robotic gripper developed by the Yale Open-Hand Project [Yal] (Yale University, New Haven, CT, USA) focusses even more on functionality. Over the years they developed the Model M² [MSD16], Model O [Odh+14], Model T42 [OMD13], Model T [DH10; MOD13], Model VF [SCD18] and Model Q [MD14].

In this work, only the Model M², Model T42 and the Model O, which is an open-source

derivative of the iRobot-Harvard-Yale (iHY) hand [Odh+14], and the commercially available Reflex Hand (RightHand Robotics, Somerville, MA, USA) will be described further, as they give a good overview of the typical characteristics of robotic grippers with increasing complexity.

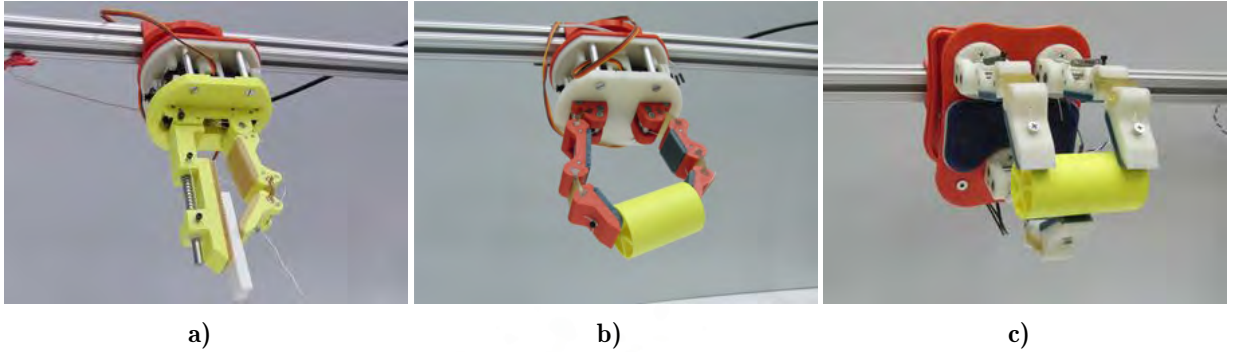


Figure 2.28: Comparison of medium-complexity Robotic Grippers from the Yale OpenHand Project
a) Model M² [MSD16]
b) Model T42 [OMD13]
c) Model O [Odh+14]

The least complex gripper, Model M² (Fig 2.28a), has one actuated and one passive finger opposing each other. The actuated finger is driven by two actuators which permit to grip both underactuated and fully-actuated. Thus, the gripper can perform basic in-hand manipulation as rolling and controlled sliding. The passive thumb can be changed depending on the application. The use of soft finger pad materials help to grasp objects with the resulting force dependent friction. The authors suggest that the design offers good possibilities to haptic exploration and controlled slip [MSD16].

Model T42 (Fig 2.28b) comes with four DOF in relation to two actuators, only offering the possibility of underactuated grasping. It offers more dexterity and is able to fulfill different types of in-hand manipulation. The design was elected to lift small, flat laying objects from plane surfaces, which was achieved in the first tests. For example, for coins with a thickness above 2 mm they had a success rate over 70 %.

The most complex of the considered grippers, Model O (Fig 2.28c), permits additional adduction/abduction. Thus, it is possible to switch from spherical to lateral gripping, respectively from the pad to the palm opposition. This feature allows to cover more grasp types. The adduction/abduction movement is realized by one actuator, while each underactuated finger is driven by one actuator.

A brief summary of the properties of the considered grippers is presented in table 2.5.

Table 2.5: Comparison of the Model M², Model T42 and Model O

Category	Model M ²	Model T42	Model O
Grasp types	TIP, PP, InfP	TIP, PP, MW	P2F, TP, PP, MW, PreS, L
DOF	2	4	9
Base Height [mm]	55–80	55–80	90

Base Width [mm]	90–105	90–105	100–125
Grip Force [N]	-	10	11–13
# of active fingers	1	2	3
# of actuators	2	2	4
Gripper mass [g]	375	400	752
Source	[MSD16]	[OMD13]	[Odh+14]

Tip Pinch (TIP); Palmar Pinch (PP); Inferior Pincer (InfP); Medium Wrap (MW); Prismatic 2 Finger (P2F); Tripod (TP); Precision Sphere (PreS); Lateral (L).

All grippers use servo motors.

In summary, the analysis of the Yale OpenHand Project hands provides the insight that a third finger significantly expands the possibilities of grasp types. However, additional actuators are usually necessary to actuate this finger, unless a differential is used (see [MOD13]). The increased number of actuators and the additional mechanical components result in a higher mass.

Generally speaking, current research shows that adaptivity

As observed of Chen et al. the gripper with 3 fingers offers significantly more possibilities and above all stability. 2-fingered grippers do offer the advantage in dexter manipulation.

Table 2.6: Comparison of State of the Art tendon-driven, robotic Grippers

Gripper	Biomimetic	Synergy-Inspired	Model O
	Robotic Hand	Three-Fingered Hand	
Source	[XT16]	[Che+20]	[Odh+14]
Year	2016	2020	2017
Grip modes	PreD, PreS, TP, P2F, TIP, PP, L, ET, PowD, PowS, MW, AT, LT, LD, SD	PreS, TP, L, PE, FH, PP, MW, LD	P2F, TP, PP, MW, PreS, L
Degrees of Freedom	20	11	9
Number of active Fingers	5	3	3
Number of Actuators	10	5	4
Gripper mass [g]	942	-	752
Comment	highly anthropomorphic	Synergy inspired	transition between power-grasping and spherical-grasping modes

Precision Disk (PreD); Precision Sphere (PreS); Tripod (TP); Prismatic 2 Finger (P2F); Tip Pinch (TIP); Palmar Pinch (PP); Lateral (L); Extension Type (ET); Power Disk (PowD); Power Sphere (PowS); Medium Wrap (MW); Adducted Thumb (AT); Light Tool (LT); Large Diameter (LD); Small Diameter (SD); Fixed Hook (FH).

2.6.1 Actuation

One of the most difficult aspect in the development of anthropomorphic hands still is the actuation. Due to the high functionality of the human hand, most of the current actuation technologies do not achieve the same level of power density and efficiency [PCP99]. Table 2.7 gives an overview on the most relevant actuators used in the development of Soft Robotic Grippers.

Table 2.7: Comparison of the most relevant actuators for Soft Robotic grippers, adapted from [HFA97]

Actuator type	ρ $\left[\frac{\text{W}}{\text{kg}}\right]$	σ_{max} [MPa]	ϵ_{max}	E [GPa]	η
DC motors	100	0.1	0.5	*	0.6–0.8
Pneumatic	400	0.5–0.9	1	$5-9 \times 10^{-4}$	0.4–0.5
Hydraulic	2 000	20–70	1	2–3	0.9–0.98
SMA	1 000	100–700	0.07	30–90	0.01–0.02
Human muscle	500	0.1–0.4	0.3–0.7	0.005–0.09	0.2–0.25

Power density ρ = Power per unit of weight, σ_{max} = Maximum force exerted by the actuators per area, ϵ_{max} = Maximum run per length, E = Actuator stiffness, η =Efficiency . Maximum stress and strain are indexes specifically designed for linear actuators. *Depending on gearhead

One of the main advantages of tendon-based force transmission is the low inertia and low friction. Additionally, it usually offers a more adaptable design at even lower cost and maintenance [PCP99].

3 Design of the Manipulator

This chapter is meant to present the development process of the robotic manipulator according to the guidelines given by the VDI 2206 [VDI04]. Thus, the list of requirements (Sec. A.3.1) was first drawn up and the tasks were specified. However, in contrast to the applicable

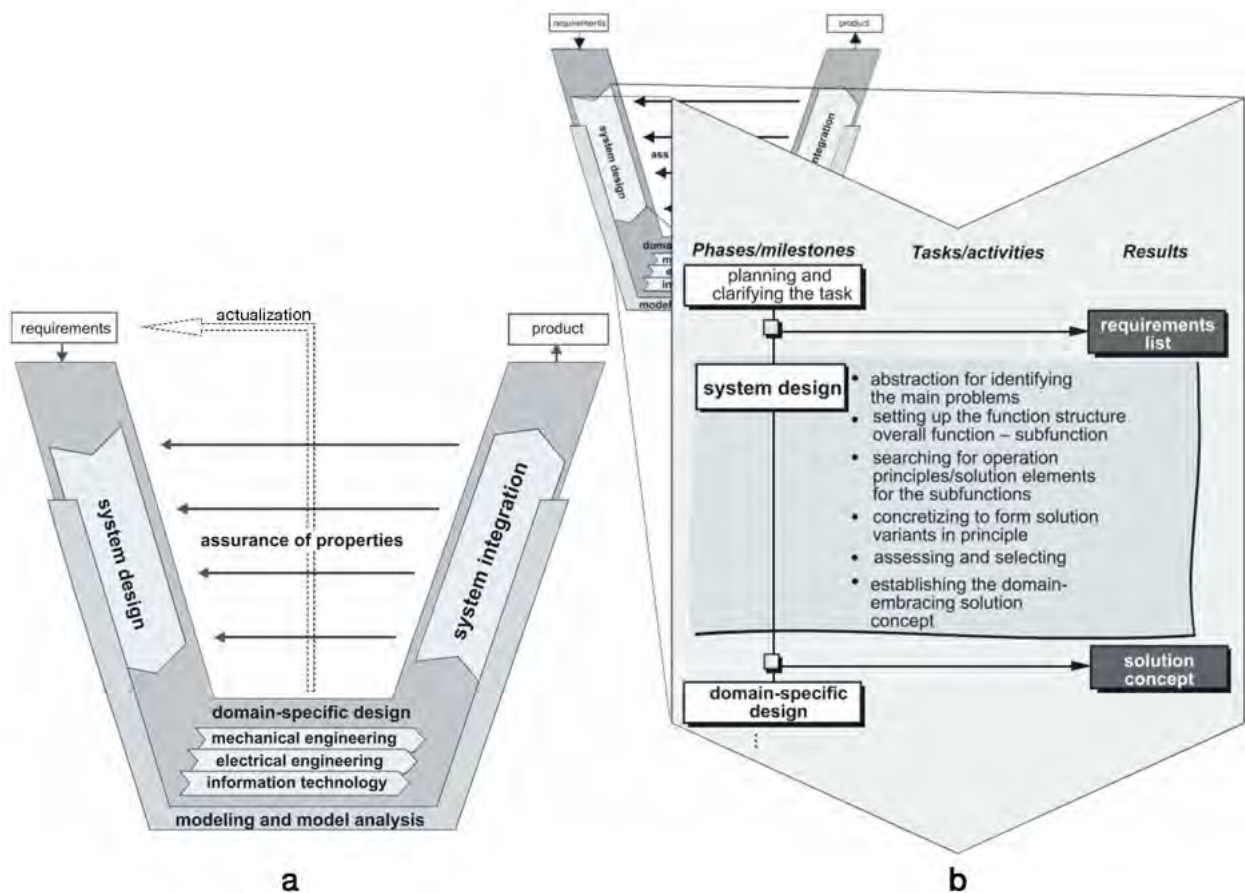


Figure 3.1: Graphical illustration of the design methodology according to the VDI 2206 and VDI 2221

- a) V-Model with continuous actualization of requirements, modified from VDI 2206 [VDI04]
- b) Activities in system design [VDI04]

VDI norm, the list of requirements was constantly updated during the development process as soon as new issues to be planned arose (see Fig. 3.1). Thus, also the function structure was continuously actualized and was expanded respectively.

The system design was conducted according to the VDI 2221 [VDI19a; VDI19b]. Based on the list of requirements, the overall function (Sec. 3.1.2) and subsequently subfunctions were

identified. Afterwards, operation principles and solution elements for the subfunctions were investigated.

3.1 Conceptual Design

The following section describes the design process of the project in more detail. First the functional requirements of the gripper will be specified. All other components were handled analogously to this procedure.

3.1.1 Requirements for the Soft Robotic Gripper

In the first step of the design process, the tasks were specified and a list of requirements was drawn up. It is divided into different sections, such as requirements for the mechanics, the motor, the sensors or the safety requirements. Table 3.1 shows an excerpt of the requirements for the functionality of the gripper, the complete tables can be found in the appendix (see 3.2.1)

The main goal of the development process is to create a tendon-driven Soft Robotic gripper that can manipulate fragile objects, such as a tomato or a glass. Here it is important to mention that the manipulation can be understood as a grasping or handling in a particularly skillful way [BLG08]. This skillfulness is to be realized by the implementation of force control. The force transmission is to be realized via a rope transmission, whereby adaptivity is to be used in the system in order to reduce the effects of rigid manipulation.

The following Table 3.1 provides a specified overview of the hard requirements for the gripper to be developed.

Table 3.1: List of the hard requirements for the Soft Robotic gripper

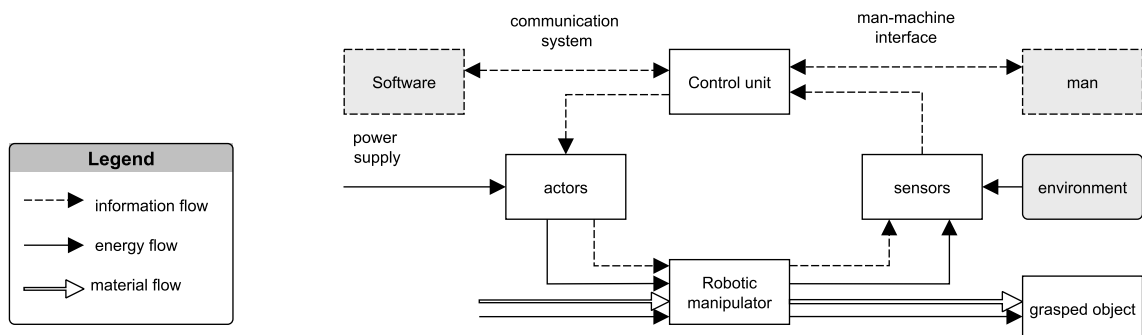
Description	Priority	Comment
Functional Properties		
Soft grasping of fragile objects	H	Tomatos, glass, eggs etc.
Controlled force application	H	characterization of force control
Reduction of the influence of rigid manipulation	H	adaptive finger tips, compliant structures
Performance of various grasp types	H	realization of grasps like the Medium Wrap (see [Fei+16])
Mechanical Design		
Human inspired	H	e.g. proportions of the phalanges, human like contact area etc.
Tendon-driven	H	force transmission via tendons

Table 3.1: List of the hard requirements for the Soft Robotic gripper (prosecution)

Description	Priority	Comment
Legend		
H	Hard requirement	
D	Desired requirement	
M	Minimum requirement	

3.1.2 Overall Function and Technical Principles

Once the main components had been identified from the task and the various requirements for the gripper, the main function of the test setup could be established (Fig. 3.2). This is the manipulation of a fragile object by means of a tendon-driven softrobotic gripper. Incoming parameters are an operator and an energy supply, outgoing parameters are the measured values. It is important to take into account the environmental influences acting on the system from the outside, as well as the effects of the system on the environment. Information flows (measured variables, control pulses or data), Energy flows (mechanical, electrical energy, forces etc.) and Material flows (tested objects, solid bodies, treated objects etc.) [VDI04].

**Figure 3.2:** Basic System Structure (based on VDI 2206 [VDI04])

Subsequently, the main function was subdivided into further components and the function structure was formed from this. This consists of the entire gripper, which on the one hand contains the fingers themselves, and on the other hand also an actuator. From the outside, the operator and environmental influences act on the system boundaries of the experimental setup, and energy is also supplied to the system. The system itself in turn acts on the environment, and feedback signals are sent to the operator.

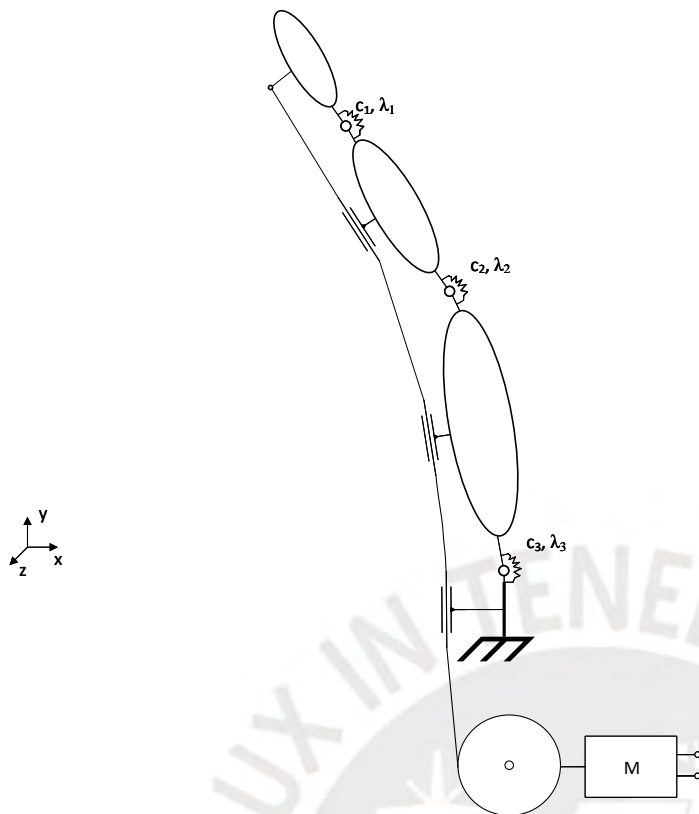


Figure 3.3: Technical principle of a finger with 3 phalanges and compliant joints

The design process of the finger can be exemplified in the following Figure 3.3, as an technical principle.

Where c is the stiffness of the torsional springs and λ is the spring length. The system is driven by a motor through a pulley.

3.2 Mechanical Design

The components defined in the value sensing tables were combined into a model in the design program Autodesk Inventor Professional 2019 [Inv18].

The focus of the design is modularity. This makes it possible to use the chassis as the basis for varying different types of fingers, flexible joints or even the number of fingers without having to make any major changes to the assembly. Furthermore, it was important that the components are designed mostly parametrically, so that, for example, tolerances for the fit of the finger joints with the phalanges or with the MCP joint can be adjusted simply by changing the tolerance value (backlash_s) for all components involved. All parameters were stored in the output file of the palm (palm_base.ipt) and linked to all derived components. This chapter provides an overview of the functional components of the “Soft Robotic Gripper” assembly by referring to the design of the functional components. Here, the design process

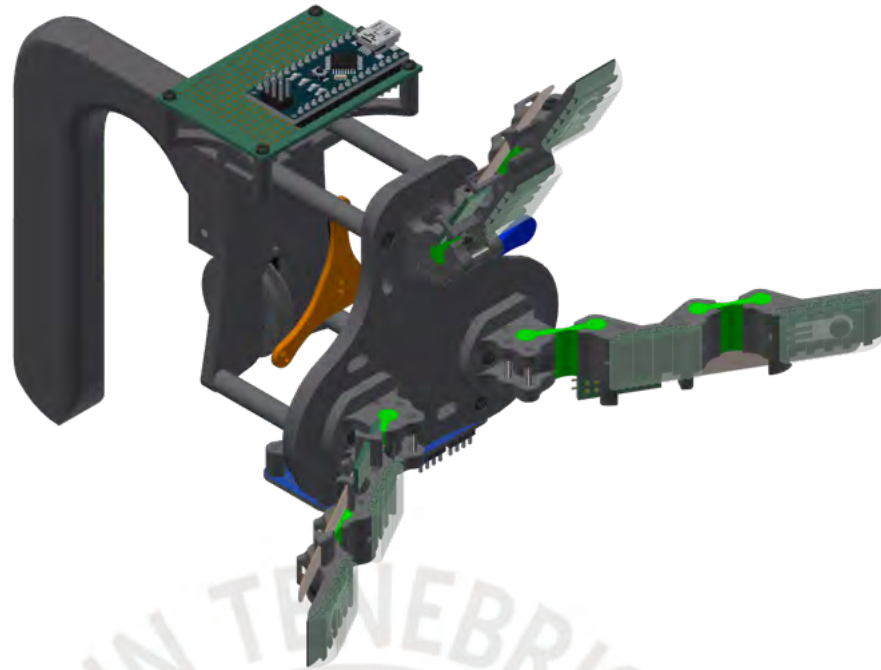


Figure 3.4: CAD-Model of the assembled Soft Robotic Gripper

of the palm, the fingers, the gear train and finally the cable train is described. All CAD files are provided in the digital appendix.

The design of the PLA components was done according to these rules:

- wall thickness $t \geq 2 \text{ mm}$
- thread depth $m_{req} \geq 3 \cdot d$ bore diameter
- Always cut thread or use heat-set inserts
- center of a bore always with $a \geq 1,5 \cdot d$ bore diameter to part contour

3.2.1 Design of the Finger

The total size and respective proportions of phalanges were determined on the basis of findings of anthropometric studies [BAG92]. The data of Table 2.1 in Section 2.1.1 was used to calculate adequate lengths for the phalanges.

For simplicity, based on other grippers, the structure of the fingers was chosen to be the same as other grippers (see Sec. 2.6). Thus the three finger of the gripper were designed like the human index finger, since it is the most important finger besides the thumb (see Sec. 2.1). Based on this guideline the lengths of the phalanges were determined. A hand length $H_L = 114 \text{ mm}$ was chosen according to the specified object geometry (see). It is smaller than the median hand length $HL_m = 182.94 \text{ mm}$ from Buchholz et al. [BAG92]’s study.

Finger Tip

To measure the contact force, it was decided to position the sensor in the fingertip. Here it has contact with the object both with precise pinches and with more powerful enclosing gripping methods such as the medium wrap. As considered in the implementation of the compliant joint, the finger is guided parallel as long as possible not to slip past the object. Studies have already shown that the response of an FSR is significantly improved when a small disc or similar is applied to provide a more uniform load [SJJ16]. Therefore, the design provides for such a component (see Fig. 3.5). In addition to embedding the sensor, molds for silicon pads were also designed. These are intended to improve adaptivity and friction. The fabrication of the silicon rubber molds is further explained in Section 3.5.2.

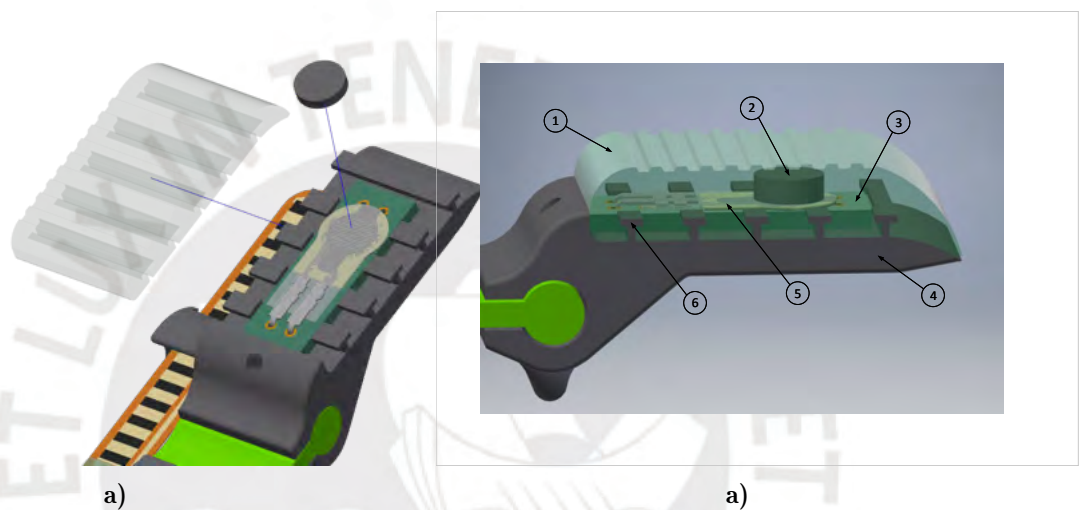


Figure 3.5: Design of the fingertip

- 1) Adaptive silicon rubber pad; 2) sensor plate for more uniform load; 3) Sensor PCB;
- 4) Phalanx distalis; 5) FSR; 6) anchor to fixate the silicon rubber mold

Tendon Routing

It is crucial to keep the friction between the tendons and the components as low as possible. When the fingers bend parasitic capstan effects [LAK13]. In addition the tendons might cut into the rigid body material when high load is applied [MOD13]. To reduce the risk of cutting and to optimize the friction, 2 mm steel tendon guide pins are used. As seen in Figure 3.6 the pins are assembled with a press-fit into the phalanges for example. The steel pins provide a harder sliding contact with significantly less friction [MOD13].

At the end, at the distal phalanx, the tendon is fixed. Due to the good frictional properties, it was decided to use Nylon fishing cables with a payload of 3.2 kg and 0.25 mm diameter.

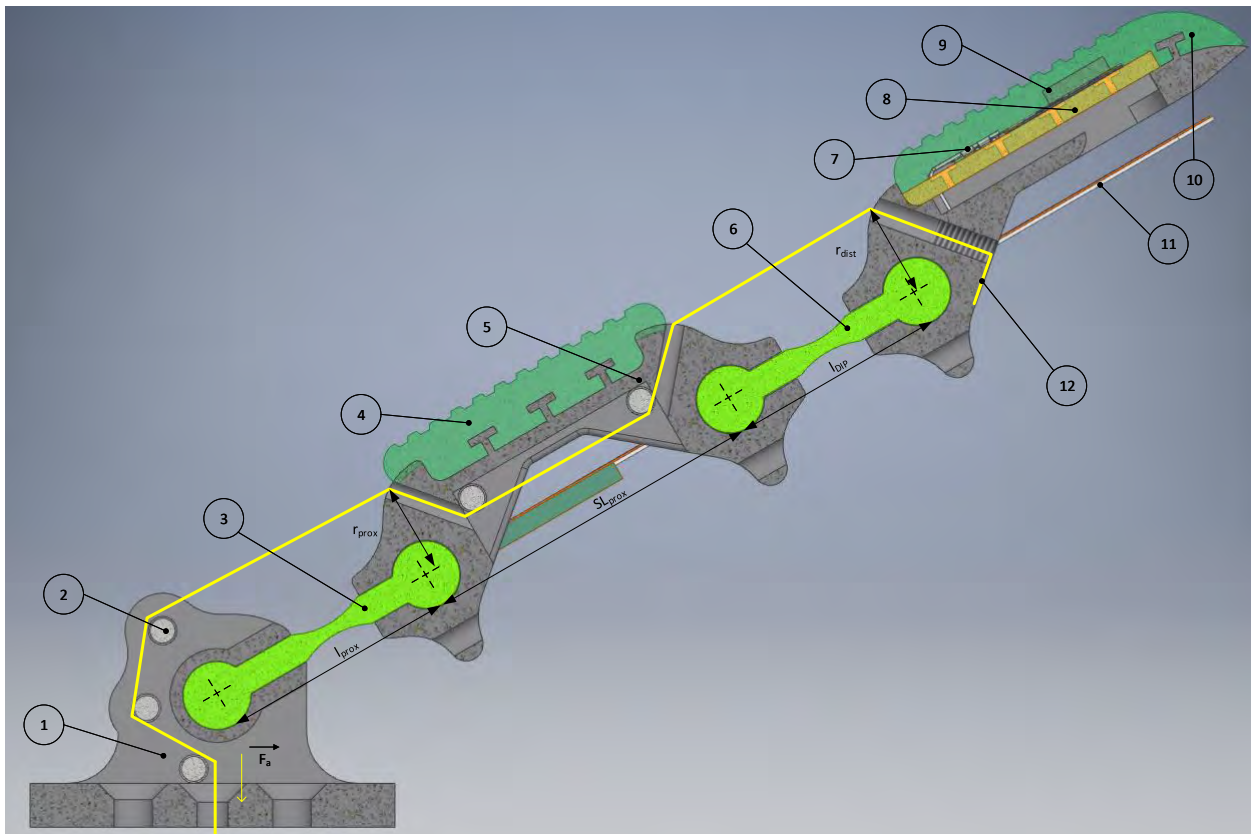


Figure 3.6: Tendon routing of the Soft Robotic fingers

- 1) MCP base; 2) steel routing pin; 3) MCP hinge; 4) Pad proximalis; 5) Phalanx proximalis; 6) DIP hinge; 7) FSR; 8) PCB; 9) sensor plate; 10) Pad distalis; 11) flex sensor; 12) cable anchor

3.2.2 Design of the Compliant Joints

In order to follow the recommendation of the state of the art, a simulation of the deformation was carried out with the aid of the flexure hinge design software DetasFLEX [Det18]. Since the literature shows a ratio of 5:2 between the stiffness of the distal and proximal joint, this ratio was simulated taking into account the available actuator power.

With regard to the modular design, care is taken to ensure that the flexible joints always have the same geometry for connection to the fixed bodies, so that they can be quickly replaced if necessary. However, in order to have an influence on the stiffness, it is possible to change the density during 3D printing (see [Hus+17]) or the geometry of the beam itself. Due to the fact that the results of the density adjustment depend very much on the printing process, it was decided to adjust the geometry. The influencing factors in 3D printing can be, for example, the temperature and especially the alignment on the print bed. To design the compliant joint, the “rigid-body replacement approach” [LFL13] was performed using their provided software.

With the help of the simulation, the stiffnesses of the compliant joints were determined. these can be achieved with the following parameters. The design was proceeded to fit in smoothly with the modular design of the assembly.

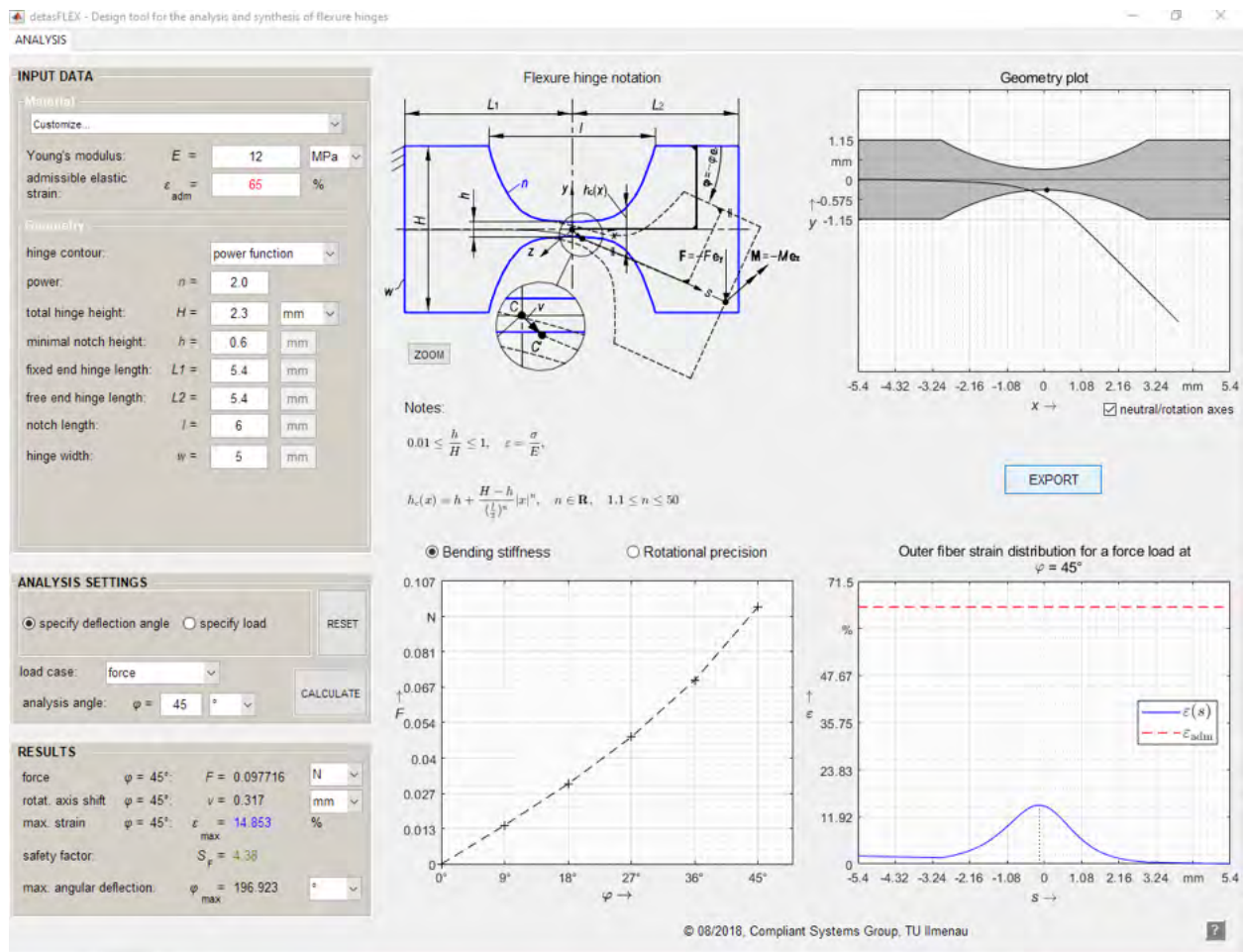


Figure 3.7: Hinge design in detasFLEX [Det18; HLZ18]

3.2.3 Design of the Tooth Gear Mechanism

In view of the requirement to realize several types of gripping (see), a toothed gear was designed that enables the position of the fingers to be changed in relation to each other by manual operation. This favors the gripping behavior, since grips such as the Medium Wrap or, in the other mode, Power Sphere can be performed. It is also possible to create pinches. In contrast to the human model, however, the adduction/abduction was not realized by the thumb, but quasi inverted by the fingers.

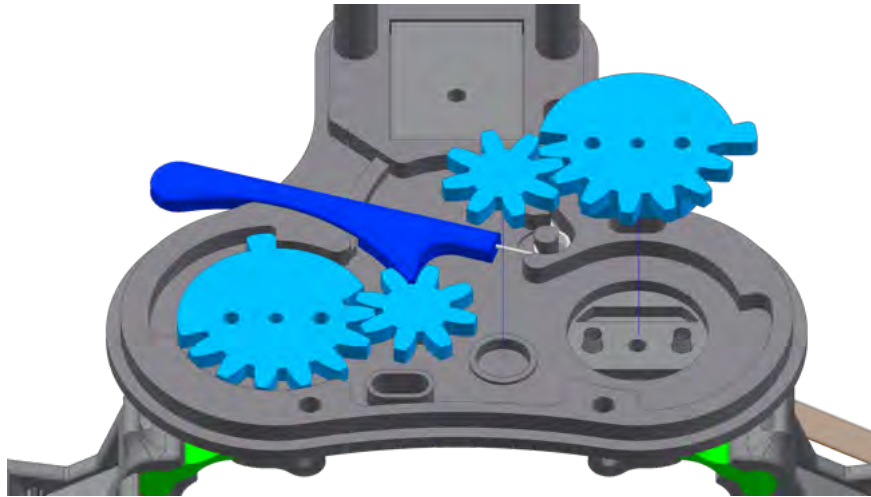


Figure 3.8: Manually lockable gear mechanism to change between different grasp modes

As seen in Figure 3.8 the gear mechanism is unlocked when the latch is pushed by the user. Once the latch is released, the torsional spring reverses it into the locked position. The large gears on which the MCP joints are mounted are supported in the palm of the hand and have a mechanical stop to prevent unwanted movement. The small transmission gears, on the other hand, are mounted on one side on the back of the palm. From above, the two types of gears are secured by the back surface of the hand (palm_backside.ipt).

The positions that can be reached in this process are shown in Figure 2.4. The total range of movement is 90 degrees.

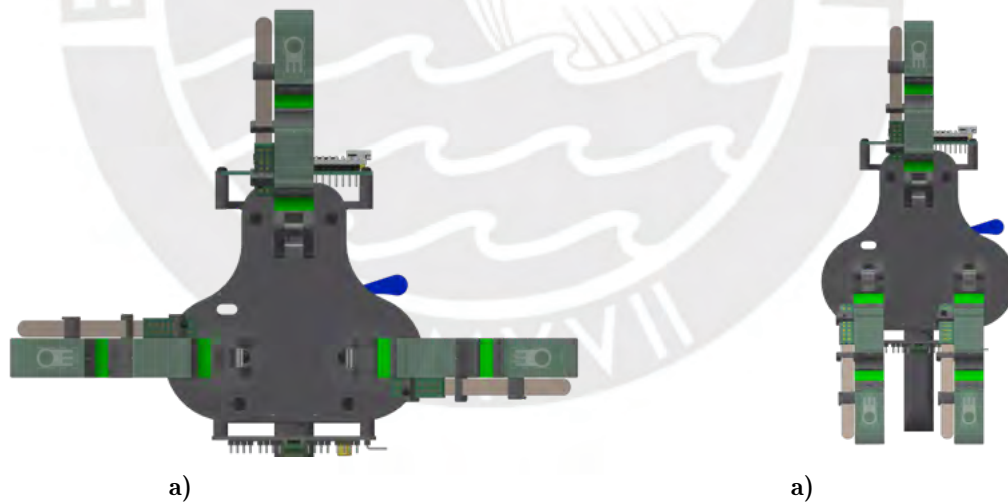


Figure 3.9: Range of motion of the gear mechanism to realize adduction/abduction. The adduction/abduction movement is between 0° and 90°

3.3 Electrical Design

The electronics required for the gripper were summarized as a circuit diagram using the Fritzing open-source software [Fri21]. This documents the wiring of the components. The

circuit diagram includes the power supply, sensors, microcontroller and circuit boards and basic components like resistors. The complete circuit diagram can be found in the digital, as well as in the printed appendix (see A.8). As an example, a section containing the necessary wiring of the FSR of the thumb (FSR_t) together with the according reference resistor $R1$ is shown in Figure 3.10.

3.3.1 Selection: Position Sensors

Compared to other position sensors (see Tab. A.3.3), the flex sensors offer flexibility, robustness and easy integration within a low range of cost [Ger+17]. A flex sensor was chosen to determine the position as shown in Table A.3.3. A FS-L-0055-253-ST (Spectra Symbol, Salt Lake City, UT, USA) was elected. One of the main advantages is the direct operation with the Arduino, since it requires 5 V supply voltage V_{cc} and provides an analog output signal V_{out} .

As mentioned before (Sec. 2.4.2), the sensor can be used with a voltage divider or RC-circuit. Since the elected microcontroller does not provide sufficient analog inputs, the RC-circuit solution (see Fig. 2.19b) got implemented, because it operates only on digital pins.

The algorithm for the RC-timing is explained in Section 3.4.1.

3.3.2 Selection: Force Sensors

Thanks to its ease of use and relatively low cost, a FSRs was chosen. According to the data sheet, the Interlink FSR 400 [Int15] model used here has a measuring range of 0.2 N to 20 N.

3.3.3 Election: Current Sensor

The elected ± 5 A Linear Current Sensor [Mic20] (Microbot, Latina, LT, Italy) carries a ACS714ELCTR-05B-T hall effect-based linear current sensor from Allegro[®] [All12] (Allegro MicroSystems Inc., Worcester, MA, USA). Its IC uses a copper conduction path to lead the measured current I_M of the motor. The magnetic field of this path is converted into a proportional voltage by a Hall IC. The sensor is implemented with a supply power V_{cc} of 5 V and has an analog output voltage V_{out} with linear characteristics.

The sensitivity of the sensor is $185 \frac{\text{mV}}{\text{A}}$ with a typical error of $\pm 1.5\%$. He offers a bidirectional current range from -5 A to 5 A.

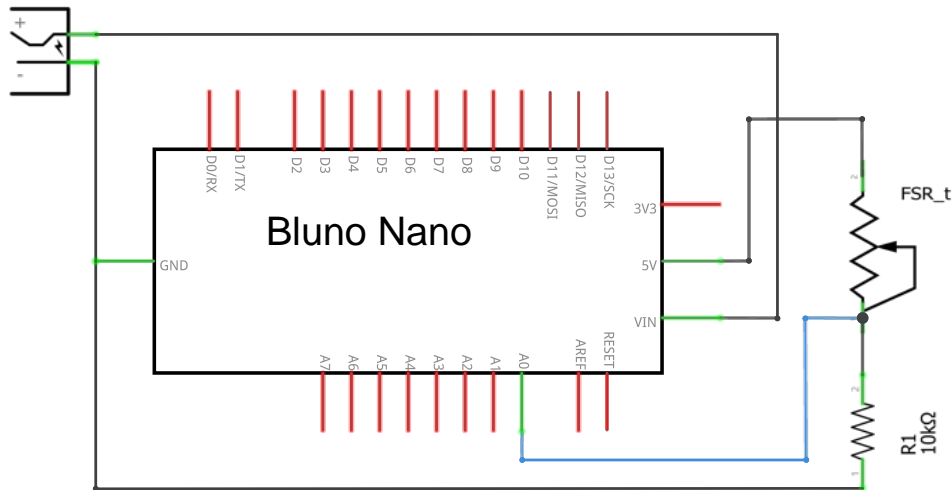


Figure 3.10: Exemplary illustration of the wiring of a FSR with the corresponding reference resistor in a voltage divider setup

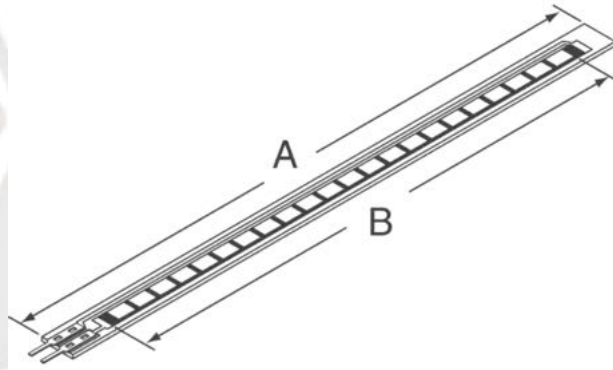


Figure 3.11: Schematic drawing of the elected Flex Sensor FS-L-0055-253-ST [Spe20]
 $A = 73.66 \text{ mm}$, $B = 55.37 \text{ mm}$

3.3.4 Calibration of the Sensors

In order to interpret the measured data it is necessary to do a referencing. This section explains the associated process and provides the knowledge needed for the conversion of the flex and force sensors.

Flex Sensor

Prior to the assembly, measurements were made to determine the characteristics (R_{flex} , V_{out}) of the flex sensor. The sensor was clamped at the beginning of the active area and the voltage and resistance were measured (see Fig. 3.13). As described in Sec. 2.1.2, the maximum deflection range of the MCP is 103° , thus only angles up to 110° are of interest. The following Figure A.2 shows the sensor's characteristics. Additionally, the electrical resistance



Figure 3.12: Linear current sensor from Microbot with an Allegro[®] Hall-effect based IC, from [Mic20]



Figure 3.13: Calibration of the flex sensor with a RC-circuit

was measured (see. A.1.1). With the help of the “Basic Fitting tool” [MAT19], the best-fit equation was determined.

$$\varphi_{flex} = 0.083634 \cdot \varphi_{Bit} - 37.946 \quad (3.1)$$

The determined data offers the possibility to quantify the analog voltage with the analog input of the microcontroller. The original data can be found in the digital appendix.

Force Sensor

The setup shown in Figure 3.14 was used to calibrate the force sensor. It was decided to use a vessel with water as reference load and to fill it up gradually and hence increase the load. At the beginning of the procedure, the vessel was weighed and filled until reaching an

adequate starting weight (see Sec. A.1.2). Then, water was added precisely by using 5 ml and 20 ml syringes, to achieve the required volume for the sampling points. Once, an effect of saturation was observed, the volume of added water was augmented.

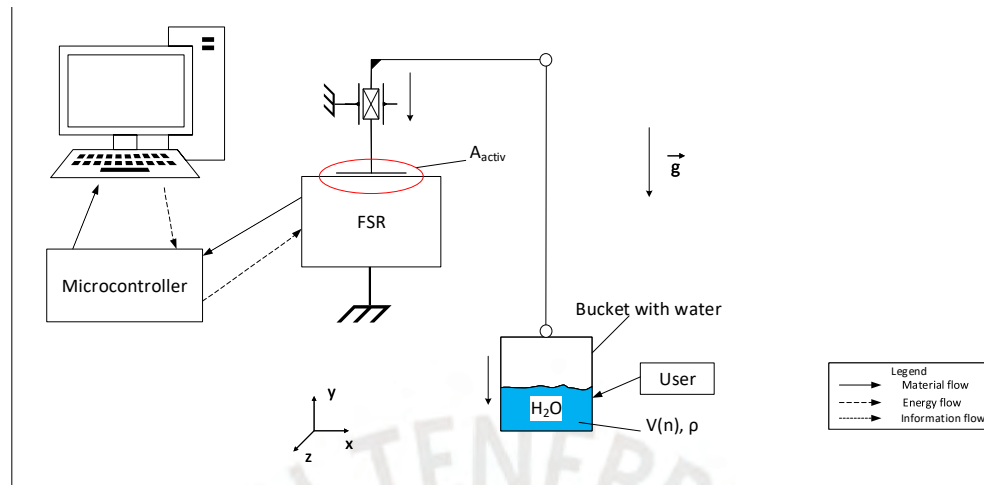


Figure 3.14: Technical principle for the referencing process

Based on 75 sample points the following characteristic curve (Fig. 3.15) was determined.

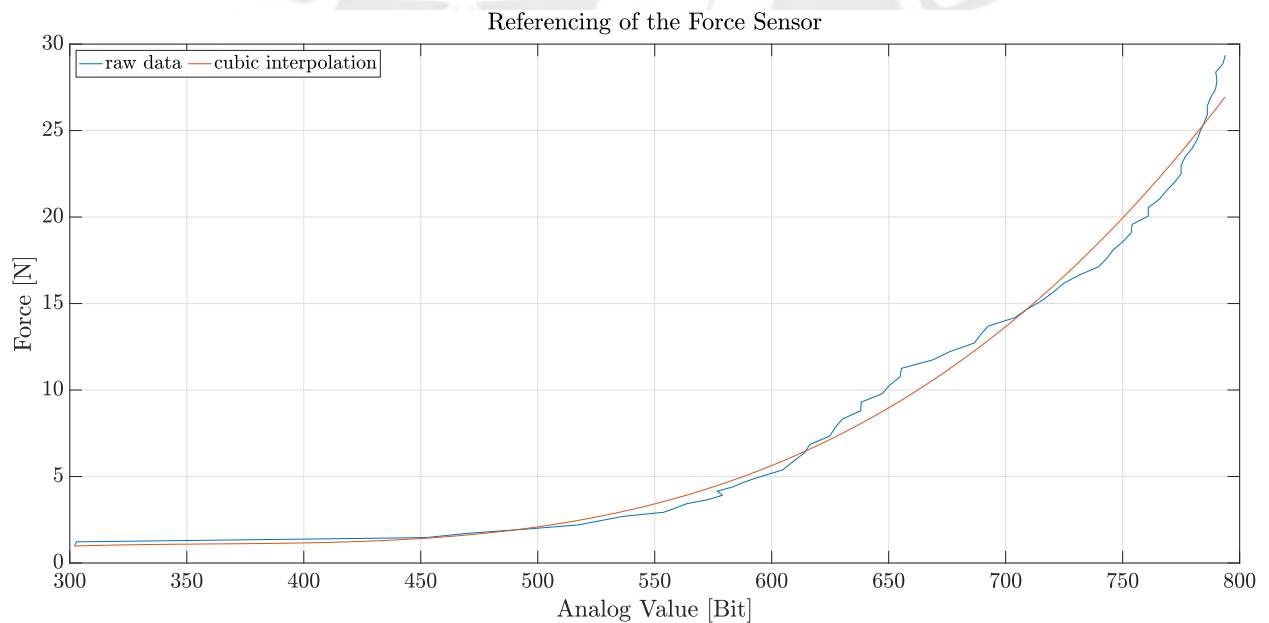


Figure 3.15: Characteristic curve of the Interlink FSR[®] 400, with a 10 kΩ Reference Resistor

As seen in Figure 3.15, the interpolated curve is cubic. The calculated parameters by the Basic Fitting tool yields the following equation.

$$F_{FSR} = 3.125 \times 10^{-7} x^3 - 0.33808 \times 10^{-3} x^2 + 0.12294x - 13.922 \quad (3.2)$$

This function allows to convert the measured analog values into the applied force of the FSRs.

3.3.5 Selection of the Actuator

Due to good availability, low price and high power density, a Feetech FT90M-FB high torque servo motor was installed [She]. However it is quite comfortable to control servo motors with the Arduino servo library, the servo consumes Arduino processing power [Ear19]. To overcome this consumption and to reduce the corresponding overhead, the motor is powered through a Adafruit 16-Channel 12-bit PWM/Servo Driver [Ear19]. The reduction of the overhead helps to enable efficient and reliable data acquisition.

3.3.6 Power Supply

Considering the requirement of a lightweight design, the decision was made to use an external power source. For a better interconnectivity, a 220 V alternating current (AC) power supply unit with a 5 V, 2 A output was elected. Thus, no converter has to be used since the microcontrollers, the motor driver and the sensors operate at 5 V.

3.4 Software Design

Apart from the mechanical and electrical design, the gripper requires software to control it. For the software development Visual Studio Code [Vis21] with the PlatformIO IDE (integrated development environment) [Pla21] extension have been used.

In addition to the functional programming, a graphical user interface (GUI) has been developed in MATLAB [MAT19] to capture, process and visualize data from the microcontroller in a more user-friendly way and to control the gripper. This section shows first the necessary conversions of the raw data (Sec. 3.4.1) and then the corresponding implementation, as well as the design and handling of the GUI.

3.4.1 Calculations

All data is transmitted via Bluetooth and received by a microcontroller which works in dongle-mode. The receiver is connected to a PC via USB. To augment the transmission speed, as much data processing as possible is done by the PC. This section gives an overview on the calculations to interpretable data.

Current Sensor

The analog output of the force sensor is linear [All12] and can be converted to the according current I_A with the following equation. Because the sensor maps ± 5 A, the zero point is at 2.5 V at the analog output. Since the sensor is only used in one direction, an offset was added to start the calculation at 0 V or 0 A.

$$I_A = \frac{\frac{5 \text{ V} \cdot I_{bit}}{1023} - 2.5 \text{ V}}{0.185 \frac{\text{mV}}{\text{A}}} \quad (3.3)$$

This equation is implemented in the Matlab[®] code and is done automatically in the background.

Flex Sensor

Because of the use of an RC-circuit a basic algorithm is necessary [Nos12]. In the course of calibration, a best-fit line was determined for the measured value curve of the bending sensor (see Sec. A.1.1), which lead to equation A.1. The according equation to calculate the deflection angle is

$$\varphi_{flex} = 0.083634 \cdot \varphi_{Bit} - 37.946 \quad (3.4)$$

FSR

Based on the data collected in Sec. A.1.2, it is possible to draw conclusions about the applied force on the basis of the analog voltage. With the help of MATLAB[®]'s "Basic Fitting Tool", the characteristic curve was interpolated. A cubic function provides sufficient accuracy. Hence, the raw data can be converted by the use of the following equation.

$$F_{FSR} = 3.125 \times 10^{-7} x^3 - 0.33808 \times 10^{-3} x^2 + 0,12294x - 13.922 \quad (3.5)$$

Where x is the read analog value sent from the microcontroller in [Bit].

3.4.2 Software Implementation

The selected microcontroller can be programmed using Visual Studio Code and the PlatformIO integrated development environment (IDE). Figure 3.16 shows the class diagram of the implementation. The complete source code can be found in the digital appendix. This also includes the source code of the Bluetooth dongle, which is trivial, however, since only the received data is passed to the PC via the serial interface.

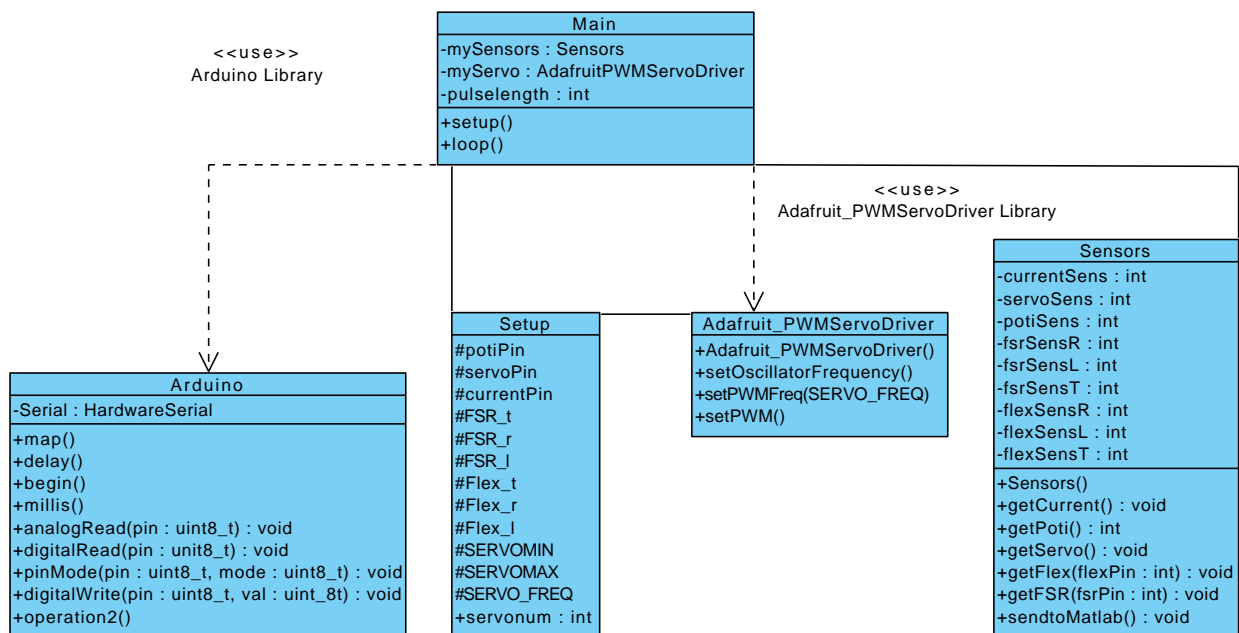


Figure 3.16: Class diagram of the Soft Robotic Gripper software

GUI Development

A GUI was developed to facilitate the recording and analysis of measured values during tests. This offers the possibility a serial connection between Matlab[®] and a Bluno Beetle, which in turn receives the measurement data from the Bluno Nano on the gripper via bluetooth.

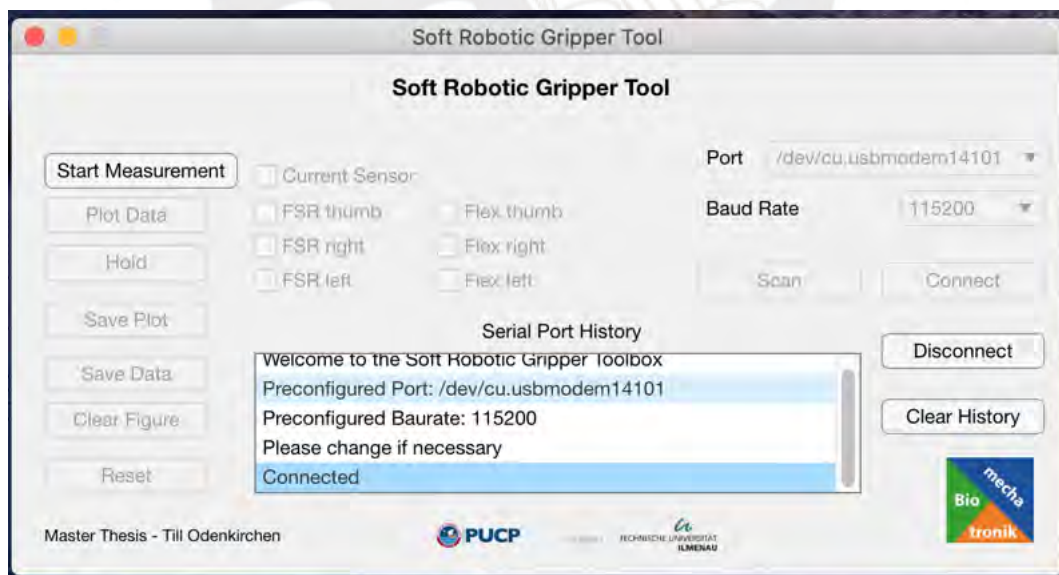


Figure 3.17: Soft Robotic Gripper Tool: A GUI to control the developed gripper

The functionality is that the available serial ports are scanned and the user can choose which one to connect to. Before connecting, it is necessary to select the baud rate specified by the terminal device. Once the baud rate is selected, the connection can be established and the measurement mode is enabled. Here the user can start the measured value recording by

pressing a button. If a test is finished, the recording is to be terminated manually. In the background, MATLAB[®] now converts all raw data into interpretable values (see Sec. 3.4.1). As seen in Figure 3.18, the user can now select which data he wants to plot. For example, it is possible to display only the measured values of a finger, e.g. FSR thumb, Flex thumb and the values of the current sensor. If one data set is to be viewed first and then another, this is also possible thanks to the implemented "Clear Figure" button.

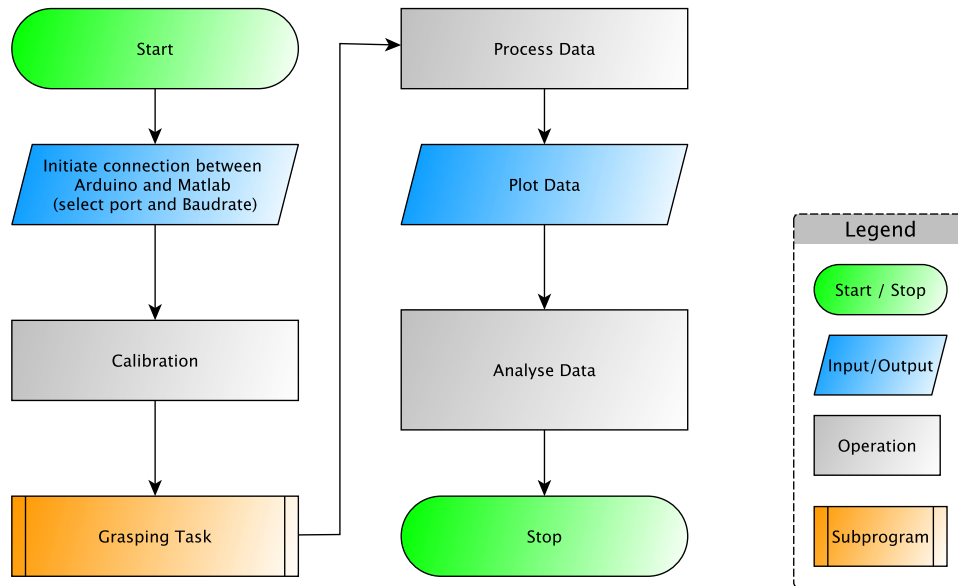


Figure 3.18: Flow chart of the data acquisition

In this case, only the figure is reset, the measured values remain in the workspace. If a plot is to be saved, this is possible via the "Save Plot" button. This exports the figure via WYSIWYG function of the "export_fig" package [Alt21]. The file name will be automatically filled with the involved fingers and the date of the measurement. Furthermore, it is also possible to save the entire dataset, i.e. the entire workspace as a .mat file, if the "Save Data" button is pressed. Also in this case the name of the saved file is provided with the date. Finally, the workspace can be reset via the "Reset" button, so that a new measurement can be started.

All MATLAB[®] files are provided in the digital appendix and can be found as "Soft Robotic Gripper Tool".

3.5 Fabrication

This chapter gives an insight on the fabrication process of the components of the soft robotic gripper. First the characteristics of the fused deposition modeling (FDM), also simply called 3D-printing, are explained and then followed by the instructions on how to make the silicon finger pads.



Figure 3.19: Fabrication of the Soft Robotic Gripper with a 3D-Printer

3.5.1 3D-Printing

Due to reproduction of components and the further development the necessary steps are documented in the following part.

After the design in Inventor (see Sec. 3.2) the .stl files were prepared for the print with the Ultimaker Cura [Ult21]) slicer software. All parts were printed in a Credity Ender 3 (Shenzhen Credity 3D Technology Co., Ltd, Shenzhen, China). The used materials were PLA [AIO21] and Ninjaflex TPU [Nin16].

The most important configurations are presented in the following table.

Table 3.2: Main parameters used for 3D-Printing

Material	PLA	TPU
Temperature	198 °C	230 °C
Build Plate Temperature	60 °C	0 °C
Build Plate Adhesion	Brim	None
Layer Height	0.2 mm	0.2 mm
Print Speed	50 $\frac{\text{mm}}{\text{s}}$	30 $\frac{\text{mm}}{\text{s}}$
Retraction	Yes	No
Support	Yes (depends on component)	No

In addition to all CAD files, the Cura profiles are also provided in the digital appendix.

3.5.2 Silicon Molds

In order to fabricate the soft finger pads, this section gives a brief overview on the procedure. The mold design consists of two parts: the component to be used in the gripper and the reusable mold press-fit part which snaps around the part. The material used is Wagnersil 20NF [Wag21], a silicone rubber that is liquid during processing and cures within approximately 90 minutes. This property makes it possible to create fine structures, such as a fluted surface of the fingertips. The model for this procedure was the work of Ma et al. [MBD15] and the Yale OpenHand Project [Yal].

Due to the hardness of Shore A20, a good adaptivity is expected, which will be tested in the following chapter (Chap. 4).

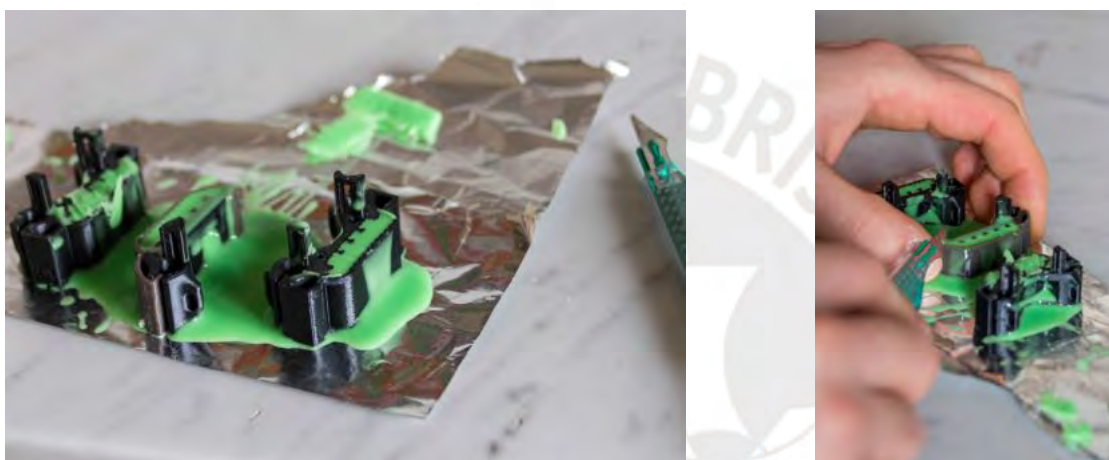


Figure 3.20: Cleaning the silicone rubbers after curing

The mold CAD parts are also provided in the digital appendix.

4 Practical Experiments

In the following, the developed underactuated soft robotic gripper will be tested for its functionality and properties by means of practical test measurements. Initial tests will be carried out on the functionality of the force sensors in the fingertips, the determination of the position by means of the flex sensors and finally the analysis of the data by measuring the actuator current.

Inspired by the AHAP [LH+19], a framework which was developed to evaluate robotic hands/grippers systematically, various objects will be grasped to determine the grasping capabilities of the developed hand. Additionally to this, the sensor performance will be looked into as well. The use of differently shaped objects leads to the need to use different types of grips. These are selected intuitively by the user by adjusting the position of the fingers in relation to the thumb.

Additionally to the approach of Llop-Harillo et al. [LH+19], the interesting idea to evaluate the performance of the gripper by Shintake et al. [Shi+16], where the grippers mass is compared to the maximal load will be considered.

During the experiments, the control of the gripper or the servo motor was realized by means of a potentiometer.

4.1 Test Measurements with the Implemented Sensors

4.1.1 Test Measurements with the FSR

For the first test of the force sensors, the gripper was left in its resting position and the fingertips were pressed against a plane surface in the following order: thumb, finger_r and finger_l. The gripper was then moved to the resting position. The according curve (Fig. 4.1) for this was recorded using the MATLAB[®] GUI (see. Sec. 3.4.2). As an example the data of the right finger is shown in Figure 4.1.

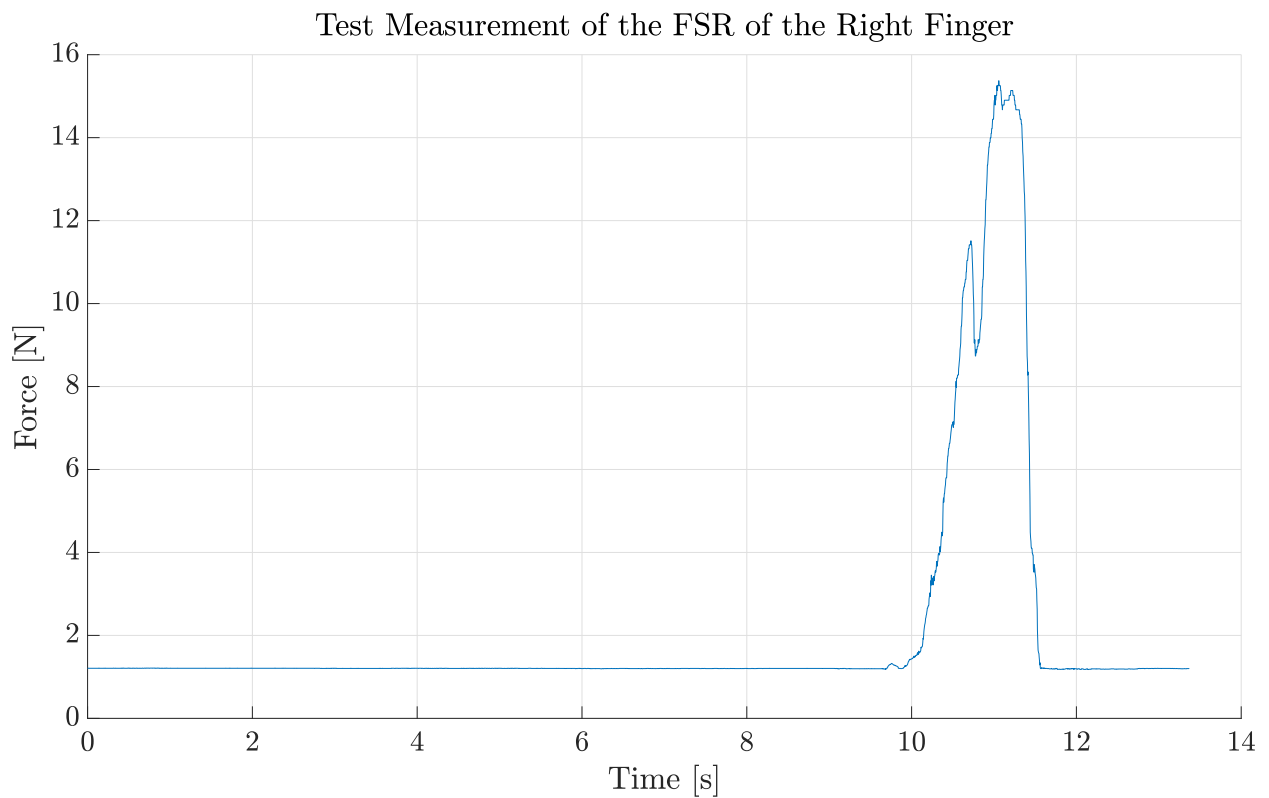


Figure 4.1: Example for the test measurements: FSR of the right finger

4.1.2 Test Measurements with the Flex Sensor

The flex sensors were tested in a similar manner to the FSRs. The gripper was placed in the rest position and then the fingers were manually bent step by step. As before, first the thumb, then the right and finally the left finger was processed. For the flexion of the fingers, the cable was tightened manually. Figure 4.2 shows the comparison of the detected deflection angle for each finger during a medium wrap.

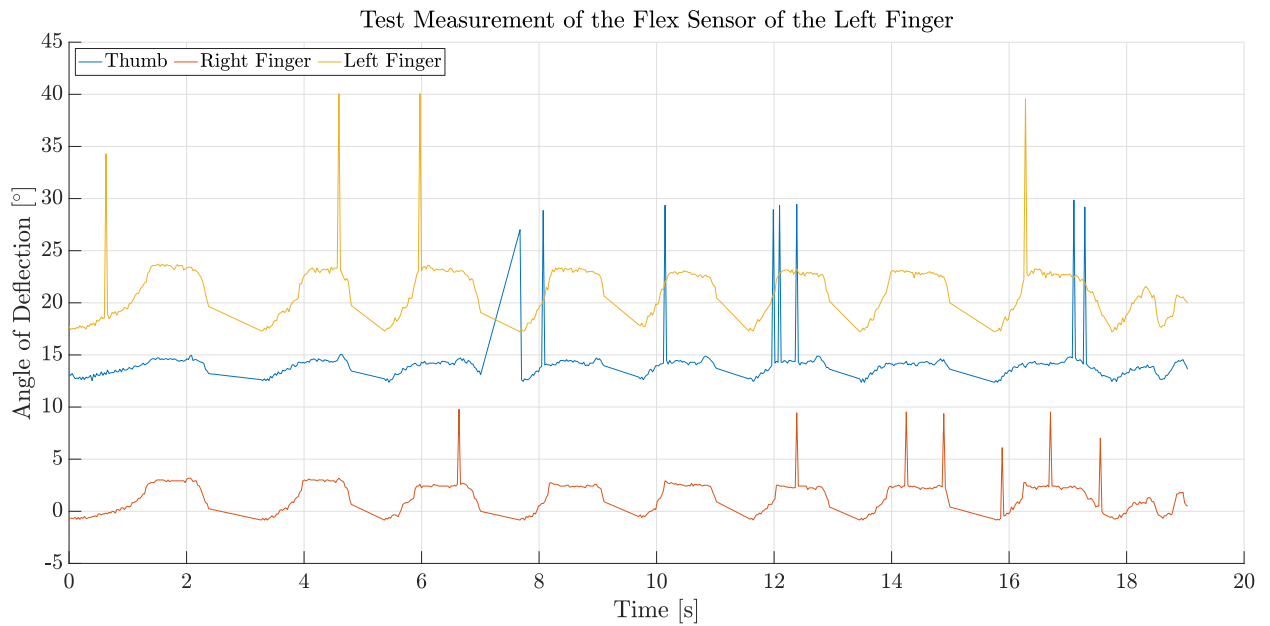


Figure 4.2: Example for the test measurements: Flex sensors during a Medium Wrap

During the test, the gripper was continuously opened and closed.

4.1.3 Test Measurements with the Current Sensor

To verify the functionality of the current sensor a basic spherical power grip was performed on a round object. This grip lead to the following curve.

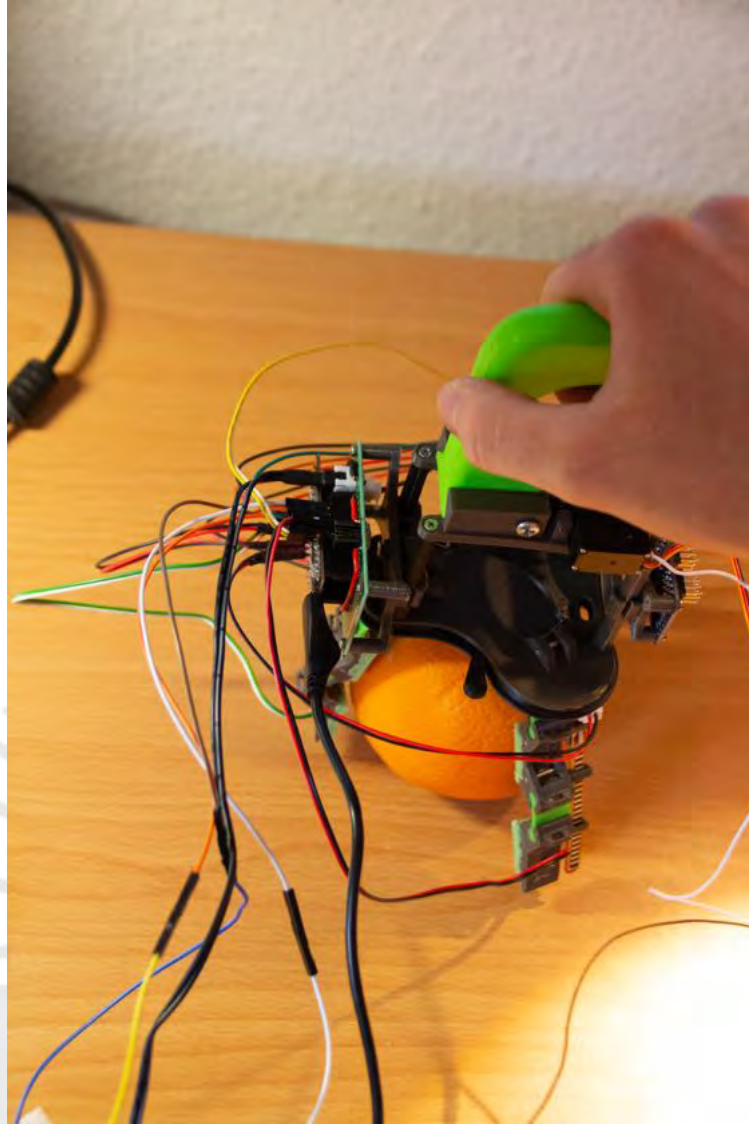


Figure 4.3: Power Sphere grip to determine the functionality of the current sensor

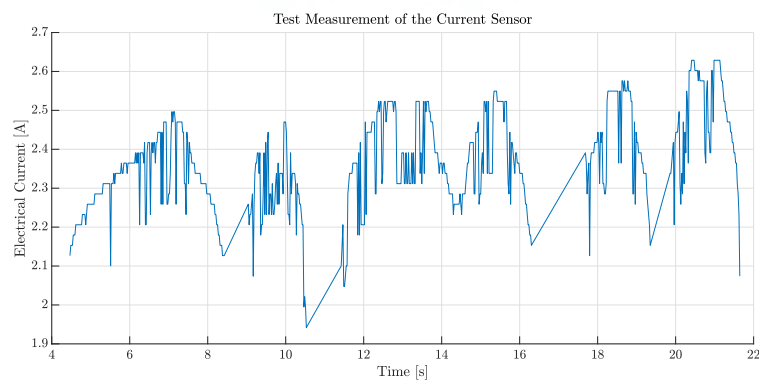


Figure 4.4: Curve of the current of the servo motor when trying to grab an orange

Since the orange is too heavy for the gripper, as previously determined, it was repeatedly re-gripped in the experiment to create a high load on the motor.

4.2 Test of the Grasping Capabilities

The following section describes the procedure for testing the gripping capabilities of the developed gripper. For this purpose, 12 objects were selected which, due to their geometry, elicit different grips in order to be manipulated. The self-weight of the gripper is 216 g

Table 4.1: Objects used for to test the grasping capabilities

Object	Mass	Grasp Type	Succesfull Grasp	Comment
Egg	56 g	yes	Tripod	only lifted from above
Tomato	11 g	yes	Lateral Pinch, Tripod, Palmar Pinch	
Banana	163 g	no	-	too heavy
Apple	206 g	no	-	
Orange	336 g	no	-	
Shot glas	112 g	yes	Lateral Pinch	
Glass S	189 g	no	-	
Glass M	285 g	no	-	
Glass L	413 g	no	-	
Plastic cup	7 g	yes	Tripod, Medium Wrap, Palmar Pinch	
Pen	8 g	yes	Prismatic 2 Finger, Tip Pinch	only lifted when over-standing
Brush	2 g	yes	Prismatic 2 Finger, Tip Pinch	only lifted when over-standing

As an example the grasping of a tomato will be showed more in detail.

First, the gripper was aligned with the tomato (see Fig. 4.6a) and slowly closed by means of the potentiometer control (see Fig. 4.6b); as soon as a stable grip became apparent, the object was lifted and gently swiveled (see Fig. 4.6a). Since slippage occurred, for example, with the glasses, visual monitoring was used in this case to readjust the control, i.e. to further tighten the rope gear.

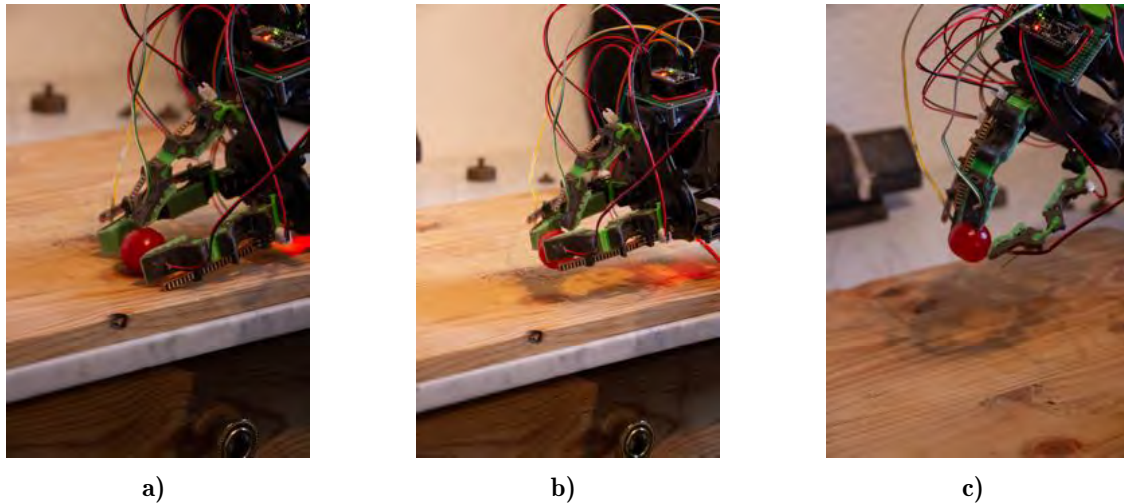


Figure 4.5: Soft Robotic Gripper performing the a) lateral tripod; b) lateral pinch and c) tripod grasp

As seen in Figure 4.5, the tomato is elevated by using the inverse adduction/abduction to change between Precision and Power Grasps.

Figure 4.6 provides an overview on sequences of a Medium Wrap. At first the gripper is aligned then closed step by step until the grasp is tough enough to lift the plastic cup.

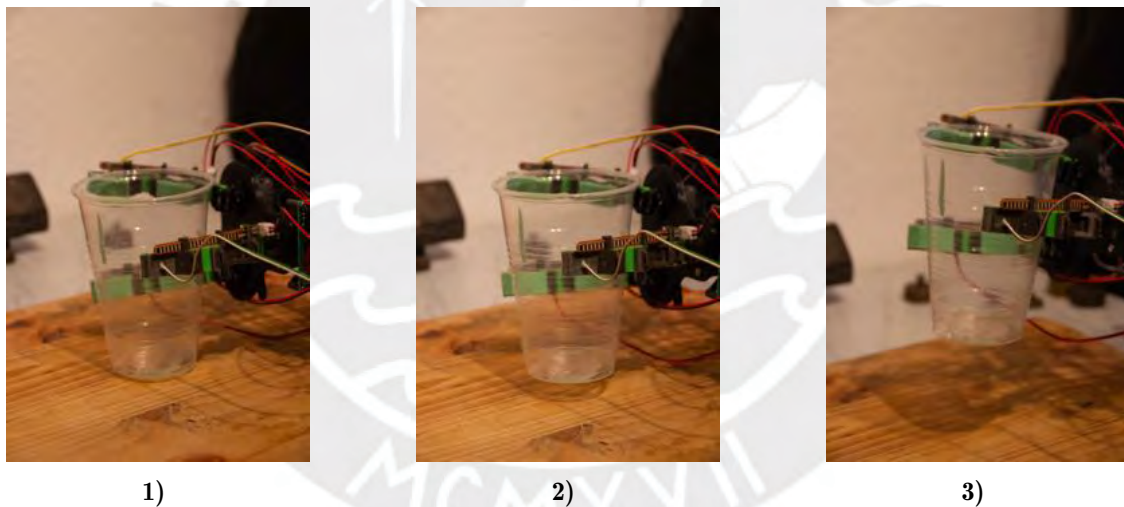


Figure 4.6: Sequences of a Medium Wrap during the manipulation of a plastic cup, chronological from 1) to 3)

4.3 Test of the Sensors during Grasping

Additional experiments were conducted to test the capabilities of the sensory system during active grasping. Figure 4.7 shows the curve of the force during the attempt to lift a shot glass from above. Since the gripper often slipped, it was always regripped.

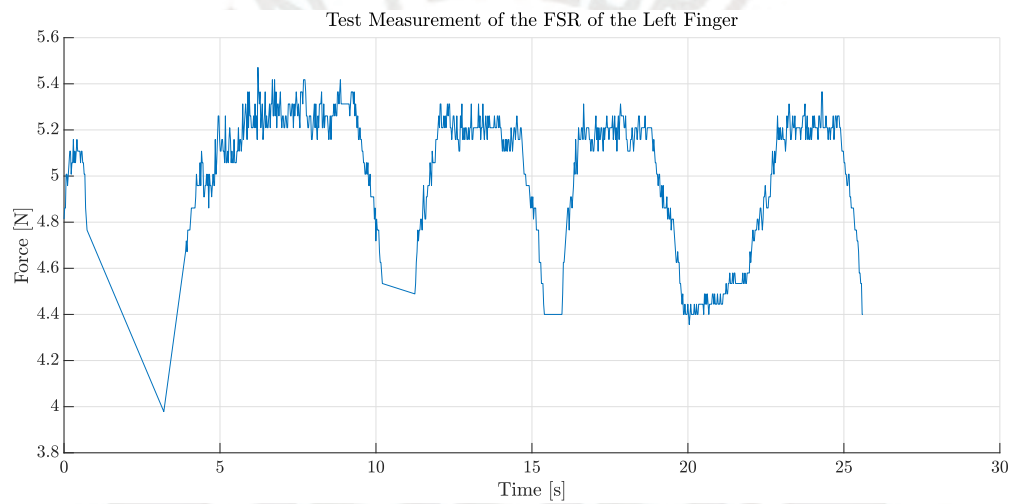


Figure 4.7: Curve of the Force of the FSR of the left finger while trying to grab a shot glass with a Medium Wrap

5 Evaluation of the Soft Robotic Gripper

The result of this work is a soft robotic gripper that enables the gripping of delicate, fragile objects. By implementing a sensor system consisting of force sensors in the form of FSRs, bending sensors and a current sensor, the system can be controlled. In addition to the sensor system, silicone rubber pads were used to provide better friction and adaptivity to the grasped object.

For measurement data analysis, a GUI was developed in MATLAB[®] to acquire, convert, visualize and store the raw data.

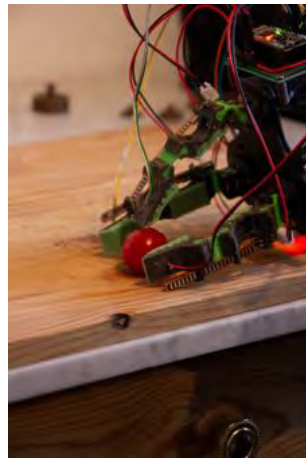
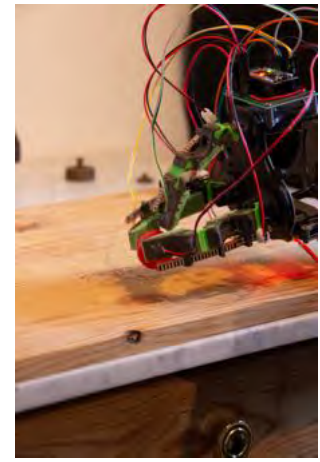
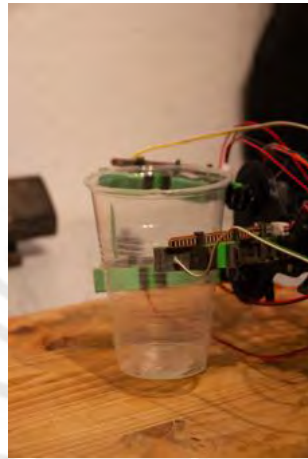
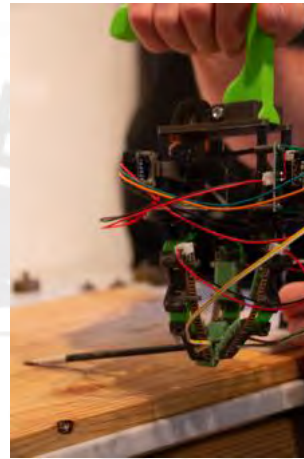
In the following, the implemented functions and the results of the practical experiments will be discussed further.

5.1 Evaluation of the Sensor Functionality

The preliminary tests of the sensor technology have shown that the sensors provide interpretable data and thus fulfill their purpose. This applies to the force and bending sensors and also the current sensor.

5.2 Evaluation of the Grasping Capabilities

The observations from the practical experiments show that the developed gripper has a good degree of adaptivity, as it can be adapted to numerous geometries. In addition to adaptivity, it also has a high degree of dexterity, with which it is even possible to manipulate small, light objects such as a tomato. The following Table 5.1 shows the types of grasps according to Feix et al. [Fei+16], which the developed gripper can handle.

**Tripod****Lateral Tripod****Palmar Pinch****Medium Wrap****Prismatic 2 Finger****Figure 5.1:** Prehensile capabilities of the Soft Robotic gripper

The practical experiments show that the manipulation of small, fragile objects works well, but effects like the roll-back phenomenon can occur (see Fig. 5.2).

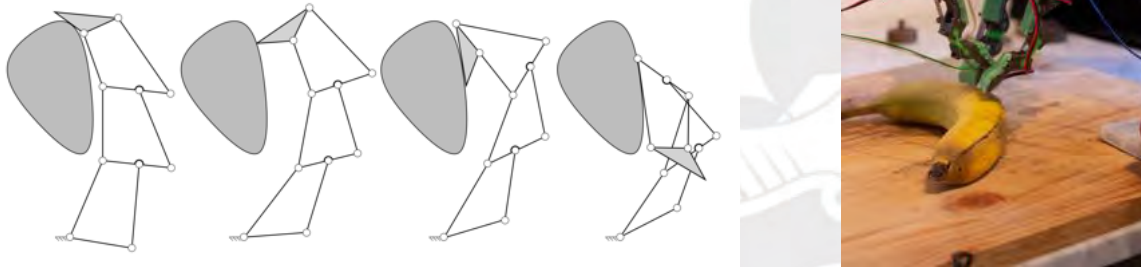


Figure 5.2: Roll-back Phenomenon during the grasp of a banana

6 Discussion

In the following chapter the achieved results of development of the Soft Robotic gripper will be discussed and successfully implemented requirements as well as points which can still be optimized will be discussed. In addition, possible causes for measurement inaccuracies will be discussed.

6.1 Design strengths and weaknesses

It was required to develop a Soft Robotic Gripper which is able to perform manipulation on fragile objects. With the help of compliant joints, adaptive contact surfaces and an underactuated tendon gear, this was achieved as far as possible.

This design allows, for example with the inverted adduction/abduction, the realization of numerous grip types, such as the medium wrap, the pinch or the power sphere.

The practical experiments show that the manipulation of small, fragile objects works well, but effects like the “roll-back phenomenon” can occur. During the design process, care was taken to ensure modularity so that components can be easily exchanged. Furthermore, the complete gripper is designed for rapid prototyping, except for the electrical components, so that it can be reproduced at will. In order to ensure as many types of gripping as possible.

The requirements for a low self-weight were taken into account as far as possible, but in the end the gripper was marginally heavier than originally anticipated.

During the practical tests it was observed that the sampling rate or the speed of the serial transmission is not very high. Thus, it is not possible to determine exactly how high the sampling rate is, since all data is only retrieved via polling.

During assembly, it became apparent that a great deal of dexterity was required when knotting the rope gear. When gripping heavy objects such as a large orange, it was noticed that the actuator force is not sufficient. However, this is also due to the high friction within the rigid bodies.

7 Conclusion and Outlook

In addition to improving the current design, there are other points of high interest. For example, an extension of the system that allows in-hand manipulation would be interesting. Regarding the sensory capabilities, an analysis of the shear forces would also be of interest to find the center of gravity of a grasped object.

With regard to the mechanical components, a refinement of the design is conceivable which, on the one hand, further reduces the overall weight and, on the other hand, improves the fit tolerances.

In view of the complicated assembly of the rope gear, it would be conceivable to integrate a tensioning mechanism to be able to adequately tension the respective tendon of each finger, like the one proposed by Gerez et al. [GL18]. Considering the rather simple electrical circuits, it would make sense to optimize the system. This includes the production of an own application specific circuit board as well as the use of more precise electrical components. For example, the measurement accuracy could be improved by using higher quality reference resistors in the FSRs circuit to provide more precise contact forces. In addition, it would be worth considering the use of measuring amplifiers (see [Int16]) and thus again increase the precision of the sensors. However, since analog values are still processed, the use of an analog-digital converter (ADC) with more than the standard 10-bit ADC of the Bluno Nano could also be considered.

Another goal could be to implement a control loop that precisely regulates the force. In combination with the position sensors and the current sensor it would be very interesting to test if it is possible to design the control to detect when an object is detected with sufficient force. This would make the manipulation much more active and further increase the level of dexterity.

Regarding the evaluation process, procedures such as AHAP [LH+19] or, regarding anthropomorphism, the procedure of Liarokapis et al. [LAK13] could be applied more completely. The last mentioned is a framework to quantify the anthropomorphism of a robotic gripper comparing the workspace of the finger phalanges and the workspace of the finger base frames, whereas Llop-Harillo et al. focus on both, anthropomorphism and functionality. The procedure uses the numerical Grasping Ability Score (GAS) to quantify the anthropomorphism and functionality of a gripper. This score is determined with the help of the publicly available *Yale-CMU-Berkeley Object and Model Set* and the grasp for the respective objects is analyzed and evaluated.

Bibliography

- [AIL85] Michael Anthony Arbib, Thea Iberall and Damian M. Lyons. “Coordinated control programs for movements of the hand”. In: *Hand Function and the Neocortex*. Ed. by Anthony W. Goodwin and Ian Darian-Smith. Vol. 10. Berlin: Springer-Verlag, 1985, pp. 111–129.
- [AIO21] Inc. AIO Robotics. *Premium PLA Filament*. Los Angeles, CA, USA, 2021.
- [All12] Allegro Microsystems Inc. *ACS714*. 2012.
- [Alt21] Yair Altman. *export_fig*. 2021. URL: https://github.com/altmany/export_fig/releases/tag/v3.14.
- [Aum+17] Gerhard Aumüller, Gabriela Aust, Jürgen Engele, Joachim Kirsch, Giovanni Maio, Artur Mayerhofer, Siegfried Mense, Dieter Reißig, Jürgen Salvetter, Wolfgang Schmidt, Frank Schmitz, Erik Schulte, Katharina Spänel-Borowski, Gunther Wennemuth, Werner Wolff, Laurenz J Wurzinger and Hans-gerhard Zilch. *Duale Reihe Anatomie*. Stuttgart: Georg Thieme Verlag, 2017.
- [BA07] Christopher Y. Brown and H. Harry Asada. “Inter-finger coordination and postural synergies in robot hands via mechanical implementation of principal components analysis”. In: *2007 IEEE/RSJ International Conference on Intelligent Robots and Systems*. IEEE, 2007, pp. 2877–2882.
- [BA92] Bryan Buchholz and Thomas J. Armstrong. “A kinematic model of the human hand to evaluate its prehensile capabilities”. In: *Journal of Biomechanics* 25.2 (1992), pp. 149–162.
- [BAG92] Bryan Buchholz, Thomas J. Armstrong and Steven A. Goldstein. “Anthropometric data for describing the kinematics of the human hand”. In: *Ergonomics* 35.3 (1992), pp. 261–273.
- [BBS01] Gabriel Baud-Bovy and John F. Soechting. “Two Virtual Fingers in the Control of the Tripod Grasp”. In: *Journal of Neurophysiology* 86.2 (2001), pp. 604–615.
- [BG06] Lionel Birglen and Clément M. Gosselin. “Force Analysis of Connected Differential Mechanisms: Application to Grasping”. In: *The International Journal of Robotics Research* 25.10 (2006), pp. 1033–1046.

- [BLG08] Lionel Birglen, Thierry Laliberté and Clément Gosselin. *Underactuated Robotic Hands*. Vol. 40. Springer Tracts in Advanced Robotics. Berlin, Heidelberg: Springer Berlin Heidelberg, 2008.
- [Boe+91] G. Boegelsack, F. J. Gierse, V. Oravsky, J. M. Prentis and A. Rossi. “Terminology for the theory of machines and mechanisms”. In: *Mechanism and Machine Theory* 26.5 (1991), pp. 435–539.
- [Bro+] Eric Brown, Nicholas Rodenberg, John Amend, Annan Mozeika, Erik Steltz, Mitchell R Zakin, Hod Lipson and Heinrich M Jaeger. “Universal robotic gripper based on the jamming of granular material”. In: ().
- [Che+20] Wenrui Chen, Zhilan Xiao, Jingwen Lu, Zilong Zhao and Yaonan Wang. “Design and Analysis of a Synergy-Inspired Three-Fingered Hand”. In: *2020 IEEE International Conference on Robotics and Automation (ICRA)*. Cmc. IEEE, 2020, pp. 8942–8948.
- [Cut89] M.R. Cutkosky. “On grasp choice, grasp models, and the design of hands for manufacturing tasks”. In: *IEEE Transactions on Robotics and Automation* 5.3 (1989), pp. 269–279.
- [CXY15] Wenbin Chen, Caihua Xiong and Shigang Yue. “Mechanical Implementation of Kinematic Synergy for Continual Grasping Generation of Anthropomorphic Hand”. In: *IEEE/ASME Transactions on Mechatronics* 20.3 (2015), pp. 1249–1263.
- [DB14] Raphael Deimel and Oliver Brock. “A Novel Type of Compliant, Underactuated Robotic Hand for Dexterous Grasping”. In: *Robotics: Science and Systems X*. Robotics: Science and Systems Foundation, 2014.
- [Det18] DetasFLEX. *Version*. Ilmenau, TH, Germany: Compliant Systems Group, 2018.
- [DH10] Aaron M Dollar and Robert D Howe. “The Highly Adaptive SDM Hand: Design and Performance Evaluation”. In: *The International Journal of Robotics Research* 29.5 (2010), pp. 585–597.
- [Ear19] Bill Earl. *Adafruit PCA9685 16-Channel Servo Driver*. New York, NY, USA: Adafruit Industries LLC, 2019, pp. 1–36.
- [FBD14] Thomas Feix, Ian M. Bullock and Aaron M. Dollar. “Analysis of Human Grasping Behavior: Object Characteristics and Grasp Type”. In: *IEEE Transactions on Haptics* 7.3 (2014), pp. 311–323.
- [Fei+09] Thomas Feix, Roland Pawlik, Heinz-Bodo Schmiedmayer, Javier Romero and Danica Kragi. “A comprehensive grasp taxonomy”. In: *Robotics, Science and Systems Conference: Workshop on Understanding the Human Hand for Advancing Robotic Manipulation* (2009), pp. 2–3.

- [Fei+16] Thomas Feix, Javier Romero, Heinz-Bodo Schmedmayer, Aaron M. Dollar and Danica Kragic. “The GRASP Taxonomy of Human Grasp Types”. In: *IEEE Transactions on Human-Machine Systems* 46.1 (2016), pp. 66–77.
- [Fes13] Festo SE & CO. *MultiChoiceGripper*. 2013. URL: <https://www.festo.com/group/en/cms/10221.htm>.
- [Fri21] Fritzing. *Version 0.9.6*. Berlin, Germany: Fritzing GmbH, 2021.
- [Gab+11] M. Gabiccini, A. Bicchi, D. Prattichizzo and M. Malvezzi. “On the role of hand synergies in the optimal choice of grasping forces”. In: *Autonomous Robots* 31.2-3 (2011), pp. 235–252.
- [GC06] Reinhard Gentner and Joseph Classen. “Modular Organization of Finger Movements by the Human Central Nervous System”. In: *Neuron* 52.4 (2006), pp. 731–742.
- [Ger+17] Giada Gerboni, Alessandro Diodato, Gastone Ciuti, Matteo Cianchetti and Arianna Menciassi. “Feedback Control of Soft Robot Actuators via Commercial Flex Bend Sensors”. In: *IEEE/ASME Transactions on Mechatronics* 22.4 (2017), pp. 1881–1888.
- [GL18] Lucas Gerez and Minas Liarokapis. “A Compact Ratchet Clutch Mechanism for Fine Tendon Termination and Adjustment”. In: *2018 IEEE/ASME International Conference on Advanced Intelligent Mechatronics (AIM)*. Vol. 2018-July. IEEE, 2018, pp. 1390–1395.
- [Her18] Ekbert Hering. *Sensoren in Wissenschaft und Technik*. Ed. by Ekbert Hering and Gert Schönfelder. Wiesbaden: Springer Fachmedien Wiesbaden, 2018.
- [HFA97] J E Huber, N A Fleck and M F Ashby. “The selection of mechanical actuators based on performance indices”. In: *Proceedings of the Royal Society of London. Series A: Mathematical, Physical and Engineering Sciences* 453.1965 (1997), pp. 2185–2205.
- [HLB16] William M. Haynes, David R. Lide and Thomas J. Bruno, eds. *Handbook of Chemistry and Physics*. 97th ed. Boca Raton: CRC Press, 2016.
- [HLZ18] Stefan Henning, Sebastian Linß and Lena Zentner. “detasFLEX – A computational design tool for the analysis of various notch flexure hinges based on non-linear modeling”. In: *Mechanical Sciences* 9.2 (2018), pp. 389–404.
- [Hus+17] Irfan Hussain, Gionata Salvietti, Monica Malvezzi and Domenico Prattichizzo. “On the role of stiffness design for fingertip trajectories of underactuated modular soft hands”. In: *2017 IEEE International Conference on Robotics and Automation (ICRA)*. IEEE, 2017, pp. 3096–3101.
- [Ibe87] Thea Iberall. “GRASP PLANNING FOR HUMAN PREHENSION”. In: *Proceedings of the 10th international joint conference on Artificial intelligence 2* (1987), pp. 1153–1156.

- [Ing+08] James N Ingram, Konrad P Kording, Ian S Howard and Daniel M Wolpert. “The statistics of natural hand movements”. In: *Experimental Brain Research* 188.2 (2008), pp. 223–236.
- [Int15] Interlink Electronics. *FSR® 400 Series Data Sheet Human - Machine Interface Solutions for a Connected World FSR ® 400 Series Data Sheet*. 2015. URL: www.interlinkelectronics.com.
- [Int16] Interlink Electronics. “FSR®Integration Guide”. In: (2016).
- [Inv18] Inventor Professional. *Version 2019.4.2*. San Rafael, CA, USA: Autodesk Corp., 2018.
- [Kap74] Ibranim Adalbert Kapandji. *The Physiology of the Joints: Upper Limb*. 1974.
- [KLV19] George P. Kontoudis, Minas Liarokapis and Kyriakos G. Vamvoudakis. “An Adaptive, Humanlike Robot Hand with Selective Interdigitation: Towards Robust Grasping and Dexterous, In-Hand Manipulation”. In: *2019 IEEE-RAS 19th International Conference on Humanoid Robots (Humanoids)*. IEEE, 2019, pp. 251–258.
- [LAK13] Minas V. Liarokapis, Panagiotis K. Artemiadis and Kostas J. Kyriakopoulos. “Quantifying anthropomorphism of robot hands”. In: *2013 IEEE International Conference on Robotics and Automation*. IEEE, 2013, pp. 2041–2046.
- [Lan96] Gordon B. Langford. “Flexible Potentiometer”. Pat. 1996.
- [Lat08] Mark L Latash. *Synergy*. Oxford University Press, 2008.
- [LFL13] Chia-Hsien Lin, Jeremy A. Fishel and Gerald E. Loeb. “Estimating Point of Contact , Force and Torque in a Biomimetic Tactile Sensor with Deformable Skin”. In: (2013), p. 6.
- [LH+19] Immaculada Llop-Harillo, Antonio Pérez-González, Julia Starke and Tamim Asfour. “The Anthropomorphic Hand Assessment Protocol (AHAP)”. In: *Robotics and Autonomous Systems* 121 (2019), p. 103259.
- [Mas18] Matthew T. Mason. “Toward Robotic Manipulation”. In: *Annual Review of Control, Robotics, and Autonomous Systems* 1.1 (2018), pp. 1–28.
- [MAT19] MATLAB. *Version 9.7.0.1190202 (R2019b)*. Natick, MA, USA: The MathWorks Inc., 2019.
- [MBD15] Raymond R. Ma, Joseph T. Belter and Aaron M. Dollar. “Hybrid Deposition Manufacturing: Design Strategies for Multimaterial Mechanisms Via Three-Dimensional Printing and Material Deposition”. In: *Journal of Mechanisms and Robotics* 7.2 (2015), pp. 1–10.

- [MD14] Raymond R. Ma and Aaron M. Dollar. “An underactuated hand for efficient finger-gaiting-based dexterous manipulation”. In: *2014 IEEE International Conference on Robotics and Biomimetics (ROBIO 2014)*. IEEE, 2014, pp. 2214–2219.
- [MD17] Raymond Ma and Aaron Dollar. “Yale OpenHand Project: Optimizing Open-Source Hand Designs for Ease of Fabrication and Adoption”. In: *IEEE Robotics & Automation Magazine* 24.1 (2017), pp. 32–40.
- [Men+12] Yiğit Mengüç, Sang Yoon Yang, Seok Kim, John A. Rogers and Metin Sitti. “Gecko-Inspired Controllable Adhesive Structures Applied to Micromanipulation”. In: *Advanced Functional Materials* 22.6 (2012), pp. 1246–1254.
- [MI94] Christine L. MacKenzie and Thea Iberall. *The Grasping Hand*. 1st ed. Vol. 104. Amsterdam: North-Holland, 1994.
- [Mic20] Microbot. *Linear Current Sensor*. 2020. URL: microbot.it.
- [MLS94] Richard M. Murray, Zexiang Li and S. Shankar Sastry. *A Mathematical Introduction to Robotic Manipulation*. CRC Press, 1994, p. 480.
- [MOD13] Raymond R. Ma, Lael U. Odhner and Aaron M. Dollar. “A modular, open-source 3D printed underactuated hand”. In: *Proceedings - IEEE International Conference on Robotics and Automation* (2013), pp. 2737–2743.
- [MR17] Wolfgang Mathis and Albrecht Reibiger. *Küpfmüller Theoretische Elektrotechnik*. Berlin, Heidelberg: Springer Berlin Heidelberg, 2017.
- [MSD16] Raymond R. Ma, Adam Spiers and Aaron M. Dollar. “M2 Gripper: Extending the Dexterity of a Simple, Underactuated Gripper”. In: *Advances in Reconfigurable Mechanisms and Robots II*. Ed. by Xilun Ding, Xianwen Kong and Jian S. Dai. Vol. 36. Cham: Springer International Publishing, 2016, pp. 795–805.
- [Nak+02] Hiroyuki Nakai, Yasuo Kuniyoshi, Masayuki Inaba and Hirochika Inoue. “Metamorphic robot made of low melting point alloy”. In: *IEEE/RSJ International Conference on Intelligent Robots and System*. Vol. 2. October. IEEE, 2002, pp. 2025–2030.
- [Nin16] NinjaTek. “NinjaFlex® 3D Printing Filament: Flexible Polyurethane Material for FDM Printers”. In: (2016), p. 1.
- [Nos12] Danny Nosonowitz. *Using an FSR | Force Sensitive Resistor (FSR) | Adafruit Learning System*. 2012. URL: <https://learn.adafruit.com/force-sensitive-resistor-fsr/using-an-fsr> (visited on 02/05/2021).
- [NR97] James S. Neely and Phillip J. Restle. “Capacitive Bend Sensor”. Pat. 1997.
- [Odh+14] Lael U. Odhner, Leif P. Jentoft, Mark R. Claffee, Nicholas Corson, Yaroslav Tenzer, Raymond R. Ma, Martin Buehler, Robert Kohout, Robert D. Howe and Aaron M. Dollar. “A compliant, underactuated hand for robust manipulation”. In: *The International Journal of Robotics Research* 33.5 (2014), pp. 736–752.

- [OMD13] Lael U. Odhner, Raymond R. Ma and Aaron M. Dollar. “Open-Loop Precision Grasping With Underactuated Hands Inspired by a Human Manipulation Strategy”. In: *IEEE Transactions on Automation Science and Engineering* 10.3 (2013), pp. 625–633.
- [Pau+14] Heinrich Paul, Josef Binder, Helmut Bäumel, Thomas Kleckers, Michael Horn and Fabian Höflinger. *Sensortechnik*. Ed. by Hans-Rolf Tränkler and Leo Reindl. VDI-Buch. Berlin, Heidelberg: Springer Berlin Heidelberg, 2014.
- [PCP99] J.L. Pons, R. Ceres and F. Pfeiffer. “Multifingered dextrous robotics hand design and control: a review”. In: *Robotica* 17.6 (1999), pp. 661–674.
- [Pet+10] A. Pettersson, S. Davis, J.O. Gray, T.J. Dodd and T. Ohlsson. “Design of a magnetorheological robot gripper for handling of delicate food products with varying shapes”. In: *Journal of Food Engineering* 98.3 (2010), pp. 332–338.
- [Pla21] PlatformIO. *Version 5.1.1*. PlatformIO labs, 2021.
- [SCD18] Adam J. Spiers, Berk Calli and Aaron M. Dollar. “Variable-Friction Finger Surfaces to Enable Within-Hand Manipulation via Gripping and Sliding”. In: *IEEE Robotics and Automation Letters* 3.4 (2018), pp. 4116–4123.
- [SFS98] Marco Santello, Martha Flanders and John F Soechting. “Postural Hand Synergies for Tool Use”. In: *The Journal of Neuroscience* 18.23 (1998), pp. 10105–10115.
- [SG96] K.B. Shimoga and A.A. Goldenberg. “Soft Robotic Fingertips”. In: *The International Journal of Robotics Research* 15.4 (1996), pp. 320–334.
- [She] Shenzhen Feetech RC Model Co. Ltd. *Feetech FT90M-FB*. Shenzhen, China.
- [Shi+16] Jun Shintake, Samuel Rosset, Bryan Schubert, Dario Floreano and Herbert Shea. “Versatile Soft Grippers with Intrinsic Electroadhesion Based on Multifunctional Polymer Actuators”. In: *Advanced Materials* 28.2 (2016), pp. 231–238.
- [Shi+18] Jun Shintake, Vito Cacucciolo, Dario Floreano and Herbert Shea. “Soft Robotic Grippers”. In: *Advanced Materials* 30.29 (2018), p. 1707035.
- [SJJ16] Amirul Syafiq Sadun, Jamaludin Jalani and Faizal Jamil. “Grasping analysis for a 3-Finger Adaptive Robot Gripper”. In: *2016 2nd IEEE International Symposium on Robotics and Manufacturing Automation (ROMA)*. September. IEEE, 2016, pp. 1–6.
- [SN17] Alapati Sreejan and Yeole Shivraj Narayan. “A review on applications of flex sensors”. In: *International Journal of Emerging Technology and Advanced Engineering* 7 (2017), pp. 97–100.
- [Spe20] Spectra Symbol. *Flex Sensor - Data Sheet*. 2020. URL: spectrasymbol.com.
- [SSS14] Michael Schünke, Erik Schulte and Udo Schumacher, eds. *Allgemeine Anatomie und Bewegungssystem*. Stuttgart: Georg Thieme Verlag, 2014.

- [Taw+19] Charbel Tawk, Andrew Gillett, Marc in het Panhuis, Geoffrey M. Spinks and Gursel Alici. “A 3D-Printed Omni-Purpose Soft Gripper”. In: *IEEE Transactions on Robotics* 35.5 (2019), pp. 1268–1275.
- [Tow00] William Townsend. “The BarrettHand grasper – programmably flexible part handling and assembly”. In: *Industrial Robot: An International Journal* 27.3 (2000), pp. 181–188.
- [Ult21] Ultimaker Cura. *Version 4.9.0*. Utrecht, ED, Netherlands: Ultimaker BV., 2021.
- [VDI04] VDI 2206. “Design methodology for mechatronic systems”. In: *VDI Richtlinien* Juni (2004).
- [VDI19a] VDI 2221 - Part 1. “Design of technical products and systems Model of product design”. In: *VDI Richtlinien* November (2019).
- [VDI19b] VDI 2221 - Part 2. “Design of technical products and systems Configuration of individual product design processes”. In: *VDI Richtlinien* November (2019).
- [Vis21] Visual Studio Code. *Version 1.54.3*. Redmond, WA, USA: Microsoft Corp., 2021.
- [Vol78] Johannes Volmer, ed. *Getriebetechnik*. Wiesbaden: Vieweg+Teubner Verlag, 1978.
- [Wag21] Wagner Dental GmbH & Co. KG. *WAGNERSIL 20 NF Premium Dubliersilikon*. Hückelhoven, NRW, DE, 2021.
- [Wan+17] Wei Wang, Nam-Geuk Kim, Hugo Rodrigue and Sung-Hoon Ahn. “Modular assembly of soft deployable structures and robots”. In: *Materials Horizons* 4.3 (2017), pp. 367–376.
- [XDM11] Zhe Xu, Brian Dellon and Yoky Matsuoka. “Design of artificial skin with integrated tactile sensors for anthropomorphic robotic hands”. In: *2011 IEEE International Conference on Robotics and Biomimetics*. IEEE, 2011, pp. 2919–2924.
- [Xio+16] Cai-Hua Xiong, Wen-Rui Chen, Bai-Yang Sun, Ming-Jin Liu, Shi-Gang Yue and Wen-Bin Chen. “Design and Implementation of an Anthropomorphic Hand for Replicating Human Grasping Functions”. In: *IEEE Transactions on Robotics* 32.3 (2016), pp. 652–671.
- [XT16] Zhe Xu and Emanuel Todorov. “Design of a highly biomimetic anthropomorphic robotic hand towards artificial limb regeneration”. In: *2016 IEEE International Conference on Robotics and Automation (ICRA)*. IEEE, 2016, pp. 3485–3492.
- [Xu+14] Kai Xu, Huan Liu, Yuheng Du, Xinjun Sheng and Xiangyang Zhu. “Mechanical implementation of postural synergies using a simple continuum mechanism”. In: *2014 IEEE International Conference on Robotics and Automation (ICRA)*. IEEE, 2014, pp. 1348–1353.
- [Yal] Yale OpenHand Project. *Yale OpenHand Project*. URL: <https://www.eng.yale.edu/grablab/openhand/>.

- [YP97] Stuart I. Yaninger and Mark C. Pickett. “Force-sensing pointing device”. Pat. 1997.
- [Zen14] Lena Zentner. *Nachgiebige Mechanismen*. München: De Gruyter Oldenbourg, 2014.
- [Zie+09] Silvio Ziegler, Robert C. Woodward, Herbert Ho-Ching Iu and Lawrence J. Borle. “Current Sensing Techniques: A Review”. In: *IEEE Sensors Journal* 9.4 (2009), pp. 354–376.
- [Zim82] Thomas G. Zimmerman. “Optical Flex Sensor Pattern”. Pat. 1982.
- [Zis+14] Agisilaos G Zisimatos, Minas V Liarokapis, Christoforos I Mavrogiannis and Kostas J Kyriakopoulos. “Open-source, affordable, modular, light-weight, underactuated robot hands”. In: *2014 IEEE/RSJ International Conference on Intelligent Robots and Systems*. Iros. IEEE, 2014, pp. 3207–3212.
- [ZL19] Lena Zentner and Sebastian Linß. *Compliant systems*. Berlin, Boston: De Gruyter, 2019.



A Appendix

A.1 Complementary Sections

A.1.1 Calibration of the Flex Sensor

In order to obtain conclusions about the deflection angle with the help of the flex sensors, a referencing was carried out. The flex sensor was clamped and gradually bent more (5° steps). The inclination was adjusted visually by means of an angle disc, as seen in Figure A.1 from 0° to 110°. Apart from the referencing directly with the measured time t_{RC} , the electrical

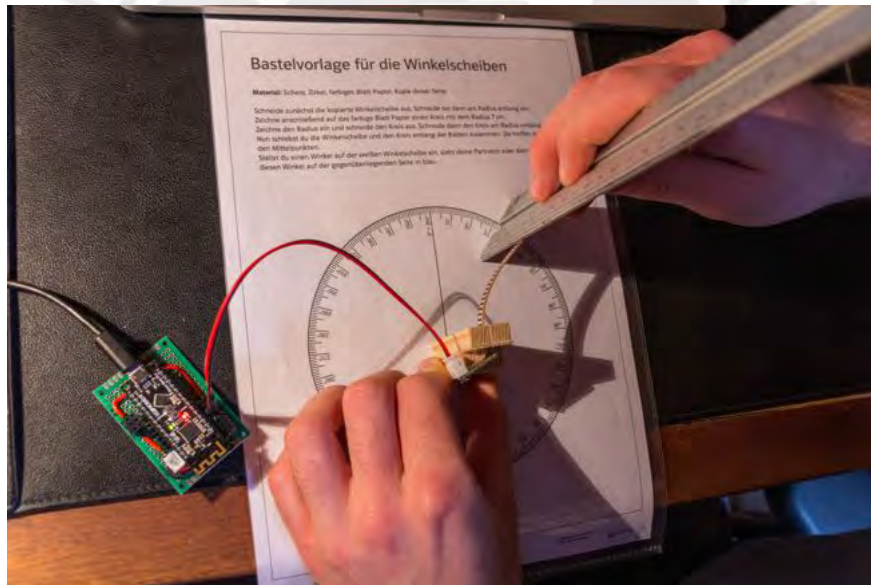


Figure A.1: Referencing of the flex sensor with an angle disc

resistances depending on the angle of deflection was measured (Fig. ??). The application of the “Basic Fitting Tool” provided the following equation.

$$\varphi = 1.7232 \cdot \varphi_{bit} - 31.873 \quad (\text{A.1})$$

Compared to the former results of the referencing with the RC-circuit, Equation 3.4, the norm of residuals is slightly higher ($r_R = 23.532$ vs. $r_{RC} = 17.242$).

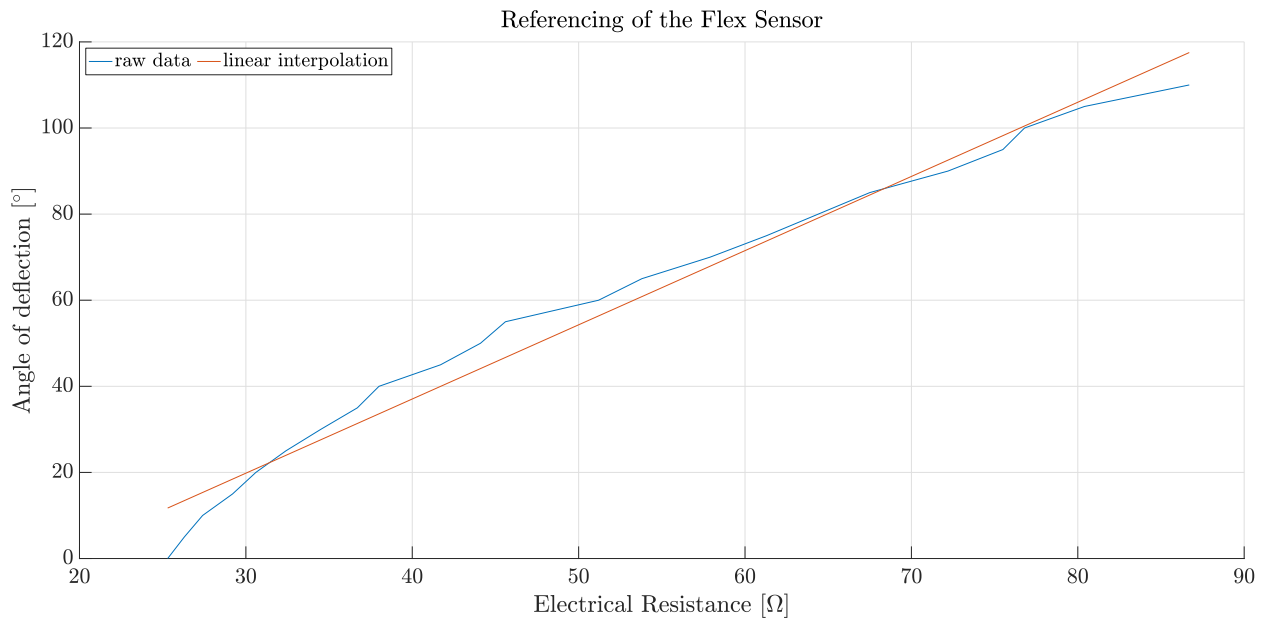


Figure A.2: Calibration of the flex sensors with a MS8233C digital multimeter (MASTECH® , Plovdiv, Bulgaria)

A.1.2 Calibration of the Force Sensor

As previously described in Section 3.3.4, the force sensor was calibrated using water as the reference weight. Here, the density of water at room temperature (296 K) was determined with $\rho_{H_2O} = 997.532 \frac{\text{kg}}{\text{m}^3}$. Based on the density the weight was calculated with $g = 9.80665 \frac{\text{m}}{\text{s}^2}$ [Pau+14, p. 493]. As drawn in the technical principle (Fig. A.3), the FSR was loaded by a

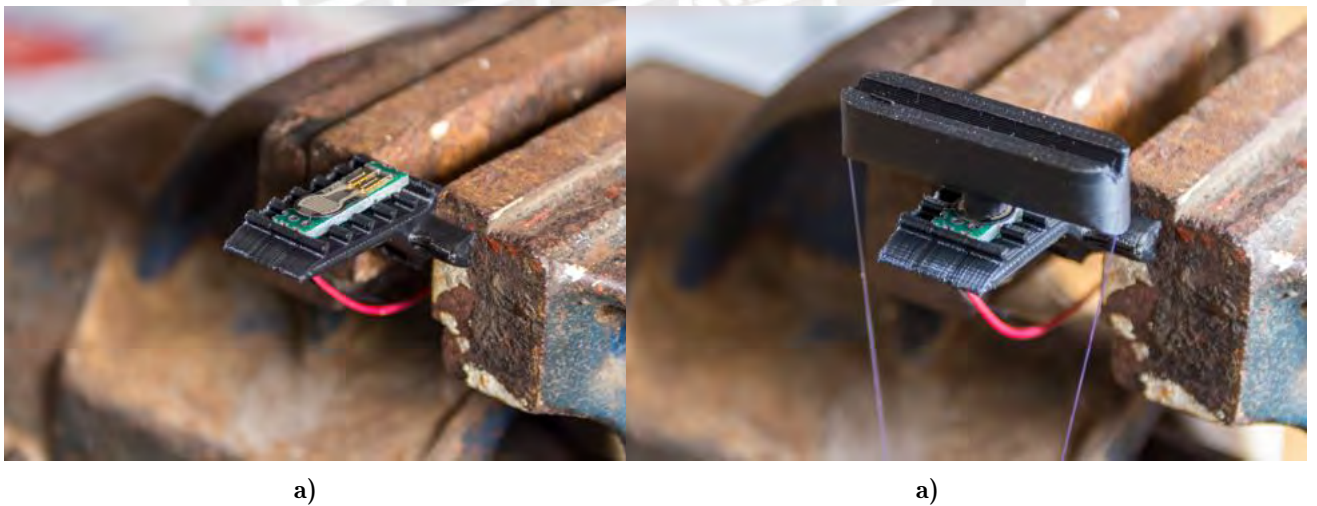


Figure A.3: Setup of the calibration by means of a beam with a flat contact surface for optimum loading of the active zone of the FSR

bucket that was constantly filled with water.



Figure A.4: Dorsal view of the calibration setup

A.2 Complementary Figures

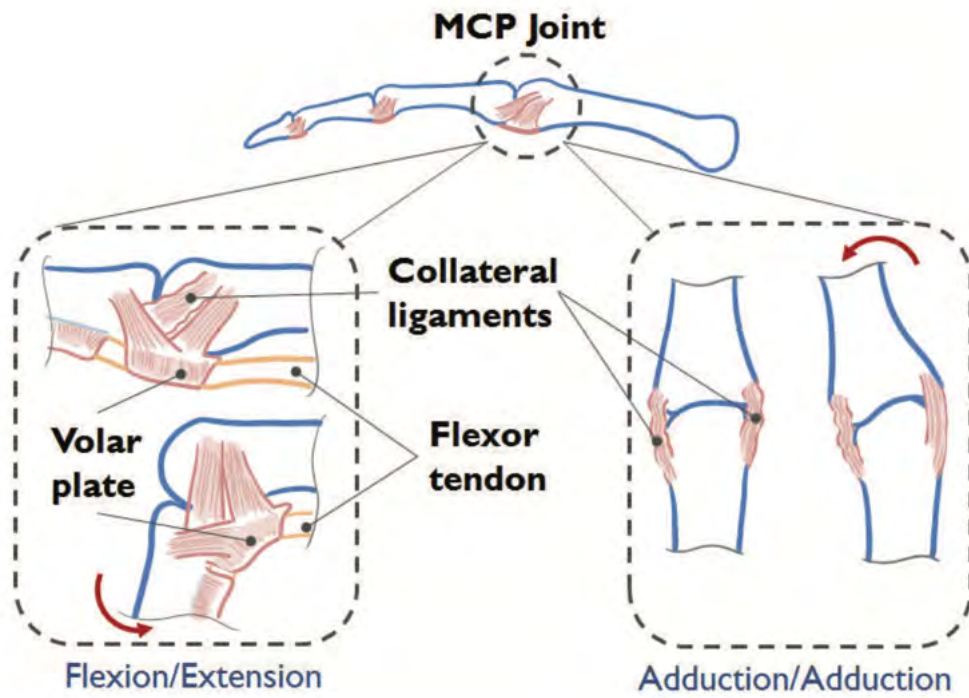


Figure A.5: Schematic drawing of the collateral ligaments and volar plate at the MCP joint [XT16, p. 3488]

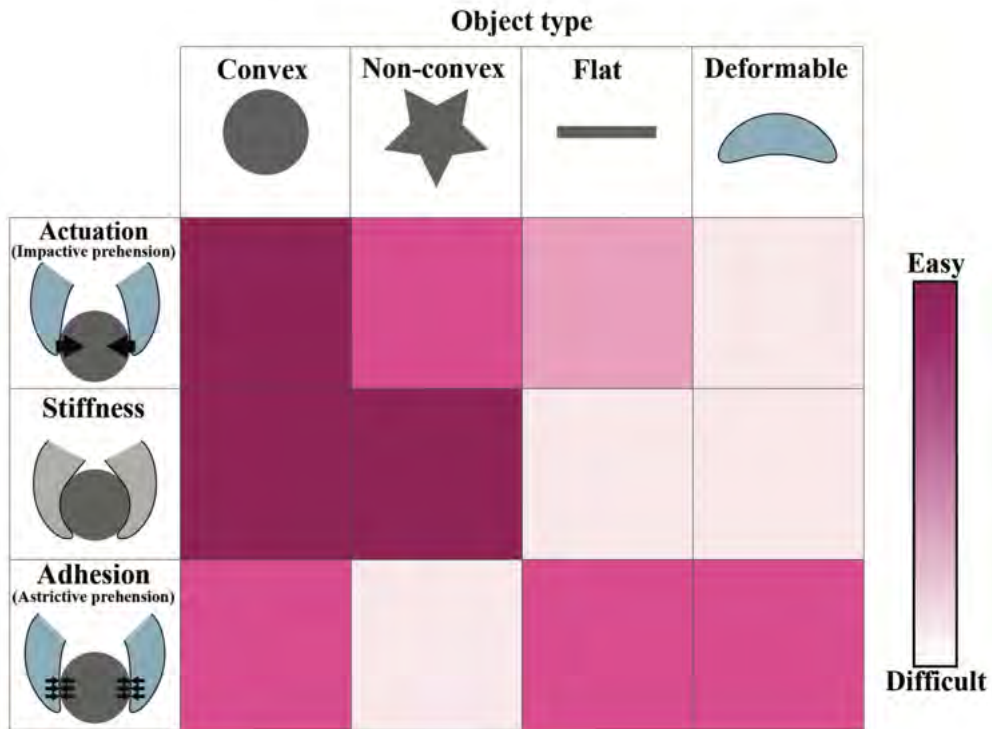


Figure A.6: Classification of gripping technologies in relation to different object geometries [Shi+16]

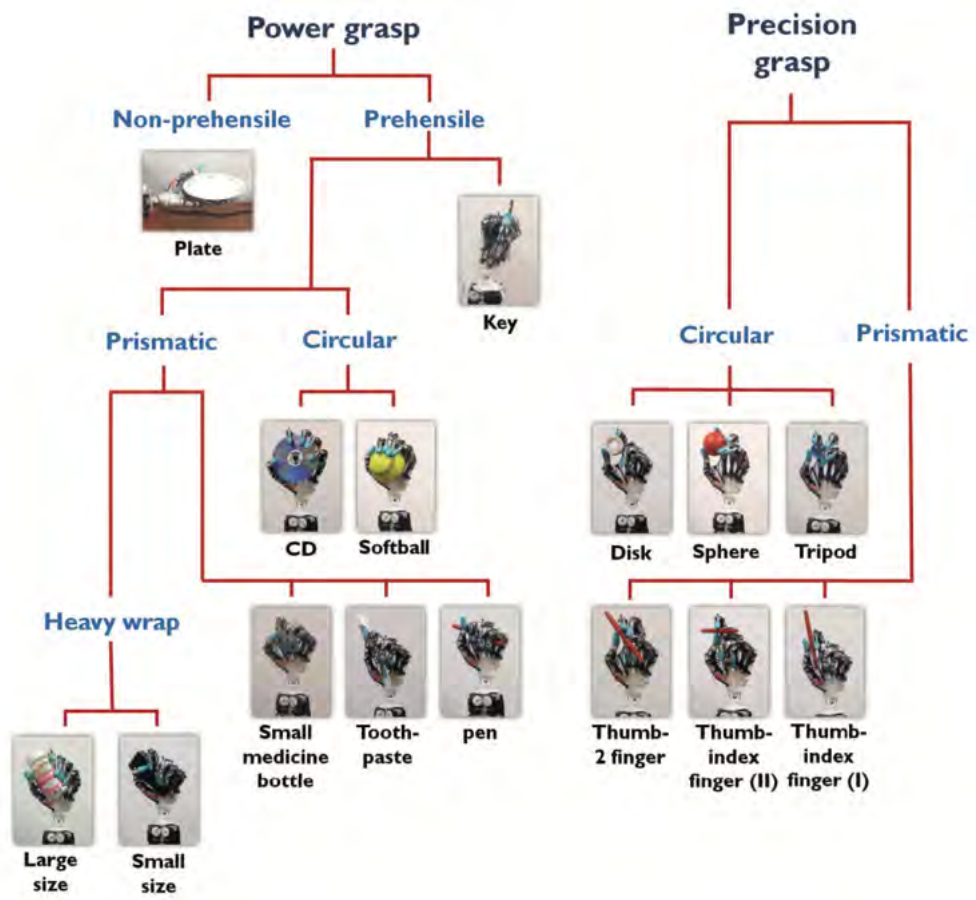


Figure A.7: Taxonomy realized by the anthropomorphic hand by Xu et al. [XT16]

A.3 Complementary Tables

A.3.1 List of Requirements



Description					
Description		Priority	Numeric		Comment
			min	max	
Functional Properties					
Soft Grasping of fragile objects		H			Tomatos, eggs etc.
Controlled force application		H			Characterization of force control
Reduction of the influence of rigid manipulation		H			Adaptive finger tips, compliant structures
Perform various grasp types		H			Grasps from the GRASP Taxonomy by Feix et. al.
Grasped objects size		M	LxWxH: 20 x 20 x 40 [cm]		Diameter 30mm
Size		D		LxWxH: 20 x 10 x 10 [cm]	Adequate size in relation to Braccio arm, scalable
Weight		D		150 [g]	Weight depending on the Tinkerkit Braccio robot arm, as lightweight as possible
Payload		M	20 [g]		E.g. Roma Tomato
Grip force		M	1 [N]		In relation to minimum payload
Grasping time		M	$t \leq 2s$		Time to grasp an object once in loading position
Release time		M	$t \leq 2s$		Time to release the grasped object
Mechanical Design					
Human inspired		H			Anthropomorphic, 3 Phalanges with tendon
Scalable		D			Possibility to fabricate the same mechanism smaller/bigger
Number of fingers		M	2		
Degrees of Freedom		M	3		
Modular		D			
Coupling points					
Joint design	Extension/flexion possible	M			
	Compensation of radial forces	M			Forces by lifting an object
	Compensation of axial forces	D			No lateral movement of the fingers
Low friction joints		D			E.g. leightweight ball bearings
Low backlash joints		D			E.g. compliant joints
Low-slip contact points		M			Human like skin, for higher friction contact with the tips

Description					
Description		Priority	Numeric		Comment
			min	max	
Number of purchased parts		D	30%		(without screws, nuts, washers,...)
Adaptive		M			Soft finger tips
Force transmission					
Tendon driven		H			E.g. cables, belt..
Holding force/torque		M			Self-locking mechanism e.g. to hold without powered motor to save energy
Routed tendons		M			E.g. Pulleys, sheaths..
Antagonistic		D			E.g. with springs or other cables
Tendon terminaton	Fixed	M			E.g. Knot
	Adjustable	D			E.g. ratchet mechanism
Protected tendons		D			Sheaths leading the cables to reduce the friction, dowels
Actuator(s)					
Speed range		D			
Torque range		M			
Output		M	5 [W]		
Motor driver	Analog	M			
	Digital	D			
Control loop	Open	M			
	Closed	D			
Simultaneous use of components		M			Ability to read data while the effector is moving
Control System					
Switching on/off Motor(s)		M			
Variable speed		D			Control of the grasping speed
Force Control		H			
Position control		D			Servo etc.
Sensors					
Measured parameter					

Description					
Description		Priority	Numeric		Comment
			min	max	
Force/Pressure		H	Accuracy: 5 %	Accuracy: 0.05 %	Exteroception
Finger Position	Relative	M	Accuracy: 5 %	Accuracy: 0.05 %	Proprioception
	Absolute	D			
Current		D	Accuracy: 5 %	Accuracy: 0.05 %	To calculate the motor's torque
Measuring unit					
Continuous reception of sensor data		M	100 [Hz]		Sampling rate
Signal Processing		M			ADC/DAC, amplifier, calculations etc.
Analog Inputs		M			Force Sensors (3), Position Sensors (3)
Digital Inputs		M			
Communication Bus		D			E.g. I2C
Feedback					
Output of calculations and measured values	Simultaneous	M		5 [s]	E.g. to Computer, LEDs,...
	After	D	1 [s]	3 [s]	
Feedback to user if used falsely used	Simultaneous	D		5 [s]	
	After	D		1 [s]	
Human Machine Interface					
Input	Vor der Messung	M			
	Simultaneous	D	0,1 [s]	1 [s]	
Control of the finger position		M			Joystick to close/loosen the grasp
Power Supply					
Portable Battery		D			higher mobility of the gripper
Only one power source		D			
Assembly					
Modular structure	Actuation	D			if necessary gearbox can be attached

Description					
Description		Priority	Numeric		Comment
			min	max	
Modular structure	Mechanical Parts (frame etc.)	D			
Use of product families for actuators		D			if necessary: replacement of parts by similar part by the same supplier
Use of product families for sensors		D			if necessary: replacement of parts by similar part by the same supplier
Easy to assemble (without special tools)		D			common screws etc.
No extensive calibration		D			Sensors etc.
Attachable to robot arms		H			experiments with robot arm
Maintenance/Reparation					
Accessibility of wearing parts		M			Quick and easy reach of wearing parts
Easy cleaning		D			i.e. openable case
Simple maintenance		D	0	30	Duration of the maintenance
Availability of spare parts		D			sensors, motors etc. special parts reproducably
Marking of maintenance parts		D			Visability of spare parts (coloured)
Maximum number of lubrication points		D	0	8	Bearings, retainer etc.
Safety					
No open cables / contacts		M			IP 54B according to ISO 20653, Protected against dust in harmful quantities, Complete protection against tangency, protection against splashing water from all sides, protected against access to dangerous active parts with fingers
Electrical isolation		D			DIN EN 60204-1:2014-10
Safety of control elements		D			EN ISO 13849-1
No sharp edges		D			DIN ISO 13735
Emergency stop button		D			DIN EN ISO 13850:2016-05
Noise emission		D			Noise exposure below the pain level, <80dB(A) (DIN EN ISO 11690 Teil 1)
Lockable if not used		D			manually resp. electrically activated

Description					
Description		Priority	Numeric		Comment
			min	max	
Locking the moving parts of the machine		D			während Wartung/Rüsten
Splash water and dust protection		D			DIN EN 60529: IP54
No safety gear for user		D			
Colour safety-related parts		M			DIN EN ISO 7010, ISO 3864-4, RAL-F14 colour index, (Emergency stop button etc.)
Grounding	total	D			
	Case	M			
	electrical components	M			
Evaluation					
Characterization of the developed gripper		M			
Assembly					
Connections can be disconnected easily		D			Connections can be separated and reconnected (without unscrewing)
Unambiguous plug connections		D			
Miscellaneous					
Overall Costs		D		150€	
Legend					
				H	Hard Requirement
				D	Desired Requirement
				M	Minimum Requirement

A.3.2 Solution Concepts

Basic Concept	1. Variation Criterion	2. Variation Criterion	Comment
Force Transmission	Printed Tendon		
	Cable	Flexible Rigid	
Cable Protection	None		
	Sheath	Entire Partial	Additional stiffness Possibility of tangency
	Pulley		
	Sheath		
Tendon termination	Pulley & Sheath		
	Fixed	Clamp Knot	see Gerez2018
	Adjustable	Ratchet mechanism Clamp	
Tendon guiding	None		
	Pulleys		
	Dowel pin		Easy to assemble, light
	Sheath		
Actuation mechanism	Rotatory	Pulley Tooth gear mechanism	
	Translatory	Tooth bar with worm drive	
Joints	Ball bearing		Expensive, more assembly effort
	Plain bearing		Higher friction see Zentner2019
	Rigid-body mechanism	Concentrated compliance Distributed compliance	
Location of the Position Sensors	Joint		
	MCP joint (root)		

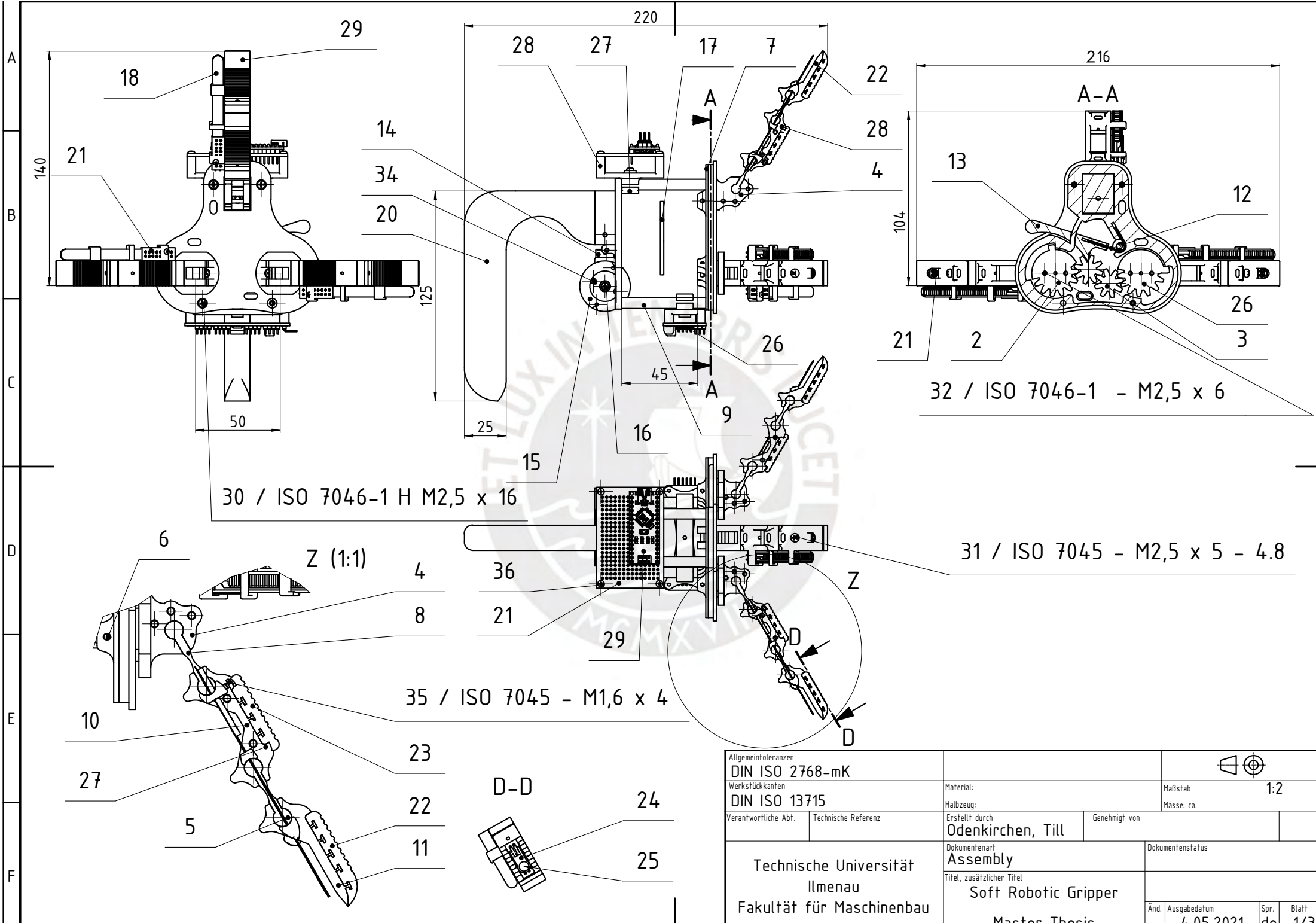


A.3.3 Evaluation Matrices

Determination of the Position	Weight	Rotary position sensor				Deflection		Comment
		Ideal solution	Points achieved	total	Points achieved	total		
Evaluation Criterion	g	g*P _i	P	g*P	P	g*P		
Resolution	2	4	1	2	2	4	1 pulse per degree	
Required Space	1	2	2	2	2	2		
Error rate	2	4	1	2	2	4		
Robustness (e.g. dust, dirt, humidity, vibration,...)	1	2	1	1	1	1	IP67/...?	
Total cost	3	6	2	6	2	6	Fabrication, accessories (AD-Converter, Amplifier etc.)	
Self-weight	3	6	1	3	2	6		
Assembly tolerances	3	6	2	6	1	3	Rotary position sensor: Magnet has to be attached exactly in the center of rotation	
Total sum		30		22		26		
Degree of Fulfillment		100,00%		73,33%		86,67%		

Legend			
Rating scheme			
Evaluation criterion	0 Points	1 Points	2 Points
Resolution	low	medium	high
Required Space	low	medium	high
Error rate	low	medium	high
Robustness (e.g. dust, dirt, humidity, vibration,...)	low	medium	high
total cost	low	medium	high
Assembly tolerances	low	medium	high
Weight			
very important	3		
important	2		
less important	1		





Allgemeintoleranzen DIN ISO 2768-mK			
Werkstückkanten DIN ISO 13715			
Material:	Maßstab		1:2
Halbzeug:	Masse: ca.		
Verantwortliche Abt.	Technische Referenz	Erstellt durch Odenkirchen, Till	Genehmigt von
Technische Universität Ilmenau Fakultät für Maschinenbau		Dokumententyp Assembly	
Titel, zusätzlicher Titel Soft Robotic Gripper		Dokumentenstatus	
And.	Ausgabedatum 4.05.2021	Spr. de	Blatt 1/3

1		2		3		4			
List of Parts: Soft Robotic Gripper									
Pos.	Menge	Einh.	Benennung	Sachnummer/Norm-Kurzbez.	Bemerkung				
A	1	1	Qty.	Palm base		PLA, 3D-printed			
	2	1	Qty.	Gear left		PLA, 3D-printed			
	3	2	Qty.	Gear right		PLA, 3D-printed			
	4	3	Qty.	MCP Base		PLA, 3D-printed			
B	5	3	Qty.	DIP Hinge		Ninjaflex TPU, 3D-printed			
	6	5	Qty.	Routing Dowel Palm		Steel			
	7	1	Qty.	Palm Backside		PLA, 3D-printed			
	8	3	Qty.	MCP Hinge		Ninjaflex TPU, 3D-printed			
	9	4	Qty.	Spacer		PLA, 3D-printed			
C	10	2	Qty.	Phalanx proximalis		PLA, 3D-printed			
	11	2	Qty.	Phalanx distalis		PLA, 3D-printed			
	12	1	Qty.	Torsional Spring					
	13	1	Qty.	Latch		PLA, 3D-printed			
	14	1	Qty.	Feetech FT90M-FB Servo Motor					
D	15	1	Qty.	Pulley		PLA, 3D-printed			
	16	1	Qty.	Servo Disk		ABS			
	17	1	Qty.	Differential		PLA, 3D-printed			
	18	3	Qty.	Spectra Symbol Flex Sensor					
	19	1	Qty.	Motor Mount		PLA, 3D-printed			
	20	1	Qty.	Handle		PLA, 3D-printed			
	21	7	Qty.	PCB FSR					
E	22	3	Qty.	Pad_dist		Wagnersil 20NF, mold			
	23	3	Qty.	Pad proximalis		Wagnersil 20NF, mold			
	24	3	Qty.	Interlink FSR400 Short Tail					
	25	3	Qty.	Sensor Plate		PLA, 3D-printed			
F	Verantwortliche Abt.		Technische Referenz		Erstellt durch		Genehmigt von		
					Odenkirchen, Till				
	Technische Universität Ilmenau Fakultät für Maschinenbau			Dokumentenart			Dokumentenstatus		
				List of Parts					
			Titel, zusätzlicher Titel						
			Soft Robotic Gripper						
			Master Thesis			Änd.	Ausgabedatum	Spr.	Blatt
							04.05.2021	de	2/3

1	2		3		4		
List of Parts: Soft Robotic Gripper							
A	Pos.	Menge	Einh.	Benennung	Sachnummer/Norm-Kurzbez.	Bemerkung	
	26	1	Qty.	Toothgear Right		PLA, 3d-printed	
	26	1	Qty.	Adafruit PCA9685			
	27	15	Qty.	Routing Dowel		Steel	
B	27	2	Qty.	PCB Fastener		PLA, 3D-printed	
	28	1	Qty.	Phalanx proximalis thumb		PLA, 3D-printed	
	28	2	Qty.	PCB Mount		PLA, 3D-printed	
	29	1	Qty.	Phalanx distalis thumb		PLA, 3D-printed	
	29	1	Qty.	Bluno Nano			
C	30	8	Qty.	Countersunk head Screw	ISO 7046-1 - M2,5 x 16 - 4.8 - H		
	31	3	Qty.	Phillips flat head screw	ISO 7045 - M2,5 x 5 - 4.8 - H		
	32	4	Qty.	Countersunk head Screw	ISO 7046-1 - M2,5 x 6 - 4.8 - H		
	33	1	Qty.	Countersunk head Screw	EN ISO 7045 - M2 x 3 - 4.8 - H		
D	34	2	Qty.	Phillips flat head screw	ISO 7045 - M1,6 x 5 - 4.8 - H		
	35	3	Qty.	Phillips flat head screw	ISO 7045 - M1,6 x 4 - 4.8 - H		
	36	5	Qty.	Phillips flat head screw	ISO 7045 - M2 x 6 - 4.8 - H		
E							
F	Verantwortliche Abt.	Technische Referenz		Erstellt durch	Genehmigt von		
	Technische Universität Ilmenau Fakultät für Maschinenbau			Odenkirchen, Till			
				Dokumentenart	Dokumentenstatus		
				List of Parts			
			Titel, zusätzlicher Titel				
			Soft Robotic Gripper				
			Master Thesis	Änd.	Ausgabedatum	Spr.	Blatt
					04.05.2021	de	3/3